University of Pavia
Department of Molecular Medicine

PhD course in Translational Medicine

XXXIII cycle

PhD thesis on

Aquaporins permeability to hydrogen peroxide may control oxidative stress

Tutor:
Prof. Umberto Laforenza

Candidate:
Dr. Giorgia Pellavio

Academic year 2019-2020

Dedicated to those who believed in me

Index

Abstract

Transmembrane water channel proteins, known as aquaporins (AQPs), play a pivotal role in many biological processes including volume regulation, cell migration and proliferation, and adipocyte metabolism. Recently, it has been demonstrated the involvement of some AQPs, known as "peroxiporins", in the transport of hydrogen peroxide (H_2O_2). H_2O_2 is the most abundant and stable reactive oxygen species (ROS) in living cells and H_2O_2 can have different effects depending on its concentration. Physiological levels of H_2O_2 induce positive adaptive responses acting as second messenger, while excessive levels provoke negative effects as apoptosis and cell death. Since AQPs allow the diffusion of H_2O_2 across plasma membranes to the extracellular fluid, they have been considered as a possible ROS scavenging mechanism. Until now, AQP1, 3, 5, 8, 9 and 11 are the mammalian AQPs involved in H_2O_2 diffusion. This project aims to understand the mechanism of AQPs as peroxiporins in mediating H_2O_2 diffusion through cellular plasma membrane.

The guiding thread of this thesis was, on the one hand, the analysis of the role of peroxiporins in some pathophysiological conditions and, on the other, the identification and characterization of new gating modulators.

In particular this thesis aimed:

1. to investigate the negative role of human Papillomavirus (HPV) infection on the aquaporin-mediated hydrogen peroxide elimination which affects human sperm functioning;
2. to clarify AQPs/peroxiporins involvement in malignant pleural mesothelioma progression (MPM);
3. to identify and characterize new aquaporin modulators to counteract the oxidative stress.

The study investigating the possible effect of human HPV on both expression and function of AQPs in normospermic and sub-fertile sperm cells found that:

- HPV infection differently influenced AQPs expression in sperm cells, which is increased in normospermic patients and is decreased in sub-fertile individuals;
- HPV infection heavily reduced water permeability of sperm cells in normospermic samples;
- confocal immunofluorescence and co-immunoprecipitation experiments unveiled a colocalization of HPV L1 protein with AQP8.

The findings may suggest that HPV infection directly inhibits AQP8 functionality and probably makes sperm cells more sensitive to oxidative stress.

The main results of the section of this thesis on the involvement of AQPs in malignant pleural mesothelioma progression are the following:

- some aquaporins (AQP3, 5, 6, 9, 11) are expressed in epithelioid and biphasic MPM cells;
- AQP6, 9 and 11 are highly expressed in some discrete areas of plasma membrane but also localized in intracellular structures, while AQP3 and 5 are only localized intracellularly;
- the water permeability of MPM cells is not influenced by H_2O_2 treatment, but, on the contrary, it is considerably increased by heat stress making these cells resistant to apoptosis;
- functional experiments performed in AQP6-null epithelioid MPM cells revealed that AQP6 is responsible, at least in part, for the increase in H_2O_2 efflux in response to heat-stress.

The study on the new aquaporin modulators able to reduce the oxidative stress condition showed that:

- well-established S1R agonists, PRE-084 and RC-33, Sigma 1 receptor (S1R) agonists can restore water permeability in heat-stressed cells and the co-administration with a S1R antagonist totally abolish this ability to restore the water permeability;
- new synthetized S1R ligands showed similar ability to restore the water permeability in heat-stressed cells and were effective in reducing the hydrogen peroxide levels within the cell in a dose-dependent fashion;
- all the compounds except one were able to counteract the oxidative stress of HeLa cells specifically knocked down for S1R.

These results support the hypothesis that the compounds analyzed act as dual aquaporin and Sigma1 receptor (DAS) modulators.

As a whole, AQPs permeability alteration (and sensitivity to oxidative stress) in HPV infection and in MPM seems to reduce the fertility of sperm cells and make MPM cells resistant to conventional chemotherapy, respectively. The possibility to modify the gating of the AQPs and ROS scavenging opens to new therapeutic strategies for the

treatment of debilitating diseases involving oxidative stress namely neurodegenerative diseases and cancer.

General Background

1. The discovery of water channels

The movement of water across cells is a fundamental biological process. Such water movement not only regulates the activity of individual cells, but it is also responsible for the functioning of many organ systems and for maintaining whole body water balance. It had long been suspected that water movement across biological cell membranes was in some way enhanced or facilitated by pores or channels, but the search to identify these channels was long and tedious (Brown, 2017).

It is well known that when the cells are placed in hyposmotic solution, they swell considerably. In contrast, when cells are placed in hyperosmotic solution, they will shrink. When osmotic swelling and shrinking were monitored at different temperatures, Solomon (Solomon, 1958) discovered a slow temperature sensitive process upon which was superimposed a much more rapid temperature-independent process. The slow process reflected diffusional permeability of water across the lipid bilayer of the plasma membrane. The fast process was consistent with the presence of aqueous pores in the membrane, which allowed the more rapid, osmotically driven passage of water that did not involve diffusion.

Macey, Farmer (Macey and Farmer, 1970) and others then showed that the compound mercuric chloride could significantly inhibit the fast component of this process, which suggested the presence of a protein pore – or water channel – within the membrane. Mercuric chloride binds to sulfhydryl groups (cysteine residues) on proteins and inhibits their function: in this case, the water permeability.

Later in 1987, Peter Agre and co-workers had purified by chance the first water pore from the red blood cell membrane while studying the Rh(D) antigen. In fact, Agre discovered a non glycosylated component of 28 kDa and a glycosylated component of 35~60 kDa, previously thought to be a degradation product of the Rh protein. The 28 kDa polypeptide was found to be highly abundant and to exist as an oligomeric protein with the physical characteristics of a tetramer (Denker et al., 1988). At the beginning the new protein was called CHIP28 (Channel-like Integral Protein of 28 kDa), but was later redubbed aquaporins-1 or AQP1 (Agre et al., 1993).

The water pore function was demonstrated by using the *Xenopus laevis* oocyte expression system (Preston et al., 1992). Transfected oocyte exhibited remarkably high

osmotic water permeability causing the cells to swell rapidly and explode in hypotonic solution (Preston et al., 1992).

In the same years, AQP1 was purified from human blood cells and reconstituted into liposomes to test its role as a molecular water channel (Zeidel et al., 1992). Liposomes with AQP1 showed a much higher water permeability than control liposomes, confirming that AQP1 is a selective water molecular channel (Zeidel et al., 1992). Agre received the Nobel Prize in Chemistry in 2003 for this discovery.

After the discovery of AQP1, other water channel family members were identified studying the homology in mammals, plants and in bacteria proteins.

2. Molecular structure of AQPs

AQP structure is largely conserved among the various AQPs classes and species isoforms, despite significant differences in sequence similarities. AQPs are tetrameric proteins composed of identical monomers, each of which functions as an independent water channel (Yang, 2017). The monomeric units of AQPs are ~30 kDa and consist of six transmembrane α-helices (known as M1, M2, M4-M6 and M8), two half helices (M3 and M7) and five loops (*a, b, c, d, e*) (Verkman et al., 2014). The polypeptide in the structure is formed by a single chain with about 270 amino acids, and amino (N) and carboxyl (C) terminals are located in the cytoplasm (Wang et al., 2015). AQP family is characterized by two conserved structural features: the two asparagine-proline-alanine (NPA) motifs and the aromatic/arginine (ar/R) constriction site (Figure 1).

The two conserved NPA motifs are located in the half-helices (M3 and M7) and they contain inward-facing asparagine polar side chains. These motifs are part of the hydrophilic surface of the amphipathic pore and are important for preventing proton conduction. In the tridimensional structure of the protein, NPA motifs are placed so as to form the pore of the channel through which water molecules can flow bidirectionally.

In fact, the NPA motifs with the polypeptide backbone α-carbonyl groups act as hydrogen-bond donors and acceptors that coordinate the transport of water (or glycerol for the aquaglyceroporins) through the pore (Verkman et al., 2014).

The ar/R constriction site is located at the extracellular side of the channel, contains highly conserved aromatic and arginine residues. Having a diameter of 3 Å, which is only slightly larger than the 2.8 Å diameter of the water molecule, the pore constriction prevents permeation of all molecules bigger than water. Therefore the ar/R constriction site is also called the “selectivity filter” (Benga, 2012).

Most members of aquaporins possess a cysteine residue in the ar/R region, which is situated near the pore responsible for functional sensitivity to mercury. In AQP1, the residue Cys189 has been shown to be the site of mercurial binding and water transport inhibition (Preston et al., 1993). However, not all AQPs are inhibited by $HgCl_2$, for examples, AQP4 (Yang et al., 1996) and AQP6. The water permeability of AQP6, on the contrary, is actually increased in the presence of this mercurial agent (Yasui et al., 1999).

Figure 1 - Secondary structure and topology of AQP molecule

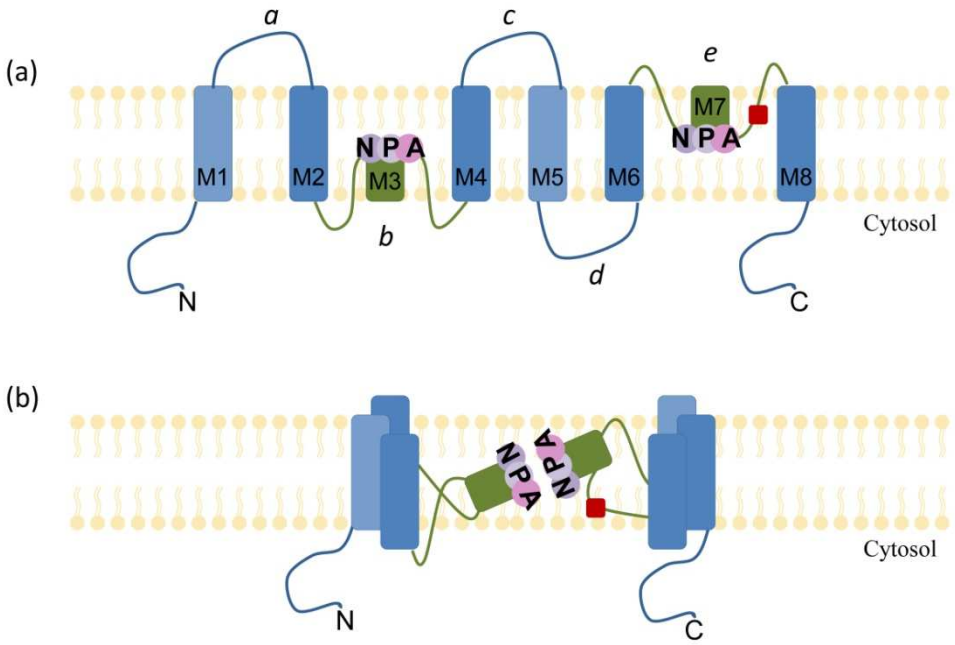

(a) AQP monomer has six transmembrane α-helices (M1, M2, M4, M5, M6, M8), two half α-helices (M3, M7), five loops (a - e) with intracellular amino and carboxyl termini. (b) In the monomer, the hydrophilic loops b and e are bent back into the cavity and meet in the middle to form the putative water-selective gate that contains two consensus NPA motifs (Asn-Pro-Ala). ar/R region (red square) is shown close to the entrance of the pore (picture created with Power Point).

3. AQPs Characteristics

Proton exclusion

It is well established that protons can be efficiently translocated across the membrane along an unbroken chain of water molecules within an open pore. This is believed to occur via a Grotthuss hop-and-turn mechanism whereby excess protons are chemically exchanged (hop) between hydrogen-bonded water molecules oriented in a single file, followed by a structural rearrangement of the hydrogen bonding network (turn) (Kreida and Törnroth-Horsefield, 2015). Remarkably, aquaporins are able to prevent proton translocation.

The proton exclusion is explained by the "hydrogen bond isolation mechanism" proposed by Murata and colleagues (Murata et al., 2000). The two asparaginases N76 and N192 belonging to the NPA motifs, have the amide group facing at the center of the pore which form hydrogen bonds with the oxygen of a water molecule, isolating it in the center of the pore. Consequently, the water molecule changes its orientation, positioning itself perpendicular to the pore axis. This mechanism determines the interruption of the continuous ideal line of water molecules connected with hydrogen bonds preventing so the transport of protons (Figure 2).

Crystallographic studies reveal that the central water molecule is still able to form hydrogen bond, but exclusively with the neighbouring water molecule, that precedes it towards the extracellular side of the pore. Moreover, positive charged residues (such as arginine and histidine) located in the extracellular and intracellular domain can also repel protons from entering the pore (Sui et al., 2001).

Figure 2 - Schematic architecture of the channel within an AQP1 subunit (sagittal section)

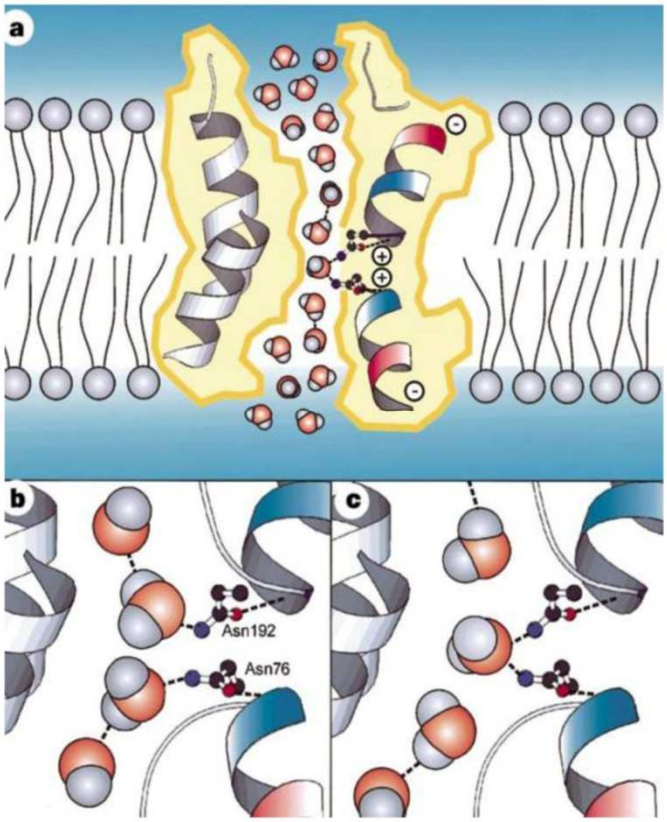

(a) Diagram illustrating how water molecoles pass through the constriction of the pore. (b) and (c), four water molecules shown represent transient interactions with Asn 76 and/or Asn 192. Note water dipole reorientation. Two partial helices meet at the midpoint of the channel, providing positively charged dipoles that reorient a water molecule as it traverses this point (Murata et al., 2000).

AQPs Permeability

The main physiological function of AQPs is to facilitate the water transport across plasma membrane of cells in response to an osmotic gradient. In addition to the primary function some AQPs (AQP3, 7, 9, 10), called aquaglyceroporins, facilitate glycerol transport (Figure 3). Such glycerol-transporting function is involved in the movement of glycerol and energy metabolism process. In aquaglyceroporins the permeability to larger molecules, than water molecules, is due to the substitution of His180 with other residues that determines the pore enlargement. As stated above, the specificity of the transport of water in AQPs is due to the ar/R constriction site, which contains a highly conserved aromatic and arginine residues (Sui et al., 2001). This site is close to the two NPA motifs and in proximity to the pore which is only a little larger than the width of a water molecule. Recent study conduct on rat AQP1 confirm that exists a solute discrimination by size; in particular specific substitution of the histidine and arginine residues of the ar/R site that determine a modification of the diameter of the pore, allowing urea permeation (Beitz et al, 2006). The double mutation Phe56Ala/His180Ala enlarged the maximal diameter of the ar/R constriction site 3-fold and made the pore permeable to glycerol and urea (Beitz et al, 2006).

Interestingly, the chemical similarity between water and H_2O_2 suggests that AQPs could likely be candidates for H_2O_2 permeation. Many studies confirmed that certain AQPs could mediate H_2O_2 transmembrane transport (Bienert and Chaumont, 2014).

The central pore, generated in the tetrameric form of AQP, is also thought to be permeable to gases. In particular, AQP1, AQP3, AQP4, AQP5, AQP8 and AQP9 could potentially transport gases such as CO_2, NO, NH_3 and O_2. However, some studies suggest that AQP1-dependent CO_2 transport has no physiological relevance (Fang et al., 2002; Yang et al., 2000). Early studies showed that NO produced by the endothelial cells relaxed adjacent vascular smooth muscle cells to regulate blood flow and blood pressure. Using AQP1 null mice, Herrera et al. subsequently identified that transport of NO by AQP1 was required for vascular function (Herrera and Garvin, 2007).

In addition, there is an increasing evidence that certain AQPs have ion channel function. In AQP1, the central pore has been proposed as a cation channel (Yool and Weinstein, 2002). The studies of Ikeda et al. indicated that AQP6 exhibited a form of anion permeation with significant specificity for nitrate (Ikeda et al., 2002).

The transport of various kinds of small molecules by AQPs is an interesting topic. However, most data about transport characteristics of AQPs are derived from *in vitro*

experiments. The physiological significance of AQPs that are permeable to gases and other small molecules is necessary to be determined by *in vivo* experiments.

Figure 3 - Overall structure of AQPs

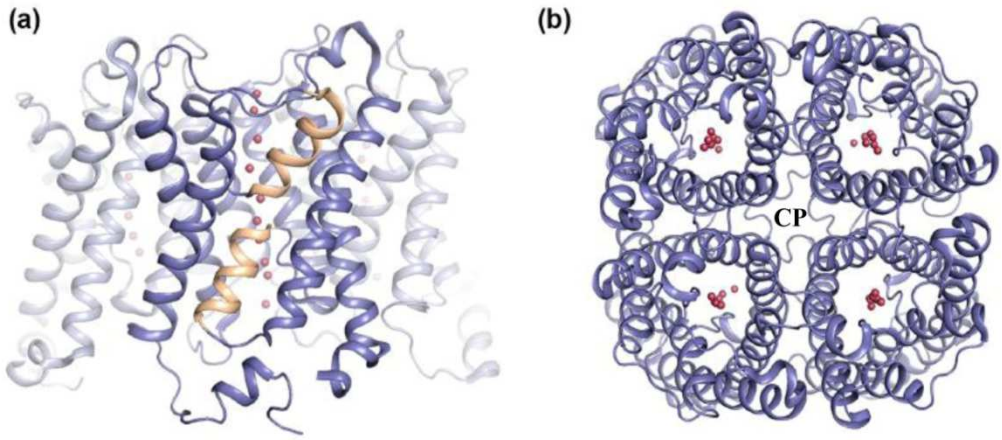

Crystal structure of human AQP5 showing the AQP tetramer viewed: (a) parallel to the membrane and (b) from the extracellular side. The AQP5 tetramer is shown in blue ribbon-representation with half-membrane spanning helices formed by loops B and E colored yellow. Water molecules in the pore are shown as red spheres. CP, central pore (modified Roche and Törnroth-Horsefield, 2017).

Inhibitors of AQPs permeability

Several molecules have been suggested as inhibitors of various AQPs over the past few years. The similarity found between AQPs and ion channels has caused interest in ion channel modulators as possible AQP inhibitors (Abir-Awan et al, 2019). For example, Tetraethylammonium (TEA) and Acetazolamide are molecules that have attracted attention as potential AQP inhibitors (Brooks et al, 2000; Yang et al, 2008). Anti-epileptic drugs (AEDs) have also been suggested to have an AQP modulating function (Tang and Yang, 2016). However due to their unconfirmed mechanisms of action and relatively non-specific action, there is no conclusive evidence showing that these molecules are effective and safe AQP inhibitors (Abir-Awan et al, 2019).

Phloretin is another small molecule that acts as a non-specific aquaglyceroporin inhibitor. It has also been shown to inhibit the urea transporter, UT-A1, found in the kidney (Esteva-Font et al, 2013). It has been speculated that the same mechanism underpinning urea inhibition is responsible for inhibition of the aquaglyceroporins, AQP3 and AQP9 (Abir-Awan et al, 2019).

For many years cancer therapy has been focus on cytotoxic treatments with heavy metal compounds such as cisplatin, a platinum compound. Many AQPs have been correlated

with cancers (Abir-Awan et al, 2019). Nickel chloride and copper ions have been shown to inhibit AQP3 function (Zelenina et al, 2003; Nave et al, 2016). It is believed that they act by binding three extracellular loop residues (Trp-128, Ser-152, and His-241) on the extracellular loops (Nave et al, 2016). Instead, mercury ions bind to Cys-189 found on several AQPs and blocks the channel (Verkman et al., 2014). In fact, a mutation in the Cys-189 residue of AQP1 prevent its inhibition by mercury, and other AQPs (such as AQP4) that lack a cysteine residue at this position are resistant to inhibition by mercury (Verkman et al., 2014).

Mercury and its compounds are known to be toxic due to their non specificity, which causes many off-target effects.

Gold-based compounds have also been used as AQP3 inhibitors and their binding is thought to be via Cys-40. Mercury and Gold compounds inhibition can be almost completely reversed by the addition of the reducing agent, 2-mercaptoethanol (Martins et al 2012).

Silver has also been used as a possible AQP inhibitor and is found to produce a rapid and irreversible inhibition of AQP1 in erythrocytes (Niemietz and Tyerman, 2002). Gold and silver are thought to bind to sulfhydryl groups on cysteine residues of AQPs, but the complete mechanisms are not yet understood (Martins et al, 2012; Niemietz and Tyerman, 2002).

In the last few years the need to find AQP inhibitors with high specificity and low toxicity led researcher to study new molecules, such as natural fito-compounds. For example curcumin, from *Curcuma longa*, is an antioxidant compound, but at the same time inhibits the functioning of AQPs in Hela cells (Pellavio et al., 2017; Portaincasa and Calamita, 2019; Sonntag et al., 2019).

4. AQPs Regulation

The water flow must occur at the appropriate locations and rates for each cell and tissue types of the human body. Therefore, the AQPs functional regulation is critical to ensure the physiological activity.

Fast regulation can be achieved by two means: by altering the water permeability rate through the pore itself (gating) or by rapidly changing the abundance of AQP molecules in the plasma membrane by shuttling the protein from the intracellular vesicles to the plasma membrane, the so-called membrane trafficking (Kreida and Törnroth-Horsefield, 2015).

The regions involved in AQP regulation are most often found outside the highly conserved transmembrane core domains, in the loops and termini. In these regions there are the phosphorylation sites that play crucial roles in the different regulation of human AQPs (Nesverova and Törnroth-Horsefield, 2019).

Through phosphorylation/dephosphorylation, the structures and properties of these regions are altered, changing their ability to bind the regulatory proteins that control the phosphorylation-dependent regulatory events. These events include: 1) translocation to and from the plasma membrane, 2) targeting degradation and 3) gating, i.e., the AQP opening (activation) or closing (by deactivation or inactivation) (Nesverova and Törnroth-Horsefield, 2019). The phosphorylation process is governed by a tight interplay of kinases and phosphatases, and is often tissue-specific, thereby allowing proteins to be regulated based on particular tissue needs (Nesverova and Törnroth-Horsefield, 2019). Protein kinases are key regulatory enzymes, reversibly attaching a phosphate group onto serine, threonine and tyrosine residues. Most of AQP0-AQP9 are phosphorylated by a member of the AGC kinase subfamily, which contains some of the most well described kinases like protein kinase A (PKA), protein kinase C (PKC), and protein kinase G (PKG). The protein phosphorylation is a reversible process allowed by the dephosphorylating activity of phosphatases. The phosphorylating and the dephosphorylating activities are equally important in protein regulation. The knowledge of how the dephosphorylation of aquaporins is regulated is very limited (Nesverova and Törnroth-Horsefield, 2019). The role of specific phosphatases has been studied mainly for AQP2 by Ren et al. (2016). The involvement of several phosphatases, including PP1, PP2A, PPA2B and PP2C (calcineurin) was demonstrated, although many of the details remain to be fully elucidated (Ren et al., 2016).

Regulation of AQPs expression

Transcriptional rates of most genes physiologically fluctuate, especially under stress and this has also been demonstrated for AQPs.

Activation of protein kinase C (PKC) decreases expression of AQPs 4 and 9, which can be prevented by the addition of PKC inhibitors. This suggests that their expression levels may be regulated by cellular stressors or signals which are mediated through PKC. Many other studies report that the upregulation and downregulation of AQP mRNAs change the AQP gene expression levels under a variety of different pathophysiological conditions, such as human renal and muscular diseases as well as after CNS trauma (Halsey et al., 2018).

Regulation of AQPs gating

The conformational 'gating' is the most common and frequently observed method for regulating AQP activity. This regulation was first reported in plant AQPs, such as those in spinach, where an intracellular loop physically barricades the intracellular pore following dephosphorylation at a local serine residue (Halsey et al., 2018).

In mammals AQP3, AQP6 and AQP0 change their water permeability in function of pH. In particular, AQP3 closes at pH <6 (Zeuthen and Klaerke, 1999) while, on the contrary, AQP6 only opens at pH <5.5 letting water and anions enter (Yasui et al., 1999a; Yasui et al., 1999b; Hazama et al., 2002; Liu et al.2005;). The permeability of the AQP0 is optimum at pH 6.5 (Németh-Cahalan and Hall, 2000).

In 2018, Gotfryd et al. discovered that the glycerol permeability of human AQP10 is pH regulated through protonation of hystidine 80. In particular the permeability to water was pH-insensitive, while glycerol passage increased at pH 5.5 (Gotfryd et al., 2018). In this case pH regulation is achieved by a cytoplasmic, glycerol specific gate and, likely, a widened ar/R filter, both unique to hAQP10, correlating with intracellular acidification of adipocytes observed during lipolysis (Gotfryd et al., 2018). Other studies report that AQP4 may also be gated by a physical narrowing of the channel pore that becomes too small for water molecules to pass through. Molecular dynamics studies reveal that a histidine residue in the cytoplasmic side of the pore may reorientate and interact with a nearby cysteine residue, which constricts the pore (Halsey et al., 2018).

In general the molecular basis for pH sensitivity of AQPs is the presence of accessible histidine residues in loop A and C (Németh-Cahalan et al., 2004). In particular, a

histidine residue in the loop A can confer sensitivity to acid or alkaline pH depending on its particular position; just by changing the histidine location of one residue the channel sensitivity to pH is altered. On the contrary, the presence of a histidine in loop C confers alkaline pH sensitivity. The protonation or deprotonation of external histidines due to pH changes, can modulate the orientation of water molecules and thus alter the electrostatic interactions between water molecules and disrupt the single-chain.

Regulation of AQPs trafficking

The main regulatory mechanism of mammalian aquaporins is trafficking and AQP2 trafficking is the canonical example. It has long been known that vasopressin is able to increase the water permeability in the collecting duct epithelium (Grantham and Burg, 1966; Morgan and Berliner, 1968), but only in the 1990s, the AQP2 was accounted for this mechanism (Zhang et al., 1993).

A decrease in blood volume or an increase in blood osmolarity causes vasopressin released from the posterior pituitary gland. Vasopressin binds to the vasopressin type-2 receptor (V2R), present on the basolateral membrane of renal collecting duct principal cells. This induces a signaling cascade, involving Gs protein mediated activation of adenylate cyclase (AC), a rise in intracellular cAMP, activation of PKA and subsequent phosphorylation of AQP2. This results in the redistribution of AQP2 from intracellular vesicles to the apical membrane. Vasopressin stimulation also results in increased intracellular Ca^{2+} levels via Ca^{2+} release from calmodulin-dependent ryanodine-sensitive intracellular stores, which induces apical membrane expression of AQP2. On the long term, vasopressin increases AQP2 expression via activating transcriptional factors, which stimulates transcription of AQP2 at the AQP2 promoter (Yang, 2017). These processes restore blood volume and normalize blood osmolarity. Upon restoration of water balance, vasopressin release from the pituitary gland returns to baseline level and AQP2 is rapidly sequestered into endosomes within cells, thus reducing collecting duct water permeability (Cheung et al., 2019) (Figure 4).

Similar to vasopressin, calcitonin, secretin, glucagon, serotonin, prostaglandin E2 and E4 all activate Gs protein and trigger a similar signaling pathway to stimulate AQP2 membrane trafficking permeability (Cheung et al., 2019).

Other AQPs are regulated by hormones. Glucagon, via activation of PKA and phosphatidylinositol-3-kinase (PI3K), induces AQP8 vesicle trafficking to the hepatocyte

canalicular domain. Thus, glucagon increases the AQP-mediated osmotic membrane water permeability, facilitating the movement of water. This process is relevant for glucagon-induced bile secretion (Soria et al., 2009).

Figure 4 – The trafficking of AQP2

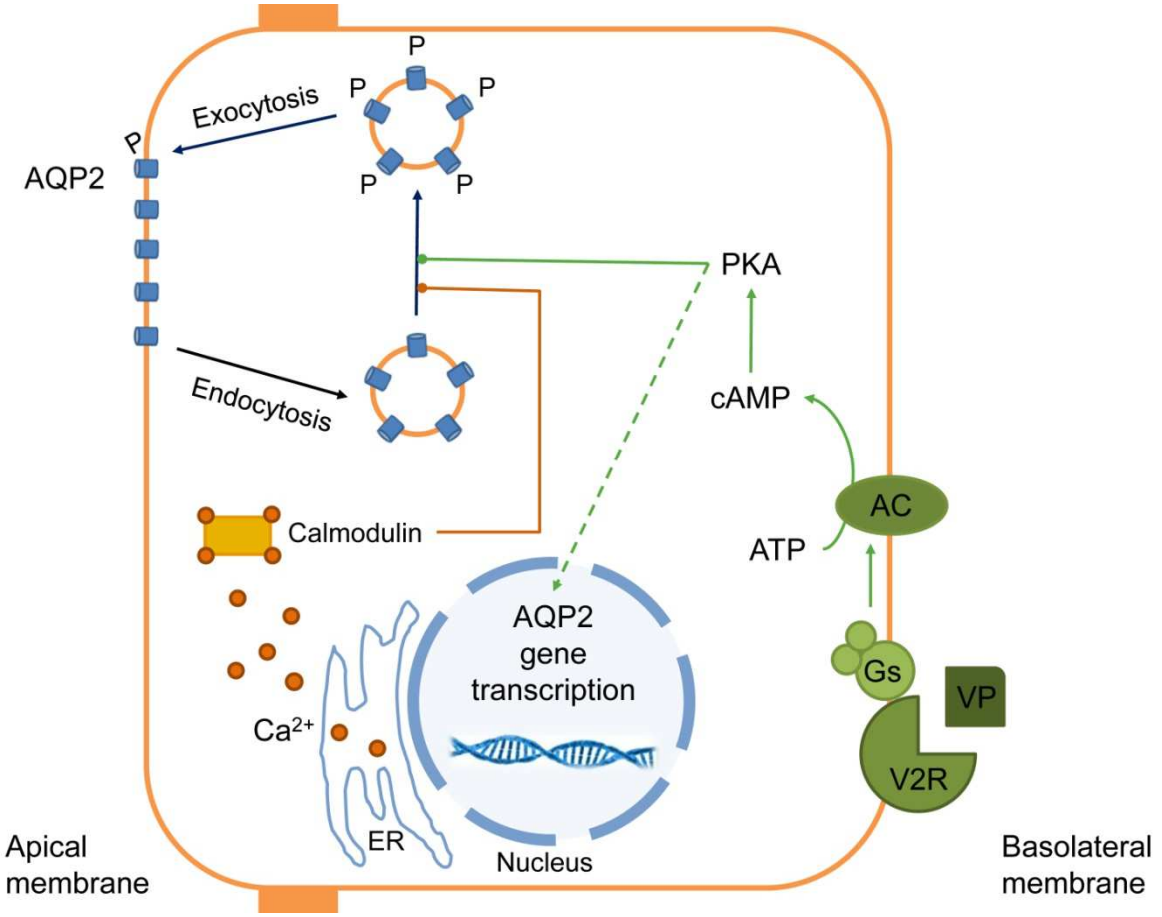

Vasopressin (VP) binds to the vasopressin type-2 receptor (V2R), present on the basolateral membrane of renal collecting duct principal cells. This induces a signaling cascade, involving Gs protein mediated activation of adenylate cyclase (AC), a rise in intracellular cAMP, activation of protein kinase A (PKA) and subsequent phosphorylation of AQP2. This results in the redistribution of AQP2 from intracellular vesicles to the apical membrane. Vasopressin stimulation also results in increased intracellular Ca^{2+} levels via Ca^{2+} release from calmodulin-dependent ryanodine-sensitive intracellular stores, which induces apical membrane expression of AQP2. On the long term, vasopressin increases AQP2 expression via activating transcriptional factors, which stimulates transcription of AQP2 at the AQP2 promoter (picture created with Power Point).

Regulation of AQPs protein-protein interactions

Protein–protein interactions play crucial roles in AQP regulation as well as alternative AQP functions and can primarily be divided into three types: interactions between AQP tetramers in supramolecular assemblies (junctions and arrays); interactions between AQP monomers of different types (hetero-tetramerization); and transient interactions with regulators (Roche and Törnroth-Horsefield, 2017) (Figure 5).

From the various identified AQP classes and paralogs, only two AQPs have been shown to accumulate in supramolecular assemblies: mammalian AQP0 found in the eye lens (Gonen et al., 2004), and AQP4, the main AQP in the brain (Rash et al., 1998). These assemblies involve interactions within the same cell membrane (arrays) and between cells (junctions). AQP0 and AQP4 both form square-formed, so-called orthogonal arrays in their native membranes. AQP0 also mediates cell adhesion through its participation in thin junctions between lens fiber cells (Gonen et al., 2004).

While most of the AQPs assemble as homo-tetramers, some AQPs have been observed to form hetero-tetramers consisting of different AQP variants. For mammalian AQPs, the hetero-tetramerization of AQP4-M1 and AQP4-M23 variants constitutes the most striking example, controlling formation of AQP4 orthogonal arrays particles. Other examples include AQP2, in which case a mutant form of AQP2 causing autosomal-dominant nephrogenic diabetes insipidus (NDI), was able to form a hetero-tetramer with wild-type AQP2 (Sohara et al., 2006). However, the existence of “true” hetero-tetramers, consisting of different AQP isoforms, rather than AQP splicing variants or mutants assembling with the wild-type form, has been reported only for plant AQPs (Jozefkowicz et al., 2017).

Interactions with regulators play crucial roles in gating, trafficking and degradation mechanisms. For mammalian AQPs, a number of interaction partners have been identified (Sjohamn and Hedfalk, 2014), including calmodulin with AQP0 and AQP6 (Rabaud et al., 2009), prolactin inducible protein (PIP) with AQP5 (Ohashi et al., 2008), perilipin-1 with AQP7 (Hansen et al., 2016), the heat shock protein Hsp70 with AQP2 (Lu et al., 2007). These examples highlight the complexity and variability of the protein–protein interactions in which different AQPs are involved. A large number of AQP interaction partners bind to the C-terminus, although other regions have been proposed to be involved in the interaction with some partners (Sjohamn and Hedfalk, 2014). The latter includes the interaction between AQP6 and calmodulin, which is suggested to be mediated by the AQP6 N-terminus (Rabaud et al., 2009). The AQP C-terminus frequently

harbors post-translational modifications sites, in particular phosphorylation sites. It is believed that post-translational modifications of these sites modulate the interactions with the regulatory proteins, allowing for dynamic control of the regulatory process (Moeller et al., 2010).

Figure 5 - Types of AQP protein–protein interactions

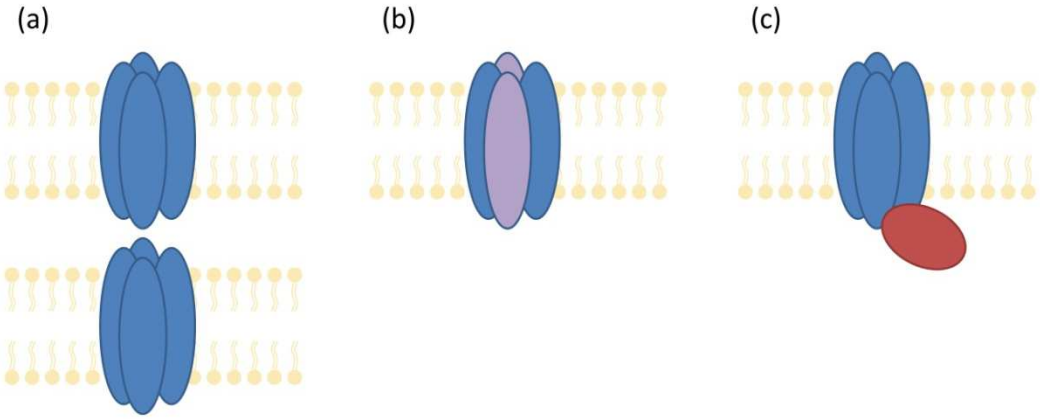

AQP protein–protein interactions can typically be divided into: (a) interactions between AQP tetramers in supramolecular assemblies; (b) interactions between different AQP monomers (blue and violet ovals) in hetero-tetramers and (c) transient interactions with regulatory proteins (in red).

5. AQPs Classification

To date, 15 classes of aquaporin genes have been identified in mammals (AQP0–AQP14), with AQP13 and AQP14 found in older lineages of mammals (Metatheria and Prototheria) (Finn et al., 2014; Finn and Cerda, 2015).

Currently there are 13 AQPs described in humans (AQP0–AQP12) that are widely distributed among the body and differentially expressed in tissues, playing an important role in a variety of physiological functions (King et al, 2004).

This family of proteins has been distributed by three subgroups according to their selectivity and primary structure (Ishibashi et al, 2011) (Figure 6):

- Classical/orthodox aquaporins (AQP0, AQP1, AQP2, AQP4, AQP5, AQP6, and AQP8) considered primarily selective to water;
- Aquaglyceroporins (AQP3, AQP7, AQP9, and AQP10) that also permeate glycerol, urea, and other small non-charged solutes;
- Nonorthodox/S-aquaporins (AQP11 and AQP12) comprising intracellular paralogs whose selectivity and function is still under investigation.

Recently, a few paralogs have also been reported to transport hydrogen peroxide and named peroxiporins (AQP3, AQP5, AQP8, AQP9 and AQP11) (Pellavio et al, 2017).

Figure 6 - Aquaporins classification

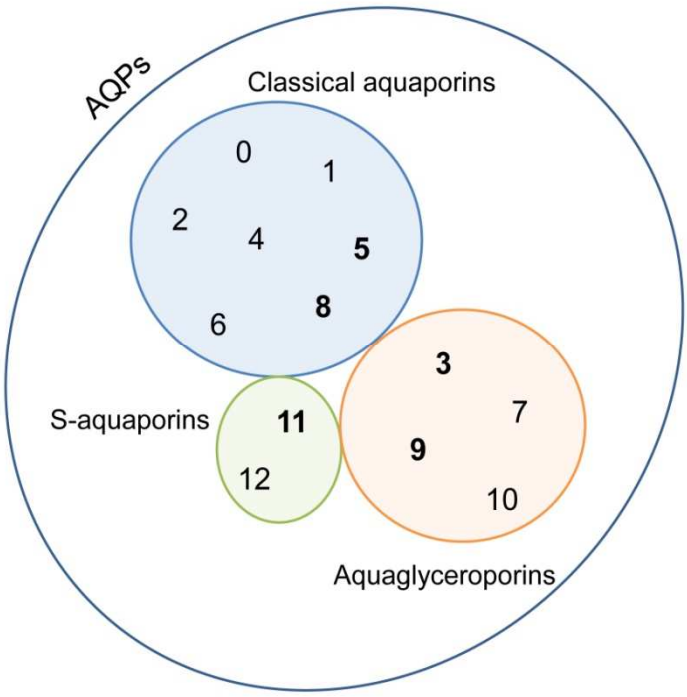

Paralogs in bold are able to transport hydrogen peroxide and were termed peroxiporins.

Classical Aquaporins: ***localization, characteristics and physiological functions in mammals.***

Classical aquaporins have been extensively studied with regard to the regulation of their expression in the body and their potential roles in physiological and pathophysiological states. Recent literature, however, appears to suggest that AQP6 and AQP8 be classified as unorthodox AQPs, due to low water permeability of AQP6 and unique, different phylogenetic of AQP8 from others (Yang, 2017) (Table 1).

AQP0 is the protein in the fiber cells of the eye lens where it is required for homeostasis and transparency of the lens (Clemens et al., 2013). AQP0 showed lower water permeability than AQP1 and this water transport is regulated by C-terminal cleavage, pH and Ca^{2+}/calmodulin (Nemeth-Cahalan et al., 2004). In particular, a low internal Ca^{2+} concentration increased AQP0 water permeability. The binding to calmodulin inhibits AQP0 water permeability by allosterically closing the cytoplasmic gate of AQP0 (Reichow et al., 2013).

AQP1 is the first water channel discovered in erythrocytes and the first AQP which was found to function as a gas channel (CO_2) (Geyer et al., 2013) AQP1 is the most widely distributed water channel in the body where it plays a central role in regulation of water transport through the tissues. AQP1 also plays an important role in angiogenesis, cell migration and cell growth (Nico and Ribatti, 2010).

AQP2 is a vasopressin-regulated aquaporin which is probably the most thoroughly studied to date. AQP2 displays permeability only to H_2O. AQP2 is expressed in principal cells of the collecting ducts and is abundant both in the apical plasma membrane and subapical vesicles in the kidney, where it is deeply involved in urine concentration (Yang, 2017). Other local, systemic factors or chemicals have been reported to regulate AQP2 expression or trafficking, such as atrial natriuretic peptide, nitric oxide, prostaglandin E2, angiotensin II, oxytocin, purine, statin (Cheung et al., 2019).
The comprehension of the shuttling mechanism has been of considerable importance for the identification of potential therapeutic targets for nephrogenic diabetes insipidus (NDI) (Noda and Sasaki, 2006). In fact, this condition can occur as a consequence of AQP2 mutations that lead to an impaired channel trafficking, which can be pharmacologically restored.

AQP4 is the main AQP located in central nervous system in glial cells plasma membranes and is also permeable to CO_2 (Geyer et al., 2013). It is known that AQP4 is responsible for the formation of brain edema following ischemic attack in the brain and thus inhibiting its activity can reduce brain damage (Papadopoulos and Verkman, 2007). AQP4 plays a pivotal role in the pathogenesis of neuromyelitis optica (NMO), a rare inflammatory demyelinating disorder affecting the optic nerves and spinal cords. The disease manifests due to the presence in the serum of the patient of autoantibodies able to bind AQP4 on plasma membrane of astrocytes and thus to activate complement leading to inflammatory demyelination (Jarius et al., 2008).

AQP5 is expressed in glandular and bronchial epithelial cells where it contributes to secretion, while in alveolar epithelium it regulates the alveolar fluid homeostasis (Song et al., 2001). AQP5 is also expressed in secretory glands where it is involved in the generation of saliva and tears (Song et al., 2002). Recent studies demonstrated that AQP5 is permeable to H_2O_2, playing an important role in cancer cell survival. By allowing a dynamic fine-tuning of intracellular H_2O_2 to activate signaling networks related to cell survival and proliferation, AQP5 can regulate cellular resistance to oxidative stress (Rodrigues et al., 2019)

AQP6 colocalizes with the H^+-ATPase in intracellular vesicles in the renal collecting duct type-A intercalated cells (Yasui et al., 1999) indicating that AQP6 may functionally interact with H^+-ATPase in the vesicles to regulate intra-vesicle pH. AQP6 appears impermeable to H_2O, but in the presence of $HgCl_2$ or at acidic pH (<5.5) the water and anion permeability of AQP6 in oocytes rapidly increased (Yasui et al., 1999). Moreover, AQP6 also enables transport of urea, glycerol, and nitrate (Holm et al., 2004; Ikeda et al., 2002).

AQP8 is a water channel first found in intracellular domains of the proximal tubule and the collecting duct cells. It was identified in the testis, in pancreas (at the apical membrane of pancreatic acinar cells), in the mitochondria of some hepatocytes in the liver (Calamita et al., 2005).
In addition to water, AQP8 transports ammonia and facilitates the diffusion of hydrogen peroxide across mitochondrial membranes when reactive oxygen species are generated (Danielli et al., 2019).

Aquaglyceroporins: ***localization, characteristics and physiological functions in mammals.***

Aquaglyceroporins are permeable to water and other small uncharged molecules such as glycerol, ammonia and urea. They also facilitate the diffusion of arsenite, antimonite and play a crucial role in metalloid homeostasis (Yang, 2017). Aquaglyceroporin are involved in cell proliferation, epidermal hydration and adipocyte metabolism; in particular, they are differently located in the adipocytes and they control glycerol uptake and release during the lipogenesis and lipolysis processes, respectively (Maeda et al., 2008) (Table 2).

AQP3 is the most abundant aquaglyceroporin in mammalian skin epidermis. It plays important roles in hydration and elasticity by facilitating water and glycerol transport, in barrier recovery and wound healing by proliferation and migration. Unfortunately, the overexpression of AQP3 in the skin, and the resulting increased transport of glycerol, may stimulate the growth of basal skin cancer cells and the onset of keratin-carcinoma (Hara-Chikuma and Verkman, 2008). AQP3 is present in the basolateral membrane of the principal cell in the collecting duct to permit water reabsorption and thus urine concentration. Recent studies revealed the pH gating of human AQP3 on both water and glycerol permeabilities using a human red blood cell model and in silico (de Almeida et al., 2016). AQP3 was also shown to transport H_2O_2 through the plasma membrane, which likely play an important role in initiating intracellular signaling in cell migration, inflammation, and cancer progression (Rodrigues et al., 2019).

AQP7 is abundantly expressed in adipose tissue, where it mediates the efflux of newly generated glycerol. Abnormal regulation of glycerol is a remarkable contributing factor to the development of metabolic disease. A deficiency of AQP7 may cause obesity and insulin resistance. Until a few years ago, AQP7 was considered the only glycerol channel in the adipose tissue; at present AQP3, AQP9 and AQP10 are also shown to be novel gateways for the transport of glycerol in human adipocytes (Laforenza et al., 2013).

AQP9 is expressed at the sinusoidal plasma membrane of hepatocytes, where it serves as a NH_3 channel and mediates the efflux of newly synthesized urea. AQP9 may also function as a glycerol channel to facilitate glycerol uptake in the liver. AQP9 is also permeable to water, glycerol, urea, carbamides, CO_2, and NH_3. Moreover, AQP9 is

suggested playing a crucial role in metalloid homeostasis by transporting antimonite and arsenite (Finn and Cerda, 2015). It also transports much larger substrates such as lactate, purine, pyrimidine (Finn and Cerda, 2015), probably due to a larger pore size disclosed by a 3D structure analysis (Viadiu et al., 2007). In addition, AQP9 was recently shown to facilitate the membrane transport of H_2O_2 in human and mice cells. Deficiency of AQP9 attenuated H_2O_2-induced cytotoxicity in human and mice cells, indicating that AQP9-mediated H_2O_2 may regulate redox-regulated downstream cell signalling (Watanabe et al., 2016).

AQP10 is an aquaglyceroporin expressed only in humans, mice did not have AQP10 since it is a pseudogene (Morinaga et al., 2002; Laforenza et al., 2013; Laforenza et al., 2016a). This aquaglyceroporin is expressed in gastrointestinal tract and in adipose tissue. Silencing AQP10 in human differentiated adipocytes resulted in a 50% decrease of glycerol and osmotic water permeability, suggesting that AQP10, together with AQP7, is particularly important for the maintenance of normal or low glycerol contents inside the adipocyte, thus protecting humans from obesity (Laforenza et al., 2013).

S-Aquaporins: ***localization, characteristics and physiological functions in mammals.***

The third subfamily of related proteins have low conserved amino acid sequences around the NPA boxes, unclassifiable to the first two subfamilies (Yang, 2017) (Table 3).

Unlike classical AQPs, AQP11 has one Asn-Pro-Ala (NPA) motif in loop E and the other NPA in loop B is atypically substituted with an Asn-Pro-Cys (NPC) motif, which appears essential for full expression of molecular function (Ikeda et al., 2011). Although detailed subcellular localization of AQP11 remains unknown, AQP11 has been observed colocalizes with markers of the endoplasmic reticulum in transiently transfected cells (Morishita et al., 2005). Deficiency of AQP11 is associated with endoplasmic reticulum stress and apoptosis in the kidney proximal tubules (Morishita et al., 2005). In fact, recent studies have demonstrated that AQP11 guarantees efficient transport of H_2O_2 across the endoplasmic reticulum membrane, functioning as a H_2O_2 scavenger (Bestetti et al., 2020).

AQP12 is more closely related to AQP11 than to other aquaporins. With regard to the signature motifs, the first NPA motif of AQP12 is substituted by an Asn-Pro-Thr NPT motif and the second NPA motif is conserved (Itoh et al., 2005). AQP12 seems to be

expressed specifically in pancreatic acinar cells and retained in intracellular structures, the physiological role of AQP12 remains to be clarified (Itoh et al., 2005). A study suggests that AQP12 may function as controlling the proper secretion of pancreatic fluid following rapid and intense stimulation (Ohta et al., 2009).

Table 1 - Mammalian Classical aquaporins and their distributions

	Transport	Distribution
Classical aquaporins		
AQP0	Water	Eye
AQP1	Water	Brain, eye, kidney, heart, lung, gastrointestinal tract, salivary gland, liver, ovary, testis, muscle, erythrocytes, spleen
AQP2	Water	Kidney, ear, ductus deferens
AQP4	Water	Brain, kidney, salivary gland, heart, gastrointestinal tract, muscle
AQP5	Water, hydrogen peroxide	Salivary gland, lung, gastrointestinal tract, ovary, eye, kidney
AQP6	Water, urea, anion	Brain, kidney
AQP8	Water, urea, ammonia, hydrogen peroxide	Testis, liver, pancreas, ovary, lung, kidney

(modified by Yang, 2017)

Table 2 - Mammalian Aquaglyceroporins and their distributions

	Transport	Distribution
Aquaglyceroporins		
AQP3	Water, urea, glycerol, ammonia, hydrogen peroxide	Kidney, heart, ovary, eye, salivary gland, gastrointestinal tract, respiratory tract, brain, erythrocyte, fat
AQP7	Water, urea, glycerol, ammonia	Testis, heart, kidney, ovary, fat
AQP9	Water, urea, glycerol, hydrogen peroxide	Liver, spleen, testis, ovary, leukocyte
AQP10	Water, urea, glycerol	Gastrointestinal tract

(modified by Yang, 2017)

Table 3 - Mammalian S-aquaporins and their distributions

	Transport	Distributions
S-aquaporins		
AQP11	Water? Hydrogen peroxide	Testis, heart, kidney, ovary, muscle, gastrointestinal tract, leukocytes, liver, brain
AQP12	Unknown	Pancreas

(modified by Yang, 2017)

6. Surprising Roles of AQPs

AQPs and Cancer

Aquaporins are implicated in the metastatic cascade, angiogenesis, Epithelial-Mesenchymal Transition (ETM), migration and invasion (De leso and Yool, 2018).

AQP1, expressed in peripheral vascular endothelial cells, is involved in tumor angiogenesis. Saadoun et al. (2005) showed AQP1 null endothelial cells from mouse aorta had reduced motility as compared to wild type, suggesting AQP1 was needed to facilitate cell migration for angiogenesis. AQP1 is upregulated by angiogenic factors in response to hypoxia, and necessary for endothelial cell migration and angiogenesis. Therapies to block the transcriptional activation of AQP1 could prevent the angiogenesis in cancer. Treatment should be spatially limited to the tumor site without affecting normal cell functions.

EMT occurs in normal physiological conditions such as implantation, embryogenesis, and organ development, as well as pathological processes such as cancer invasion and metastasis. During EMT, polarized epithelial cells undergo biochemical changes to adopt a mesenchymal phenotype, characterized by a loss of cell polarity, reduced cell-cell adhesiveness, and enhanced invasive capacity.

Aquaporins such as AQP3 have been implicated in the EMT process. AQP3 up-regulation in response to Epidermal Growth Factor (EGF) in colorectal, gastric, and pancreatic cancers, is associated with augmented cell migration, invasion, and metastasis. In addition to AQP3, AQPs 1, 4, 5, and 9 also have been involved in EMT in different types of cancer cells (De leso and Yool, 2018).

For decades, cell migration has been proposed to be driven mainly by the cytoskeletons. Recent studies have found that osmotic water flow itself could be the driving force for cell migration. The model proposed can be summarized as follows: 1) the depolymerization of cytoskeletal actin; 2) the ions influx and the increase osmolality at the front end of the cell; 3) the osmotically driven water influx into the cell through AQPs, polarized to the front end; 4) the increase local hydrostatic pressure that causes cell membrane expansion, which forms a protrusion; 5) cytoskeletal actin re-polymerizes to stabilize the emerging protrusion (Morishita et al., 2019).

Cell migration is achieved through a repeated process of polarization, protrusion of the leading edge, cell-Extracellular Matrix (ECM) adhesion, ECM degradation and retraction of the rear part (De leso and Yool, 2018).

Numerous studies have focused on the involvement of AQP1, AQP3, AQP4, AQP5, AQP7 and AQP9 in cell migration. Furthermore, AQP1, AQP4, AQP5, and AQP9 have been reported to localize to the leading-edge during migration (Morishita et al., 2019). This distribution of AQPs would enable localized water influx and subsequent volume gain, contributing to the protrusion of the leading-edge (Morishita et al., 2019). Protrusions adhere to the ECM using integrin to generate "traction" for cellular movement. AQP2 might modulate turnover of integrin to the adhesion sites, enabling forward cellular movement (De leso and Yool, 2018).

Extracellular matrix degradation widens the pathways through which cells can penetrate the tissues and reduces the distortion of the rounded cell body necessary for physical progress. AQP1, AQP3, AQP4 and AQP9 have been shown to interact with specific metalloproteinases (MMPs) to facilitate ECM degradation and invasion (De leso and Yool, 2018).

The final step in the cycle of cell movement is retraction of the trailing-edge. In this model, the role of AQP channels is to facilitate osmotic water efflux in response to K^+ efflux, presumably in parallel with electroneutral efflux of Cl^- ions (Figure 7).

It is well known that cancer cells are frequently characterized by increased levels of ROS related to a constitutive activation of growth factor pathways to sustain cellular growth and proliferation, in comparison to their normal counterparts (Moloney and Cotter, 2017). The high ROS at intracellular level, detected in various cancer types, has been shown to have several roles, for example, the activation of pro-tumorigenic signaling, the increasing cell survival and proliferation, and the DNA damage and genetic instability (Moloney and Cotter, 2017). The discovery of some AQPs, permeable to H_2O_2, is an evidence for their functional involvement in cancer progression, proliferation and metastasis. In this context, AQPs represent new and promising anticancer targets, since the channel-mediated membrane transport permits the fine adjustment of H_2O_2 levels in cell compartments, allowing it to function as a signal molecule (Bienert and Chaumont, 2014).

Figure 7 - Key contributions of aquaporins in cell migration

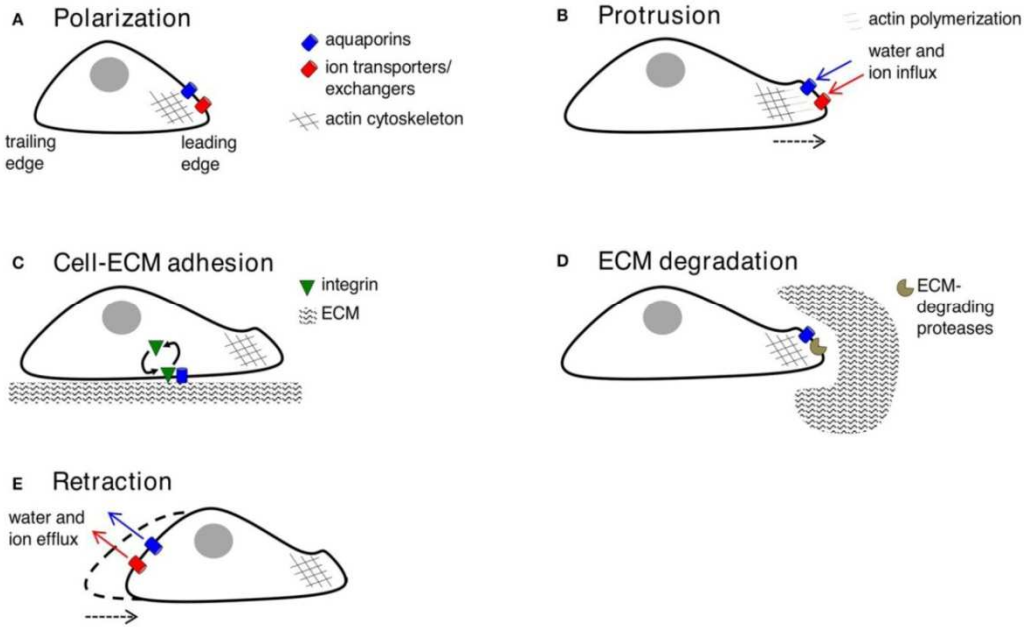

(A) Forward movement is preceded by establishing specialized loci within the cell, with redistribution of aquaporins, ion transporters/exchangers, and actin polymerization machinery to the leading edge. AQP-1,–4,–5, or–9 can be found on leading edges of migrating cancer cells. (B) Protrusions of the membrane might use water influx (down an osmotic gradient established by ion transporters/exchangers) and actin polymerization beneath the plasma membrane to dynamically push the membrane forward. AQP-1,–4, and–5 are implicated in water influx for protrusion extension in cancer cells; AQPs-1 and–4 also appear to interact with actin cytoskeleton. (C) Protrusions adhere to the ECM using integrin to generate "traction" for cellular movement. AQP2 might modulate turnover of integrin at adhesion sites, enabling forward cellular movement. (D) ECM degradation by enzymes can widen gaps through which the cell body can penetrate. AQP-1,–3,–4 and–9 are suggested to interact with ECM-degrading enzymes. (E) The final step is retraction of the cell trailing edge, thought to use aquaporins for water efflux following by K+ export. (De leso and Yool, 2018).

AQPs and Diseases: Aquaporinopathies

AQPs are expressed ubiquitously and have implications for a myriad of human diseases. Data from knockout mice support the involvement of AQPs in epithelial fluid secretion, cell migration, hypertension, brain oedema, epilepsy, adipocyte metabolism, lung injury and bronchoreactivity, which suggests that modulation of AQP function or expression could have therapeutic potential in nephrology, oncology, dermatology, ophthalmology, pulmonary area and in the treatment of obesity (Verkman et al., 2014; Krane et al., 2001).
Moreover, loss-of-function mutations in human AQPs cause pathologies, called aquaporinopathies. They include congenital cataracts, caused by AQP0 mutation; nephrogenic diabetes insipidus, caused by AQP2 mutation and neuromyelitis optica, an autoimmune neuroinflammatory disease caused by anti-AQP4 antibodies (Verkman, 2012).

Congenital cataract in mice and in humans is characterized by a loss of AQP0. The primary functions of AQP0 in the lens may be in cell–cell adhesion of lens fibers and in the regulation of gap junction channels, rather than in water transport (Verkman et al., 2014).

Non-X-linked nephrogenic diabetes insipidus (NDI) can be determined by mutations in AQP2. In the recessive mechanism a mutant AQP2 protein causes defective cellular processing and/or function, while in the dominant mechanism the mutant AQP2 prevents plasma membrane targeting of wild-type AQP2. NDI caused by AQP2 mutation is characterized by severe polyuria and polydipsia that are refractory to antidiuretic hormone (Verkman, 2012).

AQP4 is involved in neuromyelitis optica (NMO), a neuroinflammatory demyelinating disease. NMO affects optic nerve and spinal cord, causing blindness and paralysis, and has characteristic pathological and clinical features that distinguish it from multiple sclerosis. The defining feature in NMO is the presence of serum autoantibodies (NMO-IgG) directed against extracellular epitopes on AQP4. It is thought that IgG binding to AQP4 in astrocytes initiates an inflammatory cascade involving recruitment of leukocytes, cytokine release, and complement and NK cell–mediated astrocyte damage. The consequent neuroinflammation and myelin loss produce neurological deficits (Verkman, 2012).

Current NMO therapies are directed toward the possibility to use monoclonal antibodies targeting AQP4-IgG and blocking the binding to AQP4, which is the starting event in NMO disease. The recombinant monoclonal antibody named aquaporumab binds AQP4 and competes sterically with AQP4-IgG and, above all, it acts limiting the cytotoxic effect. Another potential therapeutic approach is to reduce the expression of AQP4 on astrocytes, upregulating complement inhibitor proteins or reducing the entry of AQP4-IgG into the central nervous system (Verkman, 2012).
Unfortunately, there are little useful information about the roles of AQP1, AQP3 or AQP7 in humans because human deficiencies of these AQPs are rare and phenotypes are really variable (Verkman, 2012).

AQPs and Oxidative Stress

Oxidative stress is a phenomenon caused by an imbalance between production and accumulation of reactive oxygen species (ROS) in cells and tissues and the inability of a biological system to detoxify these reactive products (Pizzino et al., 2017).
Mitochondria are the major source of ROS in cells, as consequence of active oxidative metabolism.
Superoxide anions, hydroxyl radicals, and hydrogen peroxide are the predominant forms of ROS (Huang et al., 2019).
ROS are generated from both endogenous and exogenous sources. Immune cell activation, inflammation, ischemia, infection, cancer, excessive exercise, mental stress, and aging produce endogenous free radicals. Exogenous free radical production can occur as a result from exposure to environmental pollutants, heavy metals (Cd, Hg, Pb, Fe, and As), certain drugs (cyclosporine, tacrolimus, gentamycin, and bleomycin), chemical solvents, cooking (smoked meat, used oil, and fat), cigarette smoke, alcohol, and radiations (Pizzino et al., 2017).
Hydrogen peroxide (H_2O_2) is the most abundant and stable ROS in living cells and can have a different effect, depending on its concentration. Physiological levels of ROS ("oxidative eustress") induce positive adaptive responses, while excessive levels ("oxidative distress") provoke negative effects (Sies, 2017; Sies et al., 2017).
Throughout the years, ROS have been considered to enter cells by freely diffusion through the cell membrane lipid bilayer and not via specific transporters or channels. This has been questioned since the discovery of the new membrane transport function of some AQPs, named peroxiporins (Tamma et al., 2018). H_2O_2 size and chemical and

physicochemical properties are similar to those of water (Bienert and Chaumont, 2014), which may suggest H_2O_2 passage through channel membrane proteins such as AQPs.
Many recent studies have demonstrated the H_2O_2 permeability of AQP3 (Hara-Chikuma et al., 2016; Thiagarajah et al., 2017), AQP5 (Rodrigues et al., 2019), AQP8 (Medraño-Fernandez et al., 2016), AQP9 (Watanabe et al., 2016) and AQP11 (Bestetti et al., 2020).
Since AQPs allow the diffusion of H_2O_2 across plasma membranes to the extracellular fluid, they have been considered as a possible ROS scavenging pathway (Bienert and Chaumont, 2014). Moreover, this scavenger role is corroborated by the expression of AQP8 and AQP11 in intracellular structures, involved in ROS production. AQP8 is expressed in the inner mitochondrial membrane of several mammalian tissues (Soria et al., 2010) and AQP11 is expressed in the endoplasmic reticulum membrane (Bestetti et al., 2020).
Numerous studies have shown that oxidative stress can be responsible, with varying degrees of importance, for the onset and/or progression of different diseases such as cancer, metabolic disorders, rheumatoid arthritis, atherosclerosis and cardiovascular, neurological, reproductive, respiratory, renal diseases (Pizzino et al., 2017).
In conclusion, the study of peroxiporins roles in these pathological conditions could be useful to prevent or treat them.

Objective of the thesis

In all cells, H_2O_2, the most abundant and stable ROS can act as signaling molecule or induce oxidative damage, depending on its concentration. Recently, the H_2O_2 diffusion from producing cells across plasma membranes to the extracellular fluid has been considered an important ROS scavenging possibility, mediated by some AQPs (Bienert and Chaumont, 2014).

This thesis has three different purposes:

1) to study the possible effect of HPV infection on both expression and function of AQPs in human sperm cells of patients undergoing infertility couple evaluation;

2) to clarify the involvement of AQPs (peroxiporins) in the aggressiveness and progression, as well as in its resistance to conventional chemotherapy of malignant pleural mesothelioma;

3) the identification and characterization of new aquaporin modulators capable to counteract the oxidative stress.

On the one hand, these studies will help us to understand the molecular mechanisms underlying the reduced sperm fertility caused by HPV infection and the aggressiveness and chemoresistance of mesothelioma.
On the other hand, the identification of new synthetized compounds capable to modify the permeability of AQPs and to control the ROS cellular content suggests a novel mechanism to regulate cell signaling and survival during stress and to manipulate key signaling pathways in cancer and degenerative diseases.

1st Research Plan:

Peroxiporins in Human Spermatozoa Infected by HPV

1. Introduction

AQPs in Spermatozoa

Fluid homeostasis is recognized as a critical factor during the development, maturation, and function of vertebrate male germ cells (Boj et al., 2015a). In both mammalian and teleost spermatozoa, osmotic changes associated with water and ion fluxes are vital for the activation of motility and subsequent natural fertilization. In mammals, physiological hypotonicity can facilitate the acrosome reaction in the sperm through calcium increase and acrosome swelling; this hypotonic stress is required for the activation of sperm motility once released from the epididymis. Similarly, in freshwater and marine teleosts, activation of motility is induced, respectively, by the hypo or hyperosmotic aquatic environment into which the sperm are ejaculated (Boj et al., 2015a). These processes have been associated with the presence of aquaporins in spermatozoa of both vertebrate groups.

Marine teleost's sperm cells

In the sperm of gilthead seabream (*Sparus aurata*), Aqp1aa is distributed along the entire flagellum and many sperm motility assay experiments have demonstrated that Aqp1aa is the channel mediating the water efflux during the hyperosmotic shock, which activates flagellar motility (Zilli et al., 2009; Boj et al., 2015b).

Aqp8bb, distributed along the anterior flagellum of gilthead seabream's sperm and in vesicles surrounding the nucleus, is rapidly phosphorylated and inserted into the inner membrane of the single spermatozoon mitochondrion upon seawater activation (Chauvigné et al., 2013). In addition to water, Aqp8bb, as many aquaporin paralogs, can transport H_2O_2 (Almasalmeh et al., 2014). Chauvigné et al. (Chauvigné et al., 2015) demonstrated that H_2O_2 accumulated in the mitochondria due to the hyperosmotic stress, was transported out of this compartment through Aqp8bb. Thus, Aqp8bb operates as a mitochondrial peroxiporin to allow the efflux of accumulated H_2O_2 thereby maintaining the mitochondrial membrane potential and the production of ATP needed

for the maintenance of flagellar motility (Chauvigné et al., 2015). These findings indicated that mitochondrial Aqp8bb plays an essential role in ameliorating oxidative damage by ROS in activated sperm in order to preserve flagellar motility under hypertonic conditions.

In addition to Aqp1aa and -8bb, the seabream's spermatozoa also show spatial segregation of Aqp7 in the head and of Aqp1ab and -10b in both the head and the anterior tail (Chauvigné et al., 2013). Upon sperm activation all of them are translocated to the head plasma membrane and they are involved in pattern control of sperm motion (Chauvigné et al., 2013) (Figure 8).

Mammals sperm cells

Mammalian spermatozoa consist of a head, neck, and tail.

The head contains the nucleus, which is surrounded by the cytoskeletal structures and a thin cytoplasm. The nucleus is characterized by a highly condensed chromatin and its shape is species-specific. The anterior tip of the nucleus is covered by the acrosome, which contains hydrolytic enzymes necessary for the penetration of sperm into the oocyte during fertilization. The spermatozoon flagellum is divided into four distinct segments: the connecting, middle, principal, and end pieces. In the middle piece there is the mitochondrial sheath surrounding the axoneme that spans the whole length of the flagellum (Boj et al., 2015a).

To date, four AQPs were found in mammalian spermatozoa: AQP3, AQP7, AQP8 and AQP11.

AQP3 is present in human spermatozoa and it is considered essential for their physiology and function. AQP3 is expressed in the tail membrane and when it is not expressed the spermatozoa exhibits alterations in volume regulation and excessive cell swelling in the female reproductive tract (Carrageta et al., 2020). In mouse, AQP3 was also identified in the midpiece of spermatozoa. In AQP3 null mice, sperm cells show normal motility but an impaired migration capacity into the oviduct, resulting in a reduced male fertility (Chen et al., 2011).

The localization of AQP7 in human spermatozoa is debated in the literature. Saito et al. identified AQP7 in the tail (Saito et al., 2004), Moretti et al. in the tail and midpiece (Moretti et al., 2012), while Laforenza et al. reported the presence of AQP7 only in the head (Laforenza et al., 2016b).

In fact, the different localization or even the absence of AQP7 in human spermatozoa are correlated with abnormal morphology and decreased progressive motility (Moretti et al., 2012; Laforenza et al., 2016b).

On the contrary, in the work of Yeung and coworkers, the expression of AQP8 was expressed in all of semen's donors and it was not correlated with motility. More specifically, the AQP8 was observed in the tail and in the midpiece (Yeung et al., 2010). The localization of AQP8 in the midpiece was confirmed by Laforenza et al. (2016b). An intense immunoreactivity was showed in the midpiece of the spermatozoa, apparently in the mitochondria and in 2% of sperms in the plasma membrane in the proximity of midpiece (Laforenza et al., 2016b) (Figure 8).

As mature spermatozoa exhibit an increased mitochondrial activity, and thus high reactive oxygen species and hydrogen peroxide production (Dias et al., 2014), it was postulated that AQP8 is essential to facilitate their efflux and minimize the oxidative stress damage (Laforenza et al., 2016b).

AQP11 was identified in the tail and sometimes in intracellular structures in human spermatozoa (Laforenza et al., 2016b). These findings are similar to previous observation in rodents (Yeung and Copper, 2010). Finally, it has been speculated that AQP11 may be involved in the end stage of the cytoplasm and organelle elimination process occurring during sperm maturation (Yeung and Copper, 2010).

Figure 8 - Aquaporins localization in spermatozoa

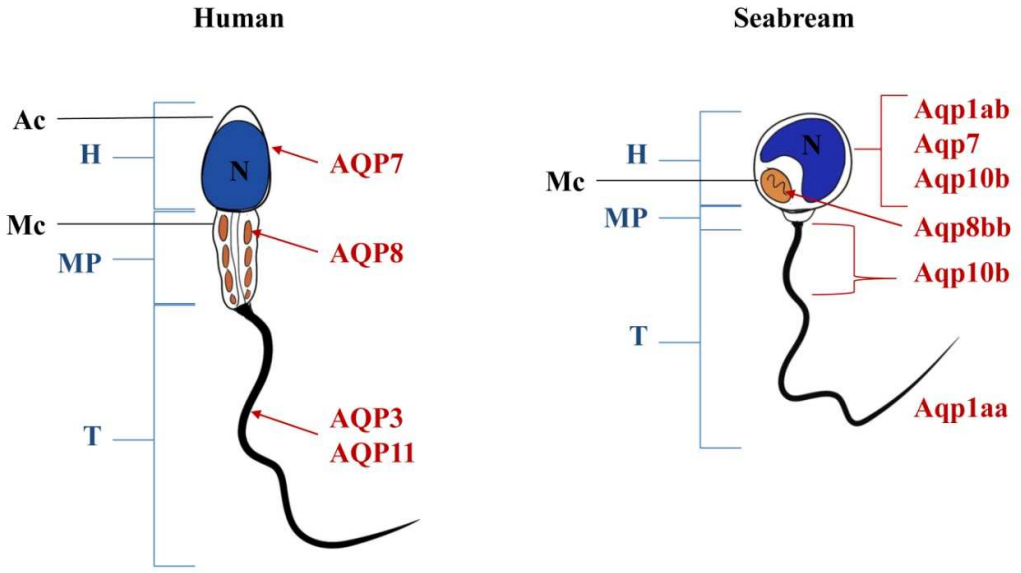

The diagram shows the differential localization of distinct aquaporin paralogs in human motile sperm and gilthead seabream activated sperm. Ac, Acrosome; Mc, mitochondria (in orange); ; N, nucleus (in blu); H, head; MP, midpiece; T, tail. (Modified with WACOM intuos by Boj et al., 2015a).

Oxidative Stress in human spermatozoa

Multiple evidence demonstrate that spermatozoa are generators of reactive oxygen species (ROS) because of the fundamental role of these molecules in the induction of sperm capacitation (Aitken and Drevet, 2020). Sperm capacitation refers to the physiological changes which spermatozoa must undergo in order to penetrate and fertilize an oocyte. These physiological changes are related to low ROS levels and include acrosome reaction, hyperactivated motility, sperm fertilizing potential and mitochondria functioning in the mid-piece which generates energy for the flagellar beat and thus sperm motility (de Lamirande and Gagnon, 1993).

On the contrary, elevated levels of ROS were found in the seminal plasma in 30%–40% of infertile subjects (Lanzafame et al., 2009). High levels of ROS determine negative effects in spermatozoa such as decreased viability, decreased motility and increased midpiece sperm morphological defects (Aitken and Drevet, 2020).

Seminal ROS originate from a variety of different endogenous and exogenous sources. Endogenous ROS are generated by spermatozoa themselves, by other cellular contaminants such as immature round germ cells, leukocytes and epithelial cells. Exogenous ROS derived from modern lifestyle and environmental factors, as an overheating of the testes, varicocele, pollutants, smoke and drugs (Aitken and Drevet, 2020; Nowicka-Bauer and Nixon, 2020).

The role of AQPs in male infertility

Sperm motility, number and morphology are the main physiological factors required for normal male fertility. Among the many factors that may compromise fertility, oxidative stress plays an important role. Reduced AQP-mediated H_2O_2 permeability may lead to an impaired efflux of ROS from sperm cells, a reduced detoxification mechanism and a loss in sperm functionality (Laforenza et al., 2016b).

Laforenza and coworkers found that the osmotic water permeability of human ejaculated semen is significantly correlated both with sperm number and progressive motility, suggesting a direct involvement of AQPs in sperm concentration and functionality (Figure 9).

They observed a decreased water permeability in stressed (H_2O_2 treatment) normospermic spermatozoa, but this decrease was not observed in stressed sub-fertile spermatozoa, suggesting a previous inhibition of the channel permeability induced by

elevated levels of H_2O_2 in sub-fertiles. They also demonstrated that AQPs are involved in both water and H_2O_2 permeation by showing the inhibitory effect of $HgCl_2$, a known water channel inhibitor. The reduction of H_2O_2 and water transport by oxidative stress suggests the existence of a new mechanism that regulates cell signaling and survival during stress. Unfortunately, the inability to perform gene silencing of individual AQPs in human sperm does not allow identifying the AQPs responsible for H_2O_2 permeation.

Human Papillomavirus (HPV) infection and infertility risk

Human Papillomaviruses (HPVs) comprise a highly diverse group of non-enveloped DNA viruses. HPV is one of the most common sexually transmitted viruses in both males and females worldwide (Lyu et al., 2017). Commonly, HPV infects mucosal genital epithelia, with an estimated 75% of humans being affected (Pérez-Andino et al., 2009).

Over 170 types of HPV have been identified and among those, at least 40 types can infect the anogenital region (Lyu et al., 2017). A subset of high-risk types (HPV-16, -18, -26, -31, -33, -35, -39, -45, -51, -52, -53, -56, -58, -59, -66, -68, -70, -73, -82, and -85) have been proved to cause neoplasms at different sites, such as cervical, vulva, vagina and anus, while low-risk types (HPV-6, -11, -40, -42, -43, -44, -54, -61, -70, -72, -81) mainly result in benign papilloma or no clinical symptoms (Lyu et al., 2017). On the contrary in males, the HPV-related cancers at penile, anal, and oropharynx sites is rare (Giuliano et al., 2015), because of the absence of dividing cells in sperm.

In addition, HPV is also responsible for a substantial part of idiopathic subfertility, but this is greatly underestimated because the dissociation between *HPV viruses* and *HPV virions* remains difficult for clinicians as well as for HPV detection (Depuydt et al., 2016).

In fact, HPVs are organisms that pass in their ontogenetic cycle through two distinct phenotypic phases: the *virions* (infectious particles) and the *viruses* (infected dividing cells) (Depuydt et al., 2016).

When the detected viral HPV DNA originates from a dividing cell, the detected HPV DNA is never infectious (dividing cells do not support virion production) and does not affect fertility, but the viral DNA can transform the dividing cell it resides in, which could in time lead to pre-cancer and cancer (Depuydt et al., 2016).

On the contrary, when the detected viral HPV DNA originates from non-dividing differentiated cells or from free *virions*, it is infectious and exerts its deleterious effects through weakening or incapacitating the cells it resides in (Depuydt et al., 2016).

To confirm this deleterious effect, a meta-analysis of case-control studies has revealed a significant association between seminal HPV infection and male infertility (Lyu et al., 2017). HPV infection can exerts its detrimental effects in different ways through its virions. Firstly, HPV virions may lead to a significant impairment of sperm parameters (e.g. concentration, morphology, and pH), especially a reduction in sperm motility, thereby affecting male fertility (Foresta et al., 2015). Lai et al. first reported the lower performance of curvilinear velocity, straight-line velocity and mean amplitude of lateral head displacement in HPV-infected sperm (Lai et al., 1997). These findings were confirmed by others (Foresta et al., 2010a; Garolla et al., 2012; Yang et al., 2013; Foresta et al., 2010b). Secondly, HPV infection is considered a risk factor for anti-sperm antibodies (ASAs) which may reduce male fertility by interfering with sperm motility and sperm-oocyte binding, and by mediating the release of cytokines that can impair sperm function (Garolla et al., 2013). Finally, HPV infection might affect the integrity of sperm DNA. Some researchers found DNA strand breakages in spermatozoa exposed to HPV E6/ E7 fragments (Connelly et al., 2001), others did not find HPV to induce sperm DNA damage (Garolla et al., 2012; Kaspersen et al., 2013). As some HPV types are more oncogenic than others, an HPV type specific effect on spermatozoa cannot be ruled out.

Whether or not human sperms express a specific receptor for HPV is not known, but Pérez-Andino et al. (Pérez-Andino et al., 2009) demonstrated that HPV-16 capsids adsorb to distinct sites on the sperm head surface at the equatorial segment, suggesting that these sites may mediate HPV binding. The presence of two distinct sites along the equator of the spermatozoa's heads was also showed in other studies (Garolla et al., 2013; Kaspersen et al., 2011).

Over the years several studies tried to wash off HPV DNA from sperm without success (Chan et al., 1994; Brossfield et al., 1999; Garolla et al., 2012), suggesting either a very strong binding of the virion to a receptor on the sperm cell surface or an entrance of HPV into the sperm cell.

In conclusion, literature data about HPV effect on fertility are still controversial, incomplete and the mechanism by which HPV could affect sperm motility is still unknown. Likewise, the exact HPV localization in the different components of semen as well as the role of infected sperm cells as transmission vectors for the virus are still unclear.

HPV needs oxidative stress to complete its life cycle

The genome of HPV is composed by three regions: the long control region (LCR), the early region and the late region.

The early region encodes E1, E2, E4, E5, E6 and E7 protein. E1 and E2 are involved in viral DNA replication, E4 permits the virions release collapsing the cytokeratin and E5-E7 are oncogenes that lead to cell immortalization and transformation. The late region encodes two proteins, L1 and L2, that compose the viral capsid (Cruz-Gregorio et al., 2018). Several evidence from past studies indicate that HR-HPV proteins are associated with oxidative stress.

The early viral proteins are involved in the production and modulation of oxidative stress (Cruz-Gregorio et al., 2018). In particular, E2 can bind some inner mitochondrial membrane proteins changing the mitochondrial cristae morphology and increasing the release of ROS. E5 is not directly associated in modulation of ROS, but this protein permits the replication of HPV stimulating the degradation of a pro-apoptotic cellular protein. A spliced E6 protein seems to decrease the levels of antioxidant cellular proteins. In addition, the combined expression E6/E7 induces overexpression of NADPH oxidase 2 (NOX2) that increase ROS levels, while E7 can confer protection against apoptosis induced by H_2O_2.

On the other side, late viral proteins need an oxidative environment to auto-assemble and build the viral capsid (Cruz-Gregorio et al., 2018).

The viral capsid is composed by 80% L1 and by 20% L2. Five units of L1 auto-assemble with each other to form an L1 pentamer. In the hollow of each L1 pentamer, an L2 protein is located, forming a complex that is called capsomere. The HPV capsid has 72 capsomeres arranged in an icosahedral structure (Li et al., 2016).

When OS surpasses the antioxidant barrier in HR-HPV-infected cells, cellular DNA becomes susceptible to rupture, probably contributing to the viral integration process.

So, the integration of the HR-HPV genome into the cellular genome is a necessary step in HR-HPV-induced carcinogenesis (Cruz-Gregorio et al., 2018).

Gender-neutral HPV vaccination

Until now there are three different types of HPV vaccines approved by the European Medicines Agency (EMA) and US Food and Drug Administration (FDA): Gardasil/Silgard, Gardasil 9 and Cervarix. The first one is active against HPV-16, -18, -6, -11, Gardasil 9 is also active against HPV-31, -33, -45, -52, -58, while Cervarix is only active against HPV-16 and -18. All three vaccinations are approved for use in boys and girls aged 9 and above and are administered in either 2–3 doses (Hintze and O'Neill, 2018).

Most countries currently only supply vaccination to females.

In 2013, Australia became the first country to start gender-neutral HPV vaccination. This was followed by USA while Austria became the first European country in 2014 (Hintze and O'Neill, 2018) and Italy in 2017.

Recent data about gender-neutral vaccination point towards both a personal benefit as well as a cost-effective population-based benefit. Data from female vaccination only have shown the vaccine to be effective in preventing premalignant cervical lesions and are believed to have the same effect for other human papillomavirus cancers. Male vaccination not only provides personal benefit but also has a “herd effect” for females by preventing the propagation of the virus (Hintze and O'Neill, 2018). In addition, a recent study showed that prophylactic HPV vaccination in men improves the clearance of HPV semen infection (Foresta et al., 2015a).

In conclusion gender-neutral vaccination provides significant cost-effective benefits for preventing human papillomavirus related diseases, and this effect is further enhanced by the use of the nonavalent vaccine (Hintze and O'Neill, 2018).

2. Objectives

This study aims to elucidate whether HPV infection could damage spermatozoa by impairing AQP functioning.

Human ejaculated spermatozoa divided in normospermic and sub-fertile both HPV-infected and non-infected samples have been analyzed to study:

1) the possible changes of AQP3, AQP7 and AQP8 protein expression by ELISA;

2) the water permeability features measured by a stopped-flow light scattering method;

3) the interaction between the AQPs and the HPV capsid protein L1 by confocal fluorescence microscope and co-immunoprecipitation;

4) protein modelling and docking simulations.

3. Materials and Methods

Sperm Samples

Ninety-four male partners were recruited from infertile couples undergoing infertility evaluation at the Center for Reproductive Medicine, Fondazione IRCCS Policlinico San Matteo (University of Pavia, Pavia, Italy) after informed consent. The consent form was specifically designed for processing of the excess of semen volume collected for diagnostic analysis, in accordance with the Declaration of Helsinki, and with our local Ethical Committee guidelines on the use of residual biological material for research purposes. Each male produced the semen by masturbation after an abstinence of 2–7 days and semen samples were collected in a sterile plastic container confirmed to be non-toxic for spermatozoa. A routine semen analysis was performed within 1 h of collection, according to the methods described by the World Health Organization (WHO) (World Health Organization, 2010). The system used for grading motility distinguishes spermatozoa with progressive (PR) or non-progressive (NP) motility from those that are immotile, as reported by the WHO manual (parameters for normospermic patients: PR+NP ≥ 40%; PR ≥ 32%) (World Health Organization, 2010). Samples were divided into two groups on the basis of their characteristics: group 1–67 were from subjects defined normospermic based on the following parameters: number of spermatozoa ≥ $15x10^6$/ml, progressive spermatozoa ≥ 32% and physiological viability ≥ 58%); group 2–27 were from patients defined sub-fertile with at least one of the principal basal seminal parameters compromised (number of spermatozoa <15x106/ml or PR<32%). In the present study, physiological morphology was not considered a parameter for discriminating between the two groups.

Routine Sperm Analysis

Macroscopic analysis

Samples were incubated at 37°C until the analysis was performed. The analysis to assess volume, pH, fluidification and viscosity was started 45 minutes from semen collection.

Determination of spermatozoa count and motility

Each semen sample was assessed for sperm motility and kinematics of movement using a disposable counting chamber (Counting Chamber Makler, Sefi Medical Instruments,

Israel). Sperm count was performed from undiluted specimens. The grid was on a glass cover. The number of spermatozoa counted in any strip of 10 squares of the grid indicated their concentration in millions/ml. No additional factors were necessary for the calculation. At least 3 strips were counted and the median value was considered. The chamber has a depth of 10 microns that eliminates blurring and allows sperm to move freely. The applied sample was observed in one focal plane. The motility of each spermatozoon was graded as follows: progressive motility (PR) (spermatozoa moving actively); non-progressive motility (NP) (all other patterns of motility with an absence of progression); immotility (no movement) (World Health Organization, 2010).

Determination of sperm morphology

To determine sperm morphology, each sample was analyzed by using Diff-Quik-stained slides (Test Simplets, Origio, Denmark). Restricted criteria by Kruger as indicated by the WHO manual were used to analyze at least 200 spermatozoa per sample (World Health Organization, 2010).

Determination of sperm viability

Samples were assessed for sperm viability by staining with 1% Eosin-Y in saline (VitalScreen, FertiPro N.V., Belgium). Briefly, 50 µl semen samples were mixed with 2 drops of 1 % Eosin-Y in a sterile test tube and a drop of semen-stain mixture was placed on a microscope slide. The smear was covered with a glass cover before the smear was dry and was read immediately under the microscope. At least 200 spermatozoa were counted and classified as stained (dead) or unstained (viable).

HPV-DNA Detection and Typing

DNA extraction was performed on sperm samples (100–300 µL) using an automatic instrument (Maxwell MDX16, Promega Italia srl, Milan, Italy) based on paramagnetic particles. 10 µL of the solution were used for PCR amplification of HPV sequences from the L1 region using SPF10 primers in a final reaction volume of 50 µL for 40 cycles. Positive and negative controls were introduced in each set of 12 reactions, including DNA from Siha and HeLa cell lines at a specified number of HPV copies, and blank reagents throughout all steps of the procedure. Concurrent amplification of human HLA-DPB1 gene was included in the assay as internal control for DNA adequacy. HPV type-specific sequences were detected by the line probe, INNO-LiPA HPV genotyping CE

assay, version INNOLIPA HPV GENOTYPING EXTRA II (Fujirebio Italia S.r.l., Italy), according to the manufacturer's instructions. The EXTRA version of the assay allows the simultaneous and separate detection of 32 HPV types: 13 high-risk HPV types (HR; 16, 18, 31, 33, 35, 39, 45, 51, 52, 56, 58, 59 and 68), 6 intermediate-risk HPV types (IR; 26, 53, 66, 70, 73 and 82), of 9 low-risk HPV types (LR; 6, 11, 40, 42, 43, 44, 54, 61 and 81), and 4 unclassified HPV types (62, 67, 83, and 89). Hybridization patterns were automatically analyzed by the LiRAS system and checked by two independent readers.

Indirect ELISA (Enzyme-linked Immunosorbent assay)

Human sperm samples were diluted in PBS and centrifuged at 1000x g for 10 min. The cell pellets were resuspended with a solution containing: 250 mM sucrose, 1 mM EDTA, 10 mM Tris-HCl, pH 7.6, 0.1 mg/mL PMSF, 100 mM β-mercaptoethanol and Protease Inhibitor Cocktail (P8340, Sigma-Aldrich S.r.l., Milan, Italy) and diluted in 300-700 µl of PBS.

Polystyrene 96-well plates (MICROTEST TM Tissue Culture Plate, 96 Well, Becton Dickinson Labware) were coated with 50 µl of semen sample and incubated for 24h at 4 °C. The total protein content of semen sample was determined with the Bradford method (Bradford, 1976) using bovine serum albumin as standard.

The plate was washed three times with PBS and then incubated with 3% BSA in PBS for 1h at room temperature to block the free protein binding sites. The plate was washed three times with PBS-T (0,1% Tween in PBS) between all the following stages. All samples were evaluated in duplicate for AQP3-7-8 and β-2-microglobulin as loading control. The plate was incubated overnight at 4 °C with anti-AQP3 rabbit polyclonal IgG (sc-20811, 1:500; Santa Cruz Biotechnology, Inc., Heidelberg, Germany), anti-AQP7 rabbit polyclonal IgG (sc-28625, 1:500; Santa Cruz Biotechnology, Inc.), anti-AQP8 rabbit polyclonal IgG affinity pure (AQP8-A, 1:500; Alpha Diagnostics Intl. Inc., San Antonio, TX, USA), RabMAb anti β-2-microglobulin antibody ((EP2978Y) ab75853, 1:10000; Abcam). The following day the plate was first incubated for 1 h at room temperature with biotinylated link universal and then with HRP-conjugated streptavidin (DAKO LSAB + System-HRP, K0690, Dako North America, CA, USA), diluted 1: 2000 in PBS-T.

o-phenylenediamine dihydrochloride (OPD powder, 25 g, Thermo scientific, Rockford, USA) was used as chromogen at a concentration of 1 mg/mL in 50 mM citric acid/sodium phosphate buffer pH 5.0 with hydrogen peroxide (30% H2O2 1 µl/mL). The plate was incubated at room temperature with the chromogen in the dark and after

enough color development the reaction was stopped with 3 N HCl. The absorbance of each well was recorded at 490 nm as measurement wavelength and 655 nm as reference wavelength using a microplate reader (Microplate Reader model 680, BioRad, Richmond, CA, USA).

The aquaporins protein content was expressed in absorbance/mg protein by the ratio between the absorbance for milliliter of semen sample and the total protein content expressed in mg/ml.

Water Permeability Measurements

Osmotic water permeability of human sperm samples was measured by a stopped-flow light-scattering method as previously described (Laforenza et al., 2016b; Laforenza et al., 2013). Briefly, the experiments were carried out at room temperature on a stopped flow apparatus (RX2000, Applied Photophysics, Leatherhead, UK) with a pneumatic drive accessory (DA.1, Applied Photophysics) coupled with a Varian Cary 50 spectrometer (Varian Australia Pty Ltd., Mulgrave, Australia). Scattered light intensity with a dead time of 6 ms was recorded at a wavelength of 450 nm. The time course of cell swelling caused by exposure to the hypotonic gradient (150 mOsm/L) was measured at the acquisition rate of one reading/0.0125 s. Cells behaved as perfect osmometers, the gradient determined an osmotic water entry, cell swelling, and decreased light scattering.

The initial rate constant of sperm cells volume changes (k) was obtained by fitting the time course of light-scattering with a one phase exponential decay (GraphPad Prism 4.00, 2003). The water permeability coefficient, *Pf*, was calculated as previously described by Wiener et al. (1989), from the following equation:

$$Pf = k \cdot \frac{V_0}{\Delta C} \cdot V_w \cdot A$$

where ΔC is the osmotic gradient, V_w the molar water volume, V_0 the cell volume and A the cell surface area. Vo and A were obtained by Curry et al. (1996). Water transport was evaluated in sperm cells from normospermic and sub-fertile subjects, with or without HPV infection, following exposure to hypoosmotic medium (150 mOsm osmotic gradient).

Immunofluorescence

Immunolocalization of AQP3, 7, 8, and HPV was evaluated in human sperm samples, which were smeared on polylysine-coated slides, air dried and fixed in 4% paraformaldehyde in PBS for 30 min, and then washed with PBS. Antigen retrieval was performed by placing the slides in a Coplin jar containing retrieval buffer (0.05% tween-20, 10 mM citrate-HCl buffer, pH 6.0) and microwaving at high power level. When the solution started to boil (5 min) the oven was turned off. Two more cycles were repeated, and the jar was left at room temperature allowing slides to cool for at least 20 min. After washing with PBS, the slides were then blocked with 3% BSA in PBS at room temperature for 30 min. Double labeling experiments were performed by incubating the slides overnight (in the cold) with affinity pure anti-AQP3 or AQP7 or AQP8 primary antibodies (Anti-AQP3, SAB5200111, Sigma-Aldrich, USA; Anti-AQP7, ab191063, Abcam, UK; Anti-AQP8, ab133667, Abcam, UK) and with a prediluted mouse monoclonal anti-HPV antibody ([K1H8] ab75574; Abcam, UK) that recognizes the major capsid L1 protein of the following HPV types: 6, 11, 16, 18, 31, 33, 42, 51, 52, 56, 58. In some experiments, other Anti-AQP8 and anti-HPV were used: Anti-AQP8 rabbit polyclonal IgG affinity pure (AQP8-A, 1:500; Alpha Diagnostics Intl. Inc., San Antonio, TX, USA) and Anti-HPV Type 16 L1 Monoclonal Antibody (CAMVIR-1; catalog # MA1-34821; Invitrogen, Life Technologies, Italia). Anti-AQP antibodies were used at the following dilutions in antibody diluent (DakoCytomation, Milan, Italy): AQP3, 1:300; AQP7 1:250; AQP8 1:250. After three 5 min washes with PBS, slides were incubated at room temperature with the fluorescent secondary antibody (ab150117, 1:400, Abcam, Cambridge, UK) and rhodamine red –X-conjugated affinity pure goat anti-rabbit IgG (H+L) (1:50 dilution; 111-295-045; Jackson ImmunoResearch Europe Ltd., Cambridge, UK) for 30 min. Slides were then washed 3 × 5 min with PBS, mounted in ProLong® Gold antifade reagent with 40,6-Diamidino-2-Phenylindole (DAPI; Molecular Probes) and examined with a TCS SP5 II confocal microscopy system (Leica Microsystems) equipped with a DM IRBE inverted microscope (Leica Microsystems). Images were visualized and analyzed by LAS AF software (Leica Microsystems Application Suite Advanced Fluorescence). Control experiments were performed simultaneously using non-immune serum.

Co-Immunoprecipitation Assay

Co-immunoprecipitation (Co-IP) of AQP8 and HPV L1 protein was performed using Capturem IP & Co-IP Kit (Cat. No. 635721; Takara Bio Europe), according to the manufacturer's instructions. Briefly, sperm cells were pelleted, resuspended in 400 µL of lysis buffer and 4 µL of protease inhibitors, and left on ice for 15 min. Cells were centrifuged at 17,000× g for 10 min at 4 °C and the supernatant (OS) was removed and kept. Protein content in the supernatant was measured as described below and 600 µg of protein lysate was incubated with 30 µL of anti- HPV Type 16 L1 Monoclonal Antibody (CAMVIR-1) for 20 min at room temperature (r.t.) with end-over-end rotation. The equilibrated spin column was loaded with the lysate and centrifuged at 1000× g for 1 min at r.t. The sample flow through (FT) was collected and 100 µL of wash buffer added to the column (the solution was kept; W). After centrifuging at 1000× g for a minute at r.t., 6 µL of Tris 1 M pH 8.0 were added to the collection tube and 60 µL Elution Buffer was added to the column and centrifuged again. Finally, the eluted solution (E) was collected for immunoblotting analysis.

Immunoblotting

Samples were heated at 80 °C in Leammli buffer (Laemmli, 1970) and loaded (30 µg OS, FT and 30 µL W and E) on Mini-PROTEAN TGX/TGX Stain-Free precast Gels 4-20 (Cat. #456-8094, Bio-Rad). Gels were transferred onto PVDF membrane (Trans-Blot Turbo Transfer Pack, #1704156, Bio-Rad Laboratories S.r.l., Italy) using Trans-Blot Turbo Transfer System (#1704150, Bio-Rad Laboratories S.r.l., Italy). Blots were blocked for 1 h with a solution containing 5% skimmed dry milk, 0.1% Tween in TBS and then incubated overnight with the recombinant Anti-AQP8 antibody (ab133667, Abcam) or the anti-HPV Type 16 L1 Monoclonal Antibody (CAMVIR-1; Invitrogen), diluted 1:750 and 1:300, respectively. The membranes were washed thrice with 0.1% tween-20 in TBS and incubated for 1 h with peroxidase-conjugated goat anti-rabbit or rabbit anti-mouse IgG diluted 1:100000 in 0.1% tween-20 in TBS. After washing, the bands were detected using the Westar Supernova (Cyanagen s.r.l. Italy). Pre-stained molecular weight markers (ab116028, Abcam) were utilized to calculate the band molecular weights. Blots were acquired using iBrightTM CL1000 Western Blot Imaging Systems (Invitrogen).

Protein Content

The protein content was determined with the Bradford method (Bradford, 1976) using bovine serum albumin as standard.

Protein Modelling and Docking Simulations

AQP8 was modelled using the I-Tasser server (Zhang, 2008) and the tetramer was generated by Z Dock (Pierce et al., 2014). The resulting model was then used to test interaction modes of AQP8 with the L1 pentamer (PDB ID: 1DZL) by the ROSIE server (Moretti et al., 2018). The resulting one thousand interaction models were manually evaluated; a lipid-embedded AQP8 model, generated by the CHARMM-GUI interface (http://www.charmm-gui.org/) was used as a reference to filter out the 987 interaction modes clashing with the lipid bilayer. The remaining 17 poses were ranked according to ROSIE total energy score. The best scoring model was visualized by Pymol (The PyMOL Molecular Graphics System, Version 2.0 Schrödinger, LLC) and analyzed by PISA (Krissinel and Henrick, 2007).

Statistics

All data were expressed as mean ± S.E.M. or S.D. (Table of semen parameters). The significance of the differences of the means was evaluated by using one-way ANOVA followed by Newman Keuls's Q test or Student's t test. To evaluate the significance of the differences of the means of the semen morphology parameters and of the osmotic water permeability, the Kruskal–Wallis test followed by Dunn's multiple comparison test was used. All statistical tests were carried out using GraphPad Prism 4.00, 2003 (GraphPad Software, La Jolla, CA, USA).

4. Results

Semen characteristics in normospermic and sub-fertile subjects with and without HPV Infection

The semen characteristics of all subjects included in the study, either normospermic (n = 67) or sub-fertile (n = 27), who attended the clinic because of infertility, are showed in Table **4**. Sperm concentration, progressive and total motility, and motile sperm count were all dramatically reduced in sub-fertile patients compared with normospermic subjects as previously shown by Laforenza et al. (2016b). No differences in the parameters were observed in the sperm from either normospermic or sub-fertile, non-infected, and HPV-infected subjects.

Table 4 - Semen parameters of normospermic and sub-fertile patients with (+ HPV) and without HPV (- HPV) infection

Semen Parameters	Normospermic HPV- (*n* = 35)	Normospermic HPV+ (*n* = 32)	Subfertile HPV- (*n* = 12)	Subfertile HPV+ (*n* = 15)
Semen volume (mL)	4.35 ± 1.69	3.69 ± 1.18	4.07 ± 0.99	4.21 ± 1.98
Sperm concentration (mil/ mL)	71.78 ± 50.50	80.61 ± 51.47	23.01 [a] ± 24.30	21.84 [a] ± 23.94
Progressive motility (PR%)	55.54 ± 13.02	54.41 ± 13.13	29.58 [a] ± 11.31	25.47 [a] ± 12.89
Motile sperm count (mil/mL)	42.85 ± 35.93	48.86 ± 34.05	5.94 [a] ± 6.62	5.86 [a] ± 6.47
Non-progressive motility (NP%)	8.69 ± 5.32	7.19 ± 3.51	9.33 ± 3.47	11.40 [b] ± 6.20
Total motility (PR%+NP%)	64.23 ± 11.43	61.59 ± 12.79	38.92 [a] ± 12.33	36.87 [a] ± 13.79
Morphology (% normal)	2..37 ± 1.77	2.70 ± 1.86	1.33 [c] ± 2.15	0.80 [d] ± 1.21

HPV-DNA detection and typing

HPV typing of human sperm samples was done by SFP10-LIPA, a robust and sensitive method for the simultaneous detection of several HPV types. Results showed that 47 out of 94 sperm samples were HPV-infected: it was possible to identify the type in only 36 samples, whereas in 11 samples the types were unidentifiable by the test. Multiple HPV types were detected in 7 samples. Twenty-five samples were infected with HR, 6 with IR, 5 with LR and 2 with unclassified HPV types. The most common HR type was HPV 16 (n = 17) followed by HPV 31 and HPV 52 (n = 3), HPV 18 (n = 2) and HPV45, 51, 56 (n.1). Three IR HPV types were found: HPV 53 (n = 3), HPV 73 (n = 2) and HPV 66 (n = 1). The most common LR type was HPV 6 (n = 4) followed by HPV 44 and 81 (n = 1). HPV 67 and 89 (n = 1) were found as unclassified HPV types.

Effect of HPV-infection on AQP3, AQP7 and AQP8 protein expression in sperm from normospermic and sub-fertile subjects

The changes of AQP3, AQP7 and AQP8 proteins expression were analyzed by indirect ELISA. in human ejaculated semen from normospermic and sub-fertile subjects with and without HPV infection

Preliminary experiments were performed to test the optimal conditions. In particular, experiments were conducted with sperm samples resuspended in lysis buffers with or without detergent. Moreover, in other experiments the AQPs expression values were normalized to the housekeeping beta-2-microglobulin. No differences were observed when detergent was added nor when values were normalized to the housekeeping (Data not showed).

The results showed that HPV-infection modified sperm AQPs expression (Figure 10). AQP3 and AQP7 expression values were significantly higher in HPV-negative sub-fertile subjects than in HPV-positive sub-fertile subjects and HPV-negative normospermic subjects (Figure 10A, 10B). AQP8 expression of HPV-negative normospermic subjects and of HPV-positive sub-fertile subjects were lower than HPV-negative sub-fertile subjects and HPV-positive normospermic subjects ($p < 0.05$, Figure 10C). In order to understand if there was a relationship between AQP protein expression and progressive motility of human ejaculated semen, the normalized expression values obtained by indirect ELISA were been plotted with the progressive motility of sperms from both

normospermic and sub-fertile HPV-positive subjects. Results showed a significant correlation for AQP8 expression (Figure 11C), but not for AQP3 and AQP7 expression (Figure 11A, 11B).

Figure 10 - AQP3, AQP7, AQP8 proteins expression changes in human ejaculated semen from normospermic and sub-fertile subjects with and without HPV infection

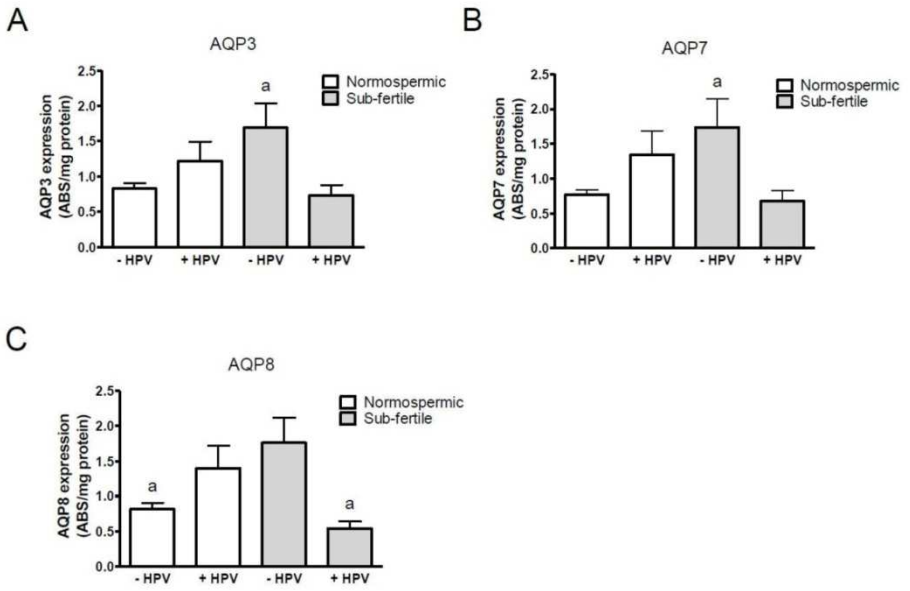

(A, B, C) The AQP3, AQP7 and AQP8 expression was assayed by indirect ELISA as described in methods and the values normalized to total protein content. Each column represents means ± SEM of 5-21 different subjects. + HPV, HPV-positive subjects; -HPV, HPV-negative subjects. AQP3 and AQP7: a, P < 0.05 vs. +HPV sub-fertile, -HPV normospermic. AQP8: a, P<0.05 vs. -HPV sub-fertile, +HPV normospermic.

Figure 11 - Relationship between the AQP3, AQP7, AQP8 protein expression assayed by indirect ELISA and the progressive motility of human ejaculated semen from HPV-positive subjects both normospermic and sub-fertile.

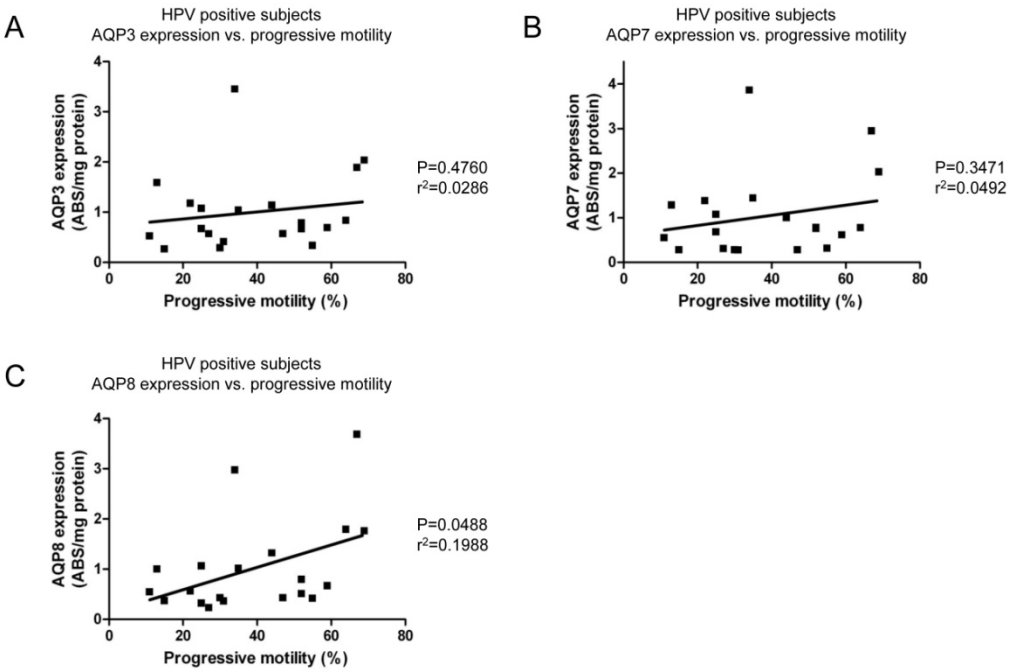

Overall linear regression (black line) is presented. P and r^2 values are shown.

Osmotic water permeability of human spermatozoa from normospermic and sub-fertile subjects with and without HPV infection

Sperm cells act as functional osmometers displaying a rapid swelling when exposed to a hypotonic medium (Figure 12B-E). The resulting scattered light intensity decay could be fitted by a single exponential decay function to calculate the initial rate constant k.

To test whether HPV infection was able to inhibit AQPs function, we measured the osmotic permeability of human sperm cells from both normospermic and sub-fertile subjects with and without HPV infection. Figure 12A shows that in subjects without HPV infection, the osmotic permeability of sperm cells from the sub-fertile group was lower than that of the normospermics, as previously demonstrated (Laforenza et al. 2016). Interestingly, the osmotic permeability of sperm cells from the HPV-infected subjects both normospermic and sub-fertile was reduced by 53% and 63% respectively compared to that of non-infected normospermic subjects. Given that the normospermic HPV-positive subjects had a reduced sperm osmotic permeability despite semen parameters in the normal range, it has been hypothesized that HPV infection could damage semen parameters over time. To test this hypothesis, the parameters of the subjects who were re-evaluated after more than 4 months were been compared with their initial parameters: there was a significant reduction only in sperm number (69.34 ± 13.1 vs. 49.2 ± 8.5; $p = 0.0171$, Student's t test for paired data).

Figure 12 -. Osmotic water permeability of human ejaculated semen from normospermic (1) and sub-fertile (2) subjects with (+HPV) and without (-HPV) HPV infection

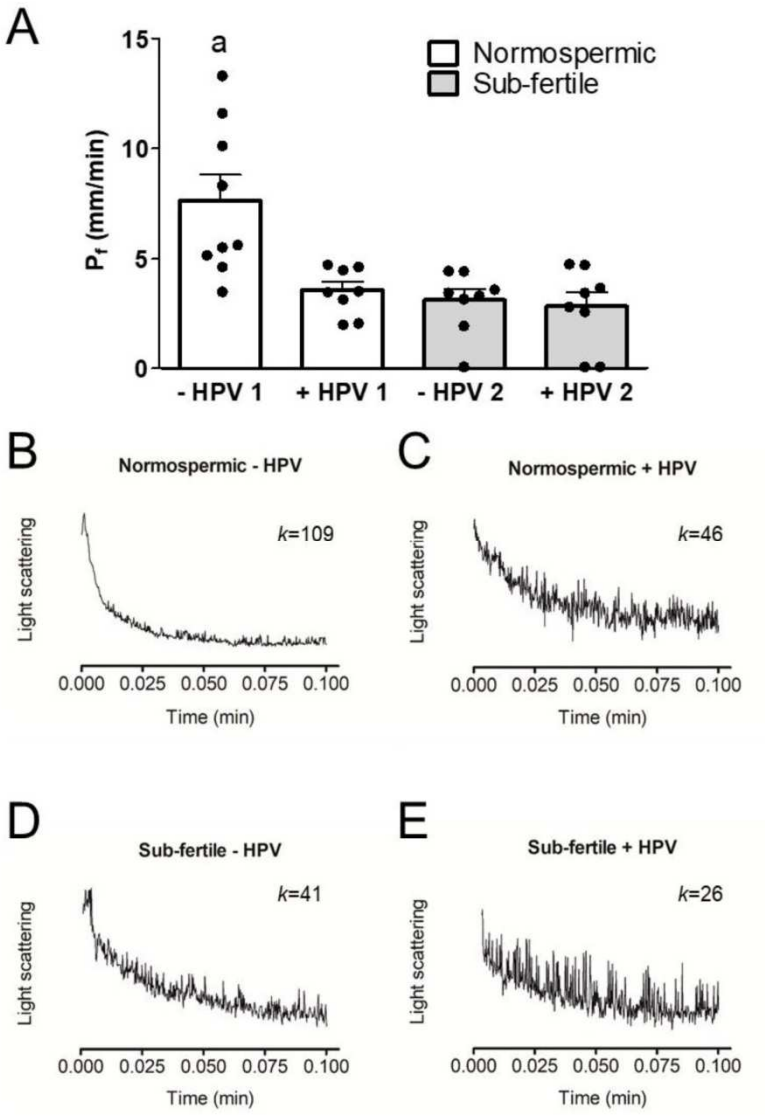

The osmotic water permeability was measured by exposing sperm cells to a 150 mOsm osmotic gradient and expressed as Pf (see Materials and methods). (A) Bars represent means ±SEM of 4–15 single shots for each of 8–10 different experiments; the individual data points are also shown (bullet point). a, $p < 0.05$ vs. normospermic HPV-positive, sub-fertile HPV-negative and sub-fertile HPV-positive (Kruskal–Wallis followed by Dunn's Multiple Comparison Test). (B–E) Representative traces of stopped-flow osmotic water permeability measurements obtained from ejaculated semen of normospermic (B,C) and sub-fertile (D,E) subjects with (C,E) and without (B,D) HPV. K relative values of single curves are also shown.

Immunolocalization of AQP3, 7, 8, and HPV evaluated in human HPV-Infected Semen

HPV localization was determined to verify its possible interaction with AQP3, AQP7, and AQP8. To this end, colocalization experiments were performed. Double label immunofluorescence showed that HPV and AQP8 proteins colocalized in the midpiece of the spermatozoa, as per the resulting yellow fluorescence in merged images (Figure 13A) of HPV (green; Figure 13B), AQP8 (red; Figure 13C) and Nuclei stained with DAPI (Figure 13D). Colocalization graphs showed the overlap of the fluorescence signals originated from HPV (green) and from AQP8 (red) labeling (Figure 13E).

Colocalization of AQP8 and L1 proteins was quantified using Pearson's correlation coefficients and intensity profile plots by LAS AF software (Leica Microsystems Application Suite Advanced Fluorescence). Image analysis revealed a Pearson's correlation coefficient of 0.612 (Figure 14). Figure 14 shows a representative colocalization analysis with the distribution scatter plot (A), the image with colocalized pixels highlighted in white (B) and the overall colocalization values obtained from the representative analysis (C). Finally, Pearson's coefficient R values obtained from colocalization experiments of L1 protein with AQP8 showed a statistically significant difference with those obtained with AQP3 and AQP7 (Figure 14D).

In contrast, AQP3 and AQP7 staining did not show any overlap of the fluorescence signal with HPV, as per the absence of yellow fluorescence in merged images of AQP3 and 7 (red) and HPV (green) (Figure 15A, B). In some experiments, a different antibody that specifically detects the L1 protein of HPV 16 (see Materials and Methods) was used. The results confirmed a colocalization of L1 with AQP8, but not with AQP3 and AQP7. Control experiments were performed simultaneously using non-immune serum which did not show any labeling (Figure 15C).

Figure 13 - Representative immunofluorescence confocal microscopy images of colocalization of AQP8 and HPV in human sperm

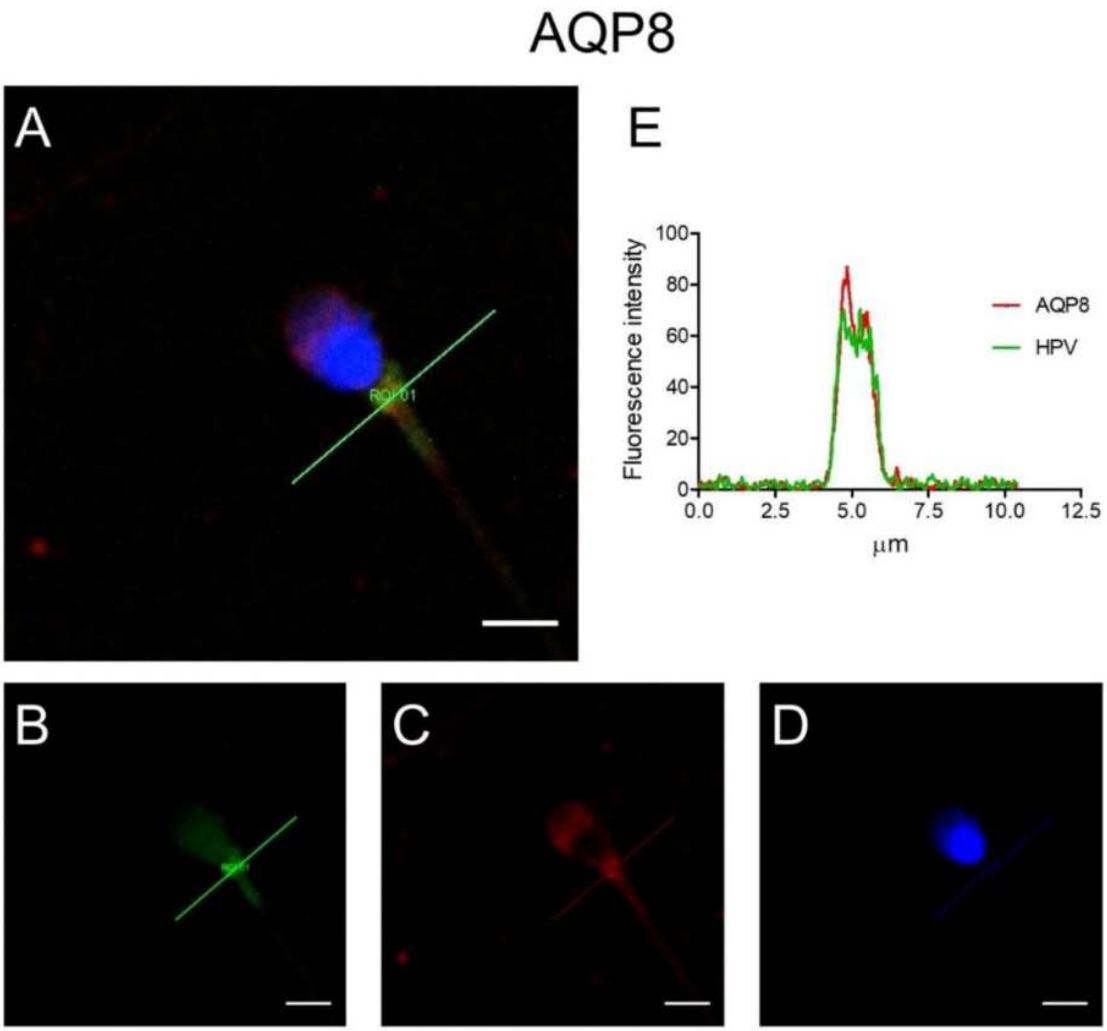

(A) Green labeling indicates the presence of HPV, red labeling the expression of AQP8, while nuclei were counterstained by DAPI (blue). Yellow labeling shows colocalization signal of AQP8 with HPV. Scale bar, 5 m. (B–D) Images show single labeling for HPV (green; B), AQP8 (red; C) and nuclei (DAPI; D). (E) Colocalization graphs, measured in the green line position in panel A, showing the overlap of the fluorescence signals originated by AQP8 and HPV staining.

Figure 14 - Representative colocalization analysis using the Leica LAS-AF image system

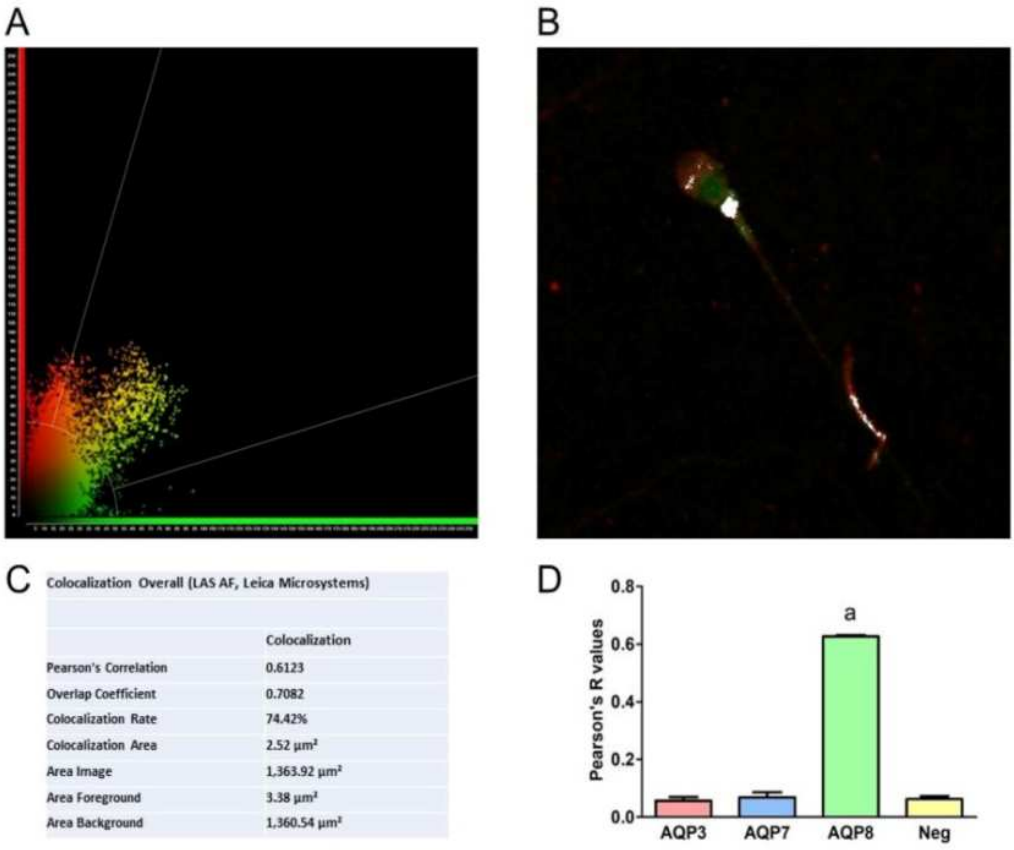

(A) Pixels distribution scatter plot: colocalized yellow pixels between the two diagonals, red (AQP8) pixels in ordinate and green (HPV) pixels in abscissa. (B) Leica LAS-AF software generates an image of colocalized pixels, highlighted in white, superimposed on an RGB-merge of two channels. (C) Overall colocalization values obtained from the representative colocalization analysis using the Leica LAS-AF image analysis of Pearson's coefficient R values was obtained from at least 6 different double immunofluorescence experiments with anti-HPV antibody and anti-AQP3, AQP7, or AQP8 antibodies. Negative controls (Neg) were also analyzed. a, $p < 0.0001$ vs. AQP3, AQP7 and Neg (ANOVA, followed by Newman–Keuls's Q test).

Figure 15 - Representative immunofluorescence confocal microscopy images of AQP3, AQP7, and HPV in human sperm

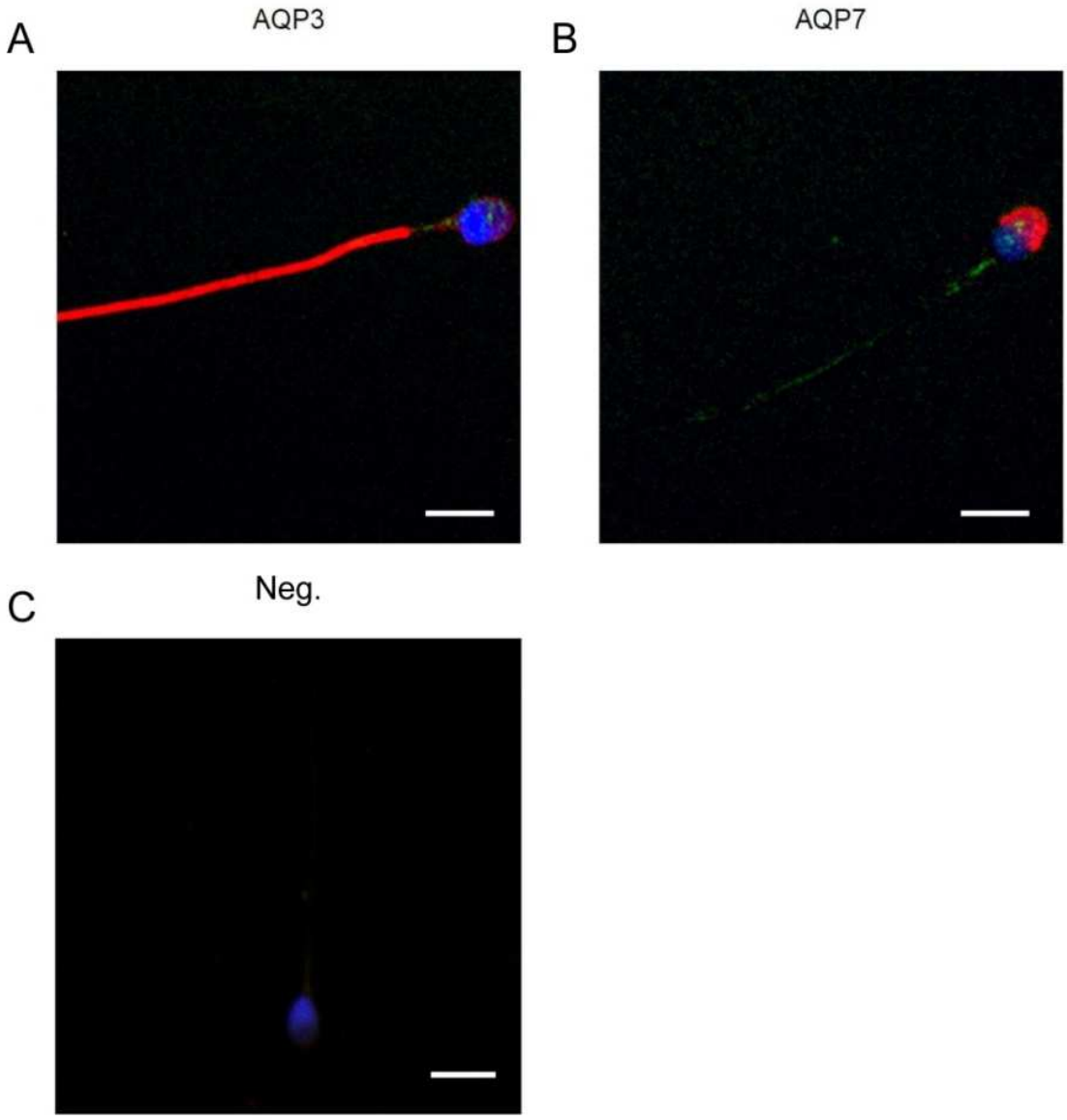

(A,B) Green labeling indicates the presence of HPV, red labeling the expression of AQP3 or AQP7, while nuclei were counterstained by DAPI (blue). Merged pictures are shown. No colocalization (no yellow signal) was observed for either AQP3 or 7 and HPV. Scale bar, 5 µm. (C) Immunofluorescence negative control. No or faint staining was observed when anti-aquaporins and anti-HPV antibodies were substituted with preimmune serum. Nuclei were counterstained by DAPI (blue). Scale bar, 10 µm.

Co-Immunoprecipitation of AQP8 and L1 Protein

To confirm the AQP8 and L1 protein interaction, we performed co-immunoprecipitation with anti-L1 protein antibody followed by western blot. L1 protein pull-down resulted in the co-immunoprecipitation of AQP8 (Figure 16A). Bands of the predicted molecular size were observed for both AQP and L1 protein in the original sample, in the FT and in the elution. No immunoreactive bands in the elution were observed when co-immunoprecipitation was performed in HPV-negative sperm cells lysates (Figure 16B) or without anti-L1 protein antibody (Figure 16C).

Figure 16 - Co-immunoprecipitation of AQP8 and HPV L1 proteins in human sperm cells

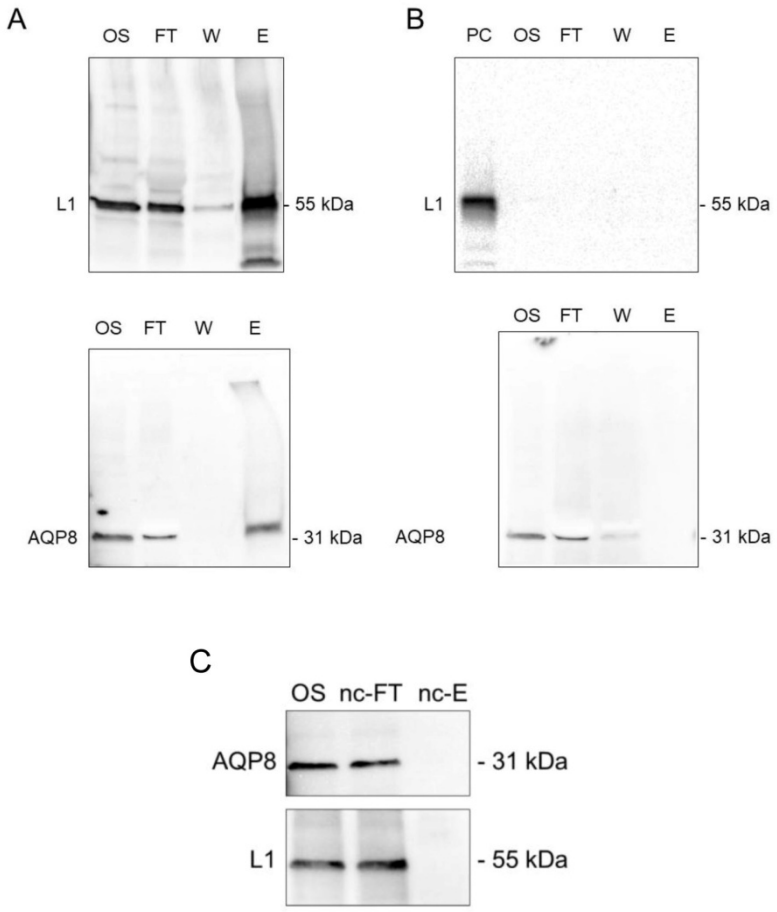

(A) The sperm cell lysates of HPV16 infected subjects were subjected to co-immunoprecipitation with a HPV L1 specific antibody; protein expression of both AQP8 and L1 was detected by immunoblotting with anti-AQP8 and with anti-HPV antibodies as indicated in Materials and methods. (B) As negative control, HPV-negative sperm cells lysates were incubated with the anti-HPV antibody. Major bands of AQP8 and L1 proteins were shown. (C) Negative control of co-immunoprecipitation of AQP8 and HPV L1 proteins in human sperm cells. As negative control (nc), lysates were incubated without the anti-HPV antibody. Major bands of AQP8 and L1 proteins were shown. OS, original sample; FT, flow-through; W, wash; E, elution, PC, positive control.

Protein Modeling and Docking Simulations

Given the experimental evidence of colocalization between AQP8 and HPV L1, a potential molecular interaction mode has been tested by molecular modelling and docking. A model for AQP8 was generated by I-Tasser; the top scoring model (C-score 0.85) was used as a base for tetramer generation by Z-Dock. The tetramer assembly with the highest similarity to available AQP structures was used for further analysis. Pentameric L1 docking onto AQP8 by ROSIE was followed by manual selection of the 1000 generated models versus a lipid-embedded AQ8 tetramer to exclude docking poses clashing with the lipid membrane. Seventeen models passed this selection criterium. The top ranking pose (total energy score: –1045.287) showed an interaction mode where the L1 pentamer is located on top of the AQP8 tetramer (Figure 17C). The interaction, however, occurs through a single L1 monomer and it especially involves the L1 extended lateral domain h4 (Chen et al., 2020) (Figure 17B). Notably, the L1 h4 helix is the point of contact between different pentamers in the HPV capsid (Chen et al., 2020). Such interaction is hydrophobic and involves a long loop. It has been proposed that the L1 h4 is a highly flexible adjustable unit (Chen et al., 2020), which therefore might adapt its conformation to bind multiple AQP8 tetramers (Figure 17D). In AQP8, the interacting surface spans two adjacent monomers (Figure 17A and B).

Figure 17 - Cartoon representation of AQP8 model and L1 interaction

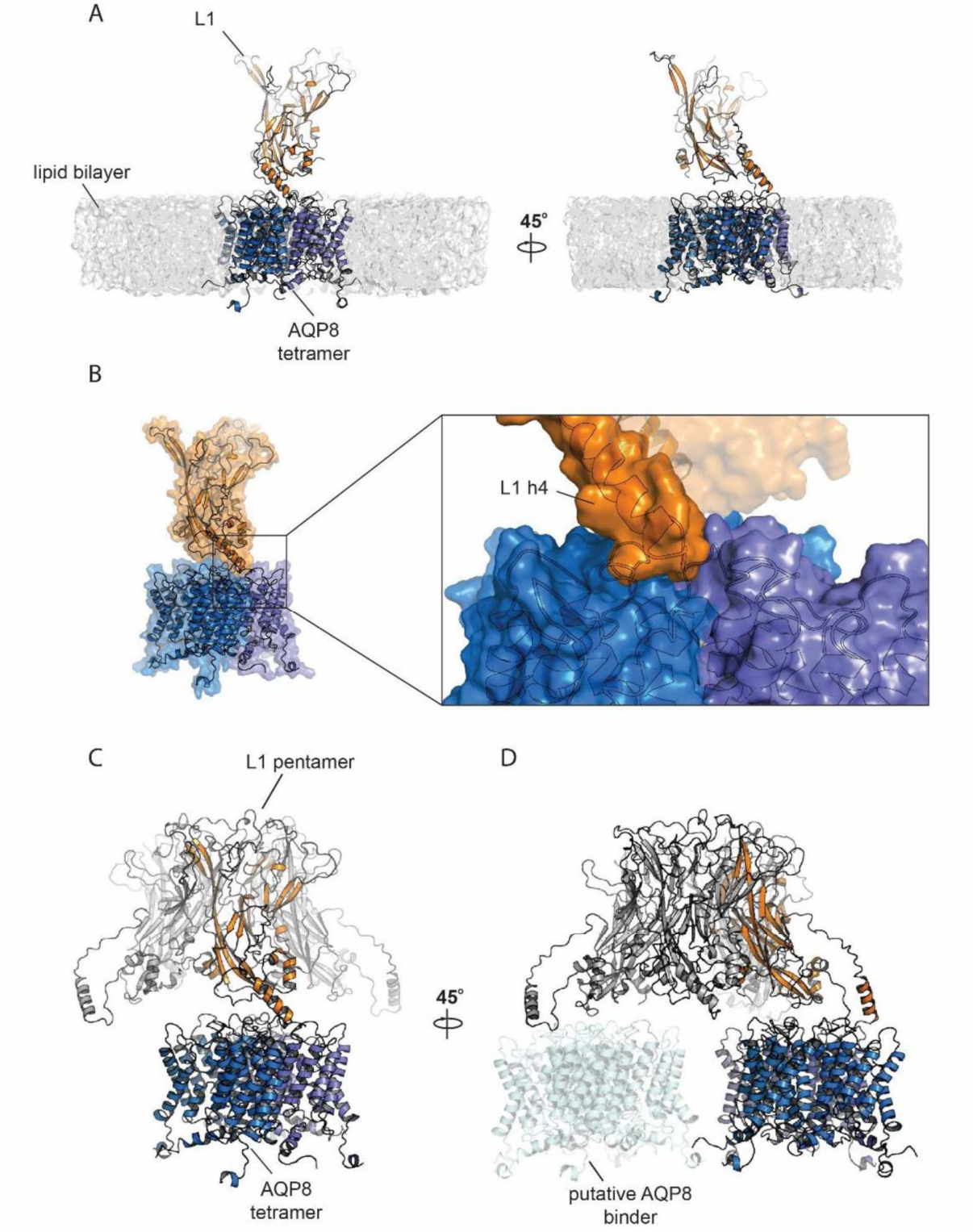

(A) AQP8 model (each monomer is colored in a different shade of blue) and L1 (orange) interaction represented in the presence of a lipid bilayer. (B) Surface representation of L1:AQP8 complex. In the box, the magnification of the interaction surface where one AQP8 monomer interacts with the L1 extended h4 helix domain. (C) Pentameric L1 used for docking simulations. (D) Possible interaction of the L1 pentamer with multiple AQP8 tetramers.

5. Discussion

The importance of fluid homeostasis during the development, maturation, and function of spermatozoa has been associated with the presence of aquaporins in spermatozoa (Boj et al., 2015a). In particular, human spermatozoa express four different AQPs: AQP3, AQP7, AQP8, AQP11. In addition to water, AQP3 and AQP8 have been proven to possess H_2O_2 transport capacity (Hara-Chikuma et al., 2016; Thiagarajah et al., 2017; Medraño-Fernandez et al., 2016) and so these AQPs are involved in ROS elimination. A low concentration of ROS is essential to sperm capacitation and mitochondria functioning related to motility (de Lamirande and Gagnon, 1993). On the contrary, elevated concentration of ROS, due to an impaired efflux from spermatozoa, lead to a loss in sperm functionality (Laforenza et al., 2016b).

Several evidence from past studies indicate that HPV needs an oxidative stress environment to complete its life cycle, in fact HR-HPV proteins are associated with oxidative stress (Cruz-Gregorio et al., 2018). The early viral proteins are involved in the production and modulation of oxidative stress, while late viral proteins need an oxidative environment to auto-assemble the viral capsid (Cruz-Gregorio et al., 2018). In this context, AQPs-mediated H_2O_2 efflux to the extracellular fluid can be considered a fundamental ROS removal system, especially in an oxidative stress status (Sies, 2017).

The first aim of this study was to elucidate the possible effect of HPV infection on AQPs expression and functioning. Results of ELISA experiments show similar expression changes for AQP3, 7 and 8 even though only for AQP8 the differences were significant. Sperms from HPV-negative sub-fertile subjects and HPV-positive normospermic subjects have higher AQPs expression compared to those from HPV-negative normospermic subjects and from HPV-positive sub-fertile subjects (Figure 10). This may suggest that normospermic subjects in the early stages of HPV infection react by increasing the expression of AQPs, especially AQP8, probably to compensate for the functional inhibition of AQPs (especially the H_2O_2 scavenging), which seems to be HPV mediated (Figure 12). Probably, at a later stage of infection (sub-fertile patients) AQPs expression decreases, becoming similar to that of normospermic HPV-negative subjects. Sub-fertile HPV-positive subjects have a normal expression of AQPs, functionally inhibited by HPV. In turn, the altered function of AQPs, especially in the response to oxidative stress, could compromise sperm functionality (current results and Laforenza et al., 2016b). Interestingly, ELISA experiments showed a significant relationship

between AQP8 protein expression and progressive motility of human ejaculated semen from normospermic and sub-fertile HPV-positive subjects (Figure 11C).

However, the reduction of the progressive motility previously reported in HPV-positive subjects (Lai et al., 1997; Foresta et al., 2010) was confirmed in this study only for sub-fertile, but not for normospermic, HPV-positive subjects (Table 4). This could explain the reason why other authors did not observe any alteration in motility in HPV-infected subjects (Brossfield et al., 1999). The comparison of semen parameters in the four groups showed a significant decreased morphology score in sub-fertile men infected with HPV compared with the normospermic HPV-positive and -negative subjects (Table 4). Moreover, subfertile HPV-positive subjects showed an increase in non progressive motility compared to the normospermic HPV-positive (Table 4). The decrease of progressive motility with the relative increase of non progressive motility and the decreased morphology score in subfertile HPV-subjects were an evidence of the harmful effect of HPV on sperm functioning during long term infection.

Permeability studies with Stopped Flow Light Scattering were performed to verify the negative effect of HPV on AQPs functionality. Actually, water movement changes could be considered representative of an H_2O_2 flux variation (Medraño-Fernandez et al., 2016). The results showed that HPV reduced the water permeability in normospermic subjects but not in the subfertiles (Figure 12). These results evaluated the hypothesis that HPV infection influences AQP functioning making the sperm more sensitive to oxidative stress even in normospermic subjects. Moreover, the same permeability in subfertile HPV-negative and positive subjects suggested that AQP inhibition by HPV could negatively affects functional parameters over time, leading to sub-fertility. A future longitudinal study of sperm parameters variation in infected subjects could clarify this issue.

The third aim of this study was to clarify the possible interaction between AQPs and HPV in order to collect more information about AQPs functional inhibition. To do that a double label immunofluorescence and a 3D structural simulation analysis were performed. The results of the double label immunofluorescence showed that AQP8 and L1, the major capsid protein of HPV, were highly colocalized in sperm middle piece (Figure 13). HPV seems to interact only with AQP8 and not with AQP3 and AQP7. The effective interaction was confirmed by co-immonoprecipitation results (Figure 16). The immofluorecence and co-immunoprecipitation results suggest that the inhibitory effect of HPV infection on AQP-mediated water permeability (see Figure 12) might be due to a

direct interaction of HPV with the AQP8 pore. Unfortunately, the inability to perform gene silencing of individual AQPs in human sperm does not allow to claim that AQP8 is the only AQPs involved in the decrease of cellular permeability.

Recently, Chauvigné and collaborators, working on spermatozoa of oviparous marine teleost, demonstrated that H_2O_2 accumulated in the mitochondria due to the hyperosmotic stress, was transported out of this compartment through Aqp8bb, an orthologue of human AQP8. Inhibition of Aqp8bb led to an insufficient elimination of ROS and to a reduction of ATP synthesis which in turn caused a reduction of sperm motility leading to progressive arrest (Chauvigné et al., 2013; Chauvigné et al., 2015).

Taking into account that the results have been obtained on fish sperms, it may be possible that in humans the inhibition of AQP-mediated H_2O_2 efflux by HPV could impair sperm function and/or cell number. Unfortunately, in literature there are no conclusive data on the subcellular localization of AQP8 in human spermatozoa, so it is not possible to speculate that HPV inhibition reduces the elimination of H_2O_2 from the sperm cells or from their mitochondria.

However, according to molecular modelling and docking simulation results, HPV has an high probability to interfere with the permeability of AQP8, impairing sperm function. L1 protein seems to have a favorite site of interaction in the region located midway of two adjacent monomers of AQP8, with the potential, in its pentameric form, to bind to multiple pore copies (Figure 17). Depending on AQP8 localization, we might speculate that during the infection phase, the whole virus could interact with the AQP8 located on the external surface of the plasma membrane and, during intracellular replication, monomeric or pentameric L1 produced ex novo could form complexes with intracellular (mitochondrial) AQP8.

Obviously, AQPs are not the only target of HPV, but in this study they showed to have a key role in worsening the oxidative stress condition, which is favorable for the virus life cycle.

6. Conclusion

This study is the first one describing the harmful effect of HPV on human sperm cells AQPs. HPV infection of sperms affects both AQPs expression and functionality. Alterations in water and hydrogen peroxide diffusion capacity are related to a direct interaction of viral L1 protein with AQP8. Thus, data suggest that HPV reduces AQP8-mediated detoxification mechanism leading to sperm distress and sperm dysfunction.

Results obtained confirm the deleterious effect of HPV on male fertility, clarifying a possible target and a mechanism by which HPV infection alters sperm functioning. The importance and peculiarity of this study also lies in the fact that the results were obtained in naturally infected sperms. In fact, previous studies investigating were performed in vitro by treating human spermatozoa with L1 protein (Garolla et al., 2015).

2nd Research Plan:

Peroxiporins in Malignant Pleural Mesothelioma

1. Introduction

Malignant Pleural Mesothelioma

Malignant pleural mesothelioma (MPM) is an aggressive cancer of the pleural mesothelium and it is associated with previous asbestos exposure (Bibby et al., 2016). Estimated data on 2008 suggested an average of 14200 cases worldwide each year (Park et al., 2011). The highest incidence is in the USA and UK, but also rank highly in Australia and Italy and it is expected to peak between 2020 and 2025 (Carbone et al., 2019). Moreover, the migratory phenomena and the unregulated use of asbestos in countries lacking legislation on asbestos use such as India, Brazil and Russia will render MPM even more frequent (Bibby et al., 2016).

Pathogenesis

Most cases of MPM are caused by previous exposure to asbestos, which often occurs 40 years previously. MPM is classified as an occupational disease since asbestos exposure occurs mainly in the workplace. However, para-occupational exposure can occur, for example in the wives of asbestos workers who wash their clothes (Bibby et al., 2016).

Asbestos is a naturally occurring silicate mineral that has two different structural forms: the curly, serpentine fibers of chrysotile or "white" asbestos and the sharp, needle-like fibers of amphibole asbestos. The risk of developing MPM is related to the type of fiber, as well as to the heaviness and duration of exposure (Bibby et al., 2016). MPM can be also caused by erionite (a mineral found in the rocks of Turkey), chest wall radiation and simian virus 40.

The mechanism of carcinogenesis in MPM is multifactorial. Asbestos fibers are inhaled and migrate to the pleura. Fibers in the pleural space cause irritation and a repeated cycle of tissue damage and repair. Then, abnormal repair and intracellular DNA damage is provoked by the presence of oxygen free radicals, released by asbestos fibers when phagocytosed by macrophages (Sekido et al., 2013). In addition, DNA mutations and chromosome structure alterations are caused by asbestos fibers penetrated in mesothelial cells, where they interfere with mitosis. A favorable tumoral

microenvironment is created by inflammatory cytokines (tumour growth factor-β, platelet-derived growth factor and vascular endothelial growth factor) released by asbestos-exposed mesothelial cells (Sekido et al., 2013). Finally, asbestos induces the phosphorylation of various protein kinases (mitogen-activated protein and extracellular signal-regulated kinases 1 and 2), leading to increased expression of proto-oncogenes and further promotion of abnormal cellular proliferation (Robinson and Lake, 2005). Compared to many tumors, MPM has a low frequency of protein-altering mutations (~25 mutations per tumor) (Guo et al., 2015).

Prognosis

Prognosis with MPM is poor and median survival ranges from 8 to 14 months from diagnosis (Bibby et al., 2016). Women have a more favorable outlook than men, but due to the occupational nature of the disease there is a male predominance of 4:1 (Beckett et al., 2015).

There are three main histological sub-types: epithelioid, sarcomatoid and biphasic or mixed.

The epithelioid variant is the most common and it is associated with most favorable prognosis (median survival 14.4 months) (Verma et al., 2018). The epithelioid subtype can exhibit a range of morphologies, including solid (the most prevalent, 44%), tubulopapillary (29%), micropapillary (13%), tubular (7%), and trabecular (2%). Most epithelioid MPM contains more than one growth pattern. The solid type is associated with high-grade nuclear features as well as shorter median overall survival, while tubulopapillary and micropapillary have the longest overall survival (Krasinskas et al., 2016). In addition to growth pattern, nuclear grade, mitotic count, and necrosis have been found to predict survival in epithelioid MPM (Rosen et al., 2018).

The biphasic variant presents a mixture of epithelial and spindle-shaped cells. The relative proportion of each cell type within biphasic tumors has implications for clinical behavior. Some studies (Vigneswaran et al., 2017) demonstrated that the amount of epithelioid differentiation in biphasic MPM is a significant predictor of survival and shorter survival is associated with increased sarcomatoid component in biphasic tumors (Harling et al., 2019).

The sarcomatoid subtype is characterized by the presence of ≥ 90% spindle-shaped cells, high nuclear/cytoplasmic ratio and frank sarcomatoid features (Dacic et al., 2020).

Sarcomatoid histology is associated with larger tumor size at diagnosis and more advanced TNM (Tumor, Node and Metastasis) stage (Paajanen et al., 2018). Patients

with sarcomatoid tumors have the lowest median overall survival of the three subtypes (median 5.3 months) (Verma et al., 2018). Gross macroscopic resection does not significantly prolong survival in sarcomatoid tumors, in contrast to epithelioid and biphasic tumors (Verma et al., 2018). These patients have a diminished response to systemic chemotherapy (Kindler et al., 2018, Mansfield et al., 2014).

Therapeutic strategies

The standard therapeutic strategies for MPM are surgery for resectable tumors, often combined with radiotherapy and/or chemotherapy (trimodality treatment), and chemotherapy or radiotherapy in unresectable tumor cases. To date, the only FDA (Food and Drug Administration) - and EMA (European Medicines Agency)-approved frontline therapy is the cisplatin-pemetrexed combination (Nicolini et al., 2019). Surgery is controversial and limited to patients with early stage disease and good functional status (Nicolini et al., 2019).

There are current studies and clinical trials on innovative approaches, such as angiogenesis inhibitors added to cisplatin-pemetrexed (Garland et al., 2011; Laurie et al., 2017; Zalcman et al., 2016), immunotherapies (Moser et al., 2015; Krishnan et al., 2015), miRNA replacement (Chung et al., 2015; Reid et al., 2013), oncoviral therapies (Sterman et al., 2011;Sterman et al., 2016), cancer vaccines (Palucka and Banchereau, 2012) and advanced cell-based therapies as Chimeric Antigen Receptor-transduced T cells (CAR-T) against mesothelin (Zeltsman et al., 2017), although the results need confirmation in larger trials.

Recently, the FDA approved an innovative first-line treatment for MPM patients as a humanitarian use device, called NovoTTF-100L, that is based on the delivery of specific electric frequencies (Tumor Treating Fields, TTF) in combination with chemotherapy, to interfere with cancer cell proliferation (Ceresoli et al., 2018).

Despite amazing efforts devoted to understanding and treating MPM better, clinical practice has not changed over the past decades, and chemotherapy remains the only standard option.

Biomarkers

Biomarkers are useful diagnostic and prognostic tools in cancers. Hence, the need emerged to identify non-invasive protein indicators, usable in the field of secondary prevention, for an early diagnosis of MPM, in order to diagnose the disease in a phase in

which the surgery and radio chemotherapy can be more effective in increasing survival (Ledda et al., 2018).

In MPM, different biomarkers have been evaluated, but have been found to be imperfect and of limited clinical use. There are early results about mesothelin, megakaryocyte potentiating factor, osteopontin and fibulin 3. In addition, the expression of AQP1 in MPM tumor cells is an independent prognostic factor to improve survival time in MPM (Ledda et al., 2018). High levels of AQP1 expression of MPM tumor cells predict an increase in survival, while in other tumors the increase of AQP1 levels is associated with worse prognosis, including breast cancer, melanoma, urothelial carcinoma and pharynx squamous cell carcinoma (Driml et al., 2016). It has been hypothesized that the highest expression of aquaporin in MPM may reflect better differentiation, since the normal mesothelium expresses AQP1 (Ledda et al., 2018).

Furthermore, a proteomics-based biomarker detection technique has been developed in the form of SOMAscan (SomaLogic Inc., Boulder, CO, USA).

Although the literature is rich in studies that have evaluated old and new biomarkers, none of them is suitable for an early diagnosis of MPM in subjects exposed to asbestos, because these studies have been disadvantaged by retrospective designs, use of selected MPM cohorts, inappropriate controls and inconsistent sampling protocols, assay methods and cut-off points (Bibby et al., 2016).

AQPs in the Lungs

Levels of AQPs expression depend on timing of lung development and pathological conditions, but in general the lungs express four AQPs: AQP1, AQP3, AQP4 and AQP5.

AQP1 is expressed in the vascular endothelium and pleural membrane, AQP3 in epithelium of large airway, AQP4 in epithelium of small airways, and AQP5 in alveolar type I cells and submucosal glands (Figure 18).

These AQPs are involved in the lung fluid transport that refers to the alveolar fluid balance, airway hydration, pleural fluid transport and submucosal glands secretion (Yang et al., 2017).

Figure 18 - AQP1 (green), AQP3 (yellow), AQP4 (blue) and AQP5 (red) localization in respiratory system

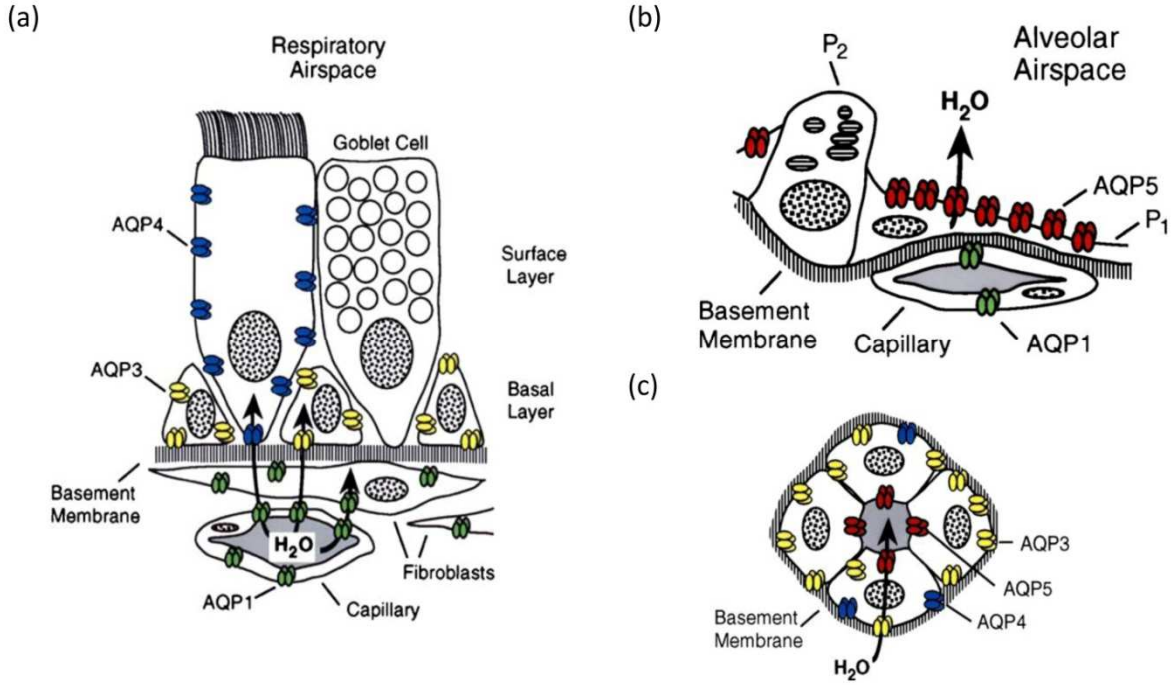

(a)Aquaporins in respiratory epithelia: absence of aquaporin expression in goblet cells, AQP4 in surface columnar cells, AQP3 in basal cells, and AQP1 in underlying fibroblasts and capillaries. (b) Aquaporins in alveolar space. P1, type 1 pneumocytes; P2, type 2 pneumocytes. (c) Aquaporins in secretory glands. (Agre, 2006).

Pleural fluid transport

Pleural mesothelial cells are specialized epithelial cells of mesodermal origin covering the lungs (visceral pleura) and the thoracic wall (parietal pleura) and between which the pleural cavity is formed (Lai-Fook, 2004). Under physiological conditions, a small amount of pleural fluid is present in the cavity, produced by plasma ultrafiltration from the parietal pleura capillaries (Agostoni and Zocchi, 2007). Pleural fluid is re-absorbed by the parietal pleura lymphatic stomata, by Starling forces across the visceral pleura and by mesothelial cell-mediated solute coupled liquid absorption and endocytosis (Agostoni and Zocchi, 2007). Pleural effusions, an excess accumulation of pleural fluid in the pleural cavity, occur in several extra-pulmonary (congestive heart failure, malignancy, post-myocardial infarction, rheumatoid arthritis) and pulmonary diseases (pneumonia, lung cancer, MPM, pulmonary embolism) (Hooper et al., 2010).

AQP1 is expressed at apical membrane of visceral and parietal pleura, and apical membrane of endothelial cell within visceral membrane (Song et al., 2000). The role of AQP1 in pleural fluid dynamics is important in cases of pleural effusions where the osmolality difference between the parietal pleura capillaries and the pleural fluid leads to compensatory increase in the activity of pleural AQP1 (Song et al., 2000). Therefore, the role of pleural AQP1 in malignant pleural effusions is potentially critical given that in a mouse model of malignant pleural effusions it has been demonstrated that pleural fluid volume is directly proportional to the tumor burden in the pleural cavity (Stathopoulos et al., 2006). Finally, AQP1 could facilitate the osmotic fluid transport within pleural space, and deletion of AQP1 could significantly reduce osmotic fluid transport (Jiang et al., 2003).

AQPs in MPM: State of Art

Due to the presence of pleural effusions in MPM, researchers decided to focus their work on AQP1 expression and permeability.

Several studies have shown that AQP1 plays a role in the equilibration of the osmotic gradient between the pleural cavity and the pleural capillaries in pleural effusions (Song et al., 2000; Klebe et al., 2015; Jagirdar et al., 2016).

Klebe and coworkers have demonstrated that AQP1 has a functional role in MPM proliferation, movement, and anchorage-independent growth. They have also demonstrated that it is possible to decrease growth and movement of MPM *in vitro* by specific blockade of AQP1 using a pharmacological blocker (AqB050) or using a specific

AQP1-siRNA. They tried to transpose the same work *in vivo* but, unfortunately, it did not result in a significant reduction of cancer growth. This could be due to many technical factors (Klebe et al., 2015).

MPM AQP1 inhibition *in vitro* inhibits cell adhesion, migration and tumor sphere formation in an extracellular component type and histological type dependent manner (Jagirdar et al., 2016).

Until now, only a group of researchers have investigated the osmotic permeability of benign mesothelial cells and epithelioid and sarcomatoid MPM cells (Katkova et al., 2019). They have found that in normal conditions, the permeability of benign cells is significantly higher from both epithelioid and sarcomatoid type of MPM cells (Katkova et al., 2019).

Unfortunately, there are no information about the expression and permeability related to other AQPs normally present in MPM cells.

2. Objectives

This study aims to investigate the functioning and the role of AQPs in redox-homeostasis of epithelioid and biphasic MPM cultured cells, evaluating:

1) the mRNA and protein expression of AQPs;

2) the immunolocalization of AQPs;

3) the water permeability features measured by a stopped-flow light scattering method. Actually, water movement changes could be considered representative of an H_2O_2 flux variation (Medraño-Fernandez et al., 2016). Moreover, time course of H_2O_2 transport will be also confirmed using the fluorescence probe CM-H2DCFDA;

4) the water permeability in silenced cells using a specific AQP-siRNA.

3. Materials and Methods

Cell Culture

Experiments were carried out on both mesothelioma and normal mesothelial immortalized cell lines. The following human cell lines were used: MeT-5A as mesothelial model (Ke et al., 1989), REN (Smythe et al., 1994) and MSTO-211H (Bepler et al., 1988) as epithelioid and biphasic MPM cells, respectively.
Cells were routinely grown in plastic tissue culture flasks using Dulbecco's modified minimal essential medium high glucose, supplemented with 10% fetal bovine serum, 1% L-glutamine, 1% penicillin and streptomycin, and maintained at 37 °C in a humidified atmosphere of 5% CO2, 95% air.

RNA Isolation and RT-qPCR

Total RNA was extracted from MeT-5A, REN and MSTO-211H cells using QIAzol Lysis Reagent (Qiagen SpA, Milan, Italy), and reverse transcription was performed according to Laforenza et al. (Laforenza et al., 2005). cDNA amplification was performed by GoTaq® Flexi DNA Polymerase (Promega, Milano, Italy), as previously described (Laforenza et al., 2005). The primers used for amplification are specific for AQP3, 5, 6, 8, 9, 11 and are listed in the Table 5 . QuantiFast SYBRGreen PCR Master Mix (Qiagen) was used to perform the qPCR. The qPCR protocol consisted of an initial denaturation of 5 min at 95 °C followed by 40 cycles of denaturation at 95 °C for 10 s, annealing (see TM in Table 5) and extension at 60 °C for 30 s. Reverse transcription was always performed both either in the presence (positive) or in the absence (negative control) of reverse transcriptase enzyme. The qPCR reactions were normalized using β-actin as housekeeping gene (Table 5). Melting curves were generated to detect the melting temperatures of specific products immediately after the PCR run. The triplicate threshold cycles (Ct) values for each sample were averaged resulting in mean Ct values for both the gene of interest and the housekeeping gene. The gene Ct values were then normalized to the housekeeping gene by taking the difference:

$$\Delta Ct = Ct(\text{AQP gene}) - Ct(\text{housekeeping gene})$$

High ΔCt values reflect low mRNA expression levels. PCR products were separated on a 3% Nusieve® (2:1) gel agarose, stained with ethidium bromide, and acquired with the

Image Master VDS (GE Healthcare, Milano, Italy). The molecular weight of the PCR products was compared with the DNA molecular weight marker VIII (Roche Molecular Biochemicals, Monza, Italy).

Table 5 - Primer sequences used for RT-qPCR

Gene		Primers sequence	Size (bp)	TM (°C)	Accession Number
AQP3	Forward Reverse	5'-CCTGGTGATGTTTGGCTGTGGCTC-3' 5'-TTCAGGTGGGCCC CAGAGACC-3'	147	60	NM_004925.5
AQP5	Forward Reverse	5'-GGTGGTGGAGCTGATTCTGA-3' 5'-GAAGTAGATT CCGACAAGGTGG-3'	142	60	NM_001651.4
AQP6	Forward Reverse	5'-CACCTCATTGGGATCCACTTC-3' 5'-CCCAGAAGACCCAGTGGACT-3'	103	60	NM_001652.4
AQP8	Forward Reverse	5'-TGGAGAGATAGCCATGTGTGAG-3' 5'-TGGCTGCACAAACCGTTCGT-3''	106	60	NM_001169.3
AQP9	Forward Reverse	5'-CCCAGCTGTGTCTTTAGCAA-3' 5'-AAGTCCATCATAGTAAATGCCAAA-3'	133	60	NM_020980.5
AQP11	Forward Reverse	5'-TTTCTCTTCCACAGCGCTCT-3' 5'-CTCCTGTTAGACTTCCTCCTGC-3'	115	60	NM_001363477.2
Hs_Actb_1_SG, QuantiTect Primer Assay QT00095431 (Qiagen)			146		

TM, Temperatura di Melting.

Gene Silencing

siRNA targeting AQP6 was purchased by Dharmacon™ (ON-TARGETplus Human AQP6 (363) siRNA – SMARTpool, L-011579-00-0005, DharmaconTM, Horizon Discovery Group, Waterbeach, UK). Scrambled siRNA was used as negative control. siRNA targeting AQP3 and AQP5 were purchased by Sigma-Aldrich Inc. MISSION esiRNA (human AQP3, EHU071641, Sigma-Aldrich, USA; human AQP5, EHU046331, Sigma-Aldrich, USA).

MeT-5A and MSTO-211H cells were transfected with siRNA oligonucleotides (5 μM), or with equimolar scramble siRNA, by using the N-ter Nanoparticle siRNA Transfection System (N2913, Sigma-Aldrich, USA). Briefly, once the monolayer cells had reached 50% confluency, the medium was removed and substituted with fresh medium containing Target siRNA Nanoparticle Formation Solution (NFS). siRNA (5 μM final concentration) was diluted in siRNA Diluition Buffer (N0413) and mixed with N-TER peptide (N2788) pre-diluted in distilled water, according to the manufacturer's instructions to create the NFS. After 30 min incubation at 37 °C, the NFS was diluited in medium and added to the cells and incubated at 37 °C for 24 h. The effectiveness of

silencing was determined by immunoblotting and silenced cells were used 24 h after transfection.

REN cells were transfected with siRNA oligonucleotides (25 nM final concentration), or with equimolar scramble siRNA, by using X-tremeGENE siRNA Transfection Reagent (04476093001, Roche Diagnostic GmbH, Mannheim, Germany). Once the monolayer cells had reached 50% confluency, the medium was removed and the cells were added with Opti-MEM I reduced serum medium without antibiotics (Life Technologies, Milan, Italy). siRNA was diluited in OptiMEM I reduced serum medium and mixed with X-tremeGENE siRNA Transfection Reagent pre-diluited in OptiMEM, according to the manufacturer's instructions. After 20 min incubation at room temperature, the mixes were added to the cells and incubated at 37 °C for 5 h. Transfection mixes were then removed and fresh culture media was added. The effectiveness of silencing was determined by immunoblotting and silenced cells were used 48 h after transfection.

Immunoblotting

Cells were homogenized in RIPA buffer (150 mM NaCl, 0.5% sodium deoxycholate, 0.1% SDS, 0.1% Triton X-100, 50 mM Tris-HCl, pH 8) supplemented with a protease inhibitor cocktail (cOmplete Tablets EASYpack, 04693116001, Roche, Mannheim, Germany).

Immunoblotting was carried out as previously described (pag. 52) loading 30 μg proteins. Membranes were incubated overnight with anti-AQP3 rabbit polyclonal IgG (ab125045,1:1000; Abcam, Cambridge, UK), anti-AQP5 rabbit polyclonal IgG (A4985, 1:1000; Sigma-Aldrich, USA), anti-AQP6 rabbit polyclonal IgG (# AQP61-A, 1:1000; Alpha Diagnostic International, San Antonio, USA), anti-AQP8 rabbit polyclonal IgG (EPR8397 ab133667, 1 :1000; Abcam, Cambridge, UK), anti-AQP9 rabbit polyclonal IgG (PA5-97110, 1:500; Invitrogen, California, USA) anti-AQP11 rabbit polyclonal IgG (#AP5805b, 1:500; ABGENT, San Diego, California) in blocking solution.

Blots were stripped (Yeung and Stanley, 2009) and reprobed with anti-β-actin rabbit polyclonal IgG (AB-81599, Immunological Sciences, Rome, Italy) diluted 1:2000 in blocking solution.

Blots were acquired with the iBrightTM CL1000 Imaging System (Invitrogen by Thermo Fisher Scientific, California, USA). Densitometric analysis of the bands was performed using the Total Lab V 1.11 program (Amersham) and iBright Analysis Software (Thermo Fisher Scientific) and results were expressed as AQP/β-actin ratio.

Immunocytochemistry

Immunolocalization of AQP3, 5, 6, 8, 9 and 11 was evaluated in MeT-5A, REN and MSTO-211H cell lines. Immortalized cells were cultured on sterile coverslips and fixed in 4% paraformaldehyde in PBS for 30 min, washed with PBS and then treated with 0.3% hydrogen peroxide in distilled water for 10 min at room temperature to block the endogenous peroxidases. After washing for 10 min with PBS, cells were blocked with 3% BSA in PBS for 30 min at room temperature. Coverslips were incubated overnight at 4 °C with affinity pure primary antibodies: anti-AQP3 rabbit polyclonal IgG (ab125045, 1:400; Abcam, Cambridge, UK), anti-AQP5 rabbit polyclonal IgG (A4985, 1:500; Sigma-Aldrich, USA), anti-AQP6 rabbit polyclonal IgG (# AQP61-A, 1:1000; Alpha Diagnostic International, San Antonio, USA), anti-AQP8 rabbit polyclonal IgG (HPA046259, 1:500; Sigma-Aldrich, USA), anti-AQP9 rabbit polyclonal IgG (ab84828, 1:200; Abcam, Cambridge, UK), anti-AQP11 rabbit polyclonal IgG (#AP5805b, 1:100; ABGENT, San Diego, California) diluted in PBS. After three 10 min washes with PBS, coverslips were incubated for 30 min at room temperature with goat anti-rabbit IgG HRP-conjugated (ab236466 – Mouse and Rabbit Specific HRP/DAB IHC Detection Kit – Micro-polymer, Abcam, Cambridge, UK). The reaction was visualized by incubation with a DakoCytomation 3,3'-diaminobenzidine chromogen solution. The cells were counterstained with haematoxylin, dehydrated and mounted in Leica CV Mount (14046430011, Leica biosystems, USA). Controls experiments were performed simultaneously omitting the primary antibody. Then, coverslips were examined by light microscopy using an Olympus BX41 and the digital images were acquired with the Nikon DS-Fi1 digital camera using Nis Element F Imaging Software (2.33, Nikon, Tokyo, Japan).

Immunofluorescence

Immunolocalization of AQP6 was evaluated in MeT-5A, REN and MSTO-211H cells, which were cultured on coverslips, incubated with 50 ug/ml Conacavalin A FITC labeled (c7642, Sigma-Aldrich, USA) in PBS for 1h at room temperature. After three washes with PBS, the cells were fixed in 4% paraformaldeyde in PBS for 30 min and then washed with PBS. The cells were then blocked with 3% BSA in PBS at room temperature for 30 min. Coverslips were incubated overnight at 4 °C with affinity pure anti-AQP6 rabbit polyclonal primary antibody (# AQP61-A, 1:250; Alpha Diagnostic International, San Antonio, USA). After three 10 min washes with PBS, coverslips were incubated at room temperature with the fluorescent secondary antibody, rhodamine red-X-conjugated affinity pure goat anti-rabbit IgG (H+L) (111-295-045, 1:1000; Jackson ImmunoResearch Europe Ltd., Cambridgeshire, UK), for 1 h. Coverslips were then washed 3 x 10 min with PBS, mounted in ProLong Gold antifade reagent with 4',6-Diamino-2-Phenylindole (DAPI; Molecular Probes) and examined with a TCS SP5 II confocal microscopy system (Leica Microsystems) equipped with a DM IRBE inverted microscope (Leica Microsystems). Images were visualized and analyzed by LAS AF software (Leica Microsystems Application Suite Advanced Fluorescence). Control experiments were performed simultaneously using non-immune serum.

Water Permeability Measurements

Osmotic water permeability of mesothelium and MPM cells was measured by stopped-flow light scattering method (Laforenza et al., 2016) (for more details pag. 50)

Initially, the water permeability coefficient, *Pf*, was calculated to compare the water permeability capacity of the three cell types, successively the initial rate constant of cells volume changes (k) was considered to determine the changes due to the different cell treatments.

As indicated above, it has been demonstrated that the osmotic water permeability of AQPs is indicative of H_2O_2 permeability (Medraño-Fernandez et al., 2016).

To study the effect of oxidative stress on water permeability, immortalized cells were divided into five groups: a) normal untreated cells (Control); b) cells treated for 45 min with 50 μM H_2O_2 (Exogenous oxidative stress); c) cells incubated for 3h at 42 °C (Endogenous oxidative stress); d) stressed cells treated for 15 min with 15 mM β-

mercaptoethanol to restore the normal condition; e) cells pretreated with 10 mM DPI and incubated for 3h at 42 °C.

Moreover, the AQPs localization on cell membranes was demonstrated in a functional way, evaluating the water permeability and the effect of mercury, an AQPs inhibitor: a) normal untreated cells (Control); b) cells treated for 15 min with 100 μM $HgCl_2$; c) cells treated with $HgCl_2$ and then restored for 15 min with 15 mM β-mercaptoethanol.
To study the effect of oxidative stress on water permeability of AQP6 silenced cell lines, silenced and not-silenced cells were divided in two groups: a) normal untreated cells (Control); b) cells treated for 45 min with 50 μM H_2O_2 (Exogenous oxidative stress).

Hydrogen Peroxide Influx Measurements

Hydrogen peroxide influx in mesothelium and MPM cells were measured by a fluorescence method using the 5-(and-6)-chloromethyl-20,70-dichlorodihydro-fluorescein diacetate, acetyl ester reagent (CM-H2DCFDA) (Invitrogen).

Briefly, cells were centrifuged at 200 rcf for 5 min. The cell pellet was resuspended in PBS and CM-H2DCFDA reagent was added (diluition 1:500). Thereafter 1h of incubation at room temperature, cells were centrifuged again, and the pellet resuspended in PBS was divided into two groups: a) normal untreated cells (Control); b) cells treated with 100 μM $HgCl_2$ for 15 min. 100 μl of Control and $HgCl_2$ treated cells were loaded in a polystyrene 96-well plate (MICROTEST TM Tissue Culture Plate, 96 Well, Becton Dickinson Labware) and then 100 μl of distilled water or 50 μM H_2O_2 was injected, just before the measurement.
Hydrogen peroxide levels were measured in the experimental conditions described above by using a CLARIOstar® microplate reader (BMG LABTECH, Ortenberg, Germany) for 15 min. Data were normalized with protein content.

Protein Content

The protein content was determined with the Bradford method (Bradford, 1976), using bovine serum albumin as standard.

Statistics

All data were expressed as means ± SEM (Standard Error Mean). The significance of the differences of the means were evaluated by using one-way ANOVA, followed by Newman–Keuls' Q test, or Student's t test. All statistical tests were carried out with GraphPad Prism 4.00, 2003.

4. Results

Quantitative RT-PCR (qRT-PCR) of AQP3, AQP5, AQP6, AQP8, AQP9, AQP11 mRNA expression in MeT-5A, REN, MSTO-211H cell lines

The expression levels of AQP3, AQP5, AQP6, AQP8, AQP9, AQP11 mRNA was evaluated by qRT-PCR in mesothelial (MeT-5A), epithelioid and biphasic MPM (REN, MSTO-211H) cell lines.

All the AQPs considered were expressed in the three cell lines. The results of agarose gel electrophoresis of qPCR reaction products showed single bands of the expected size of cDNA fragments amplified (147 bp for AQP3, 142 bp for AQP5, 103 bp for AQP6, 106 bp for AQP8, 133 bp for AQP9 and 115 bp for AQP11). Negative controls of qRT-PCR experiments were always performed by omitting the reverse transcriptase enzyme (data not shown). Significant data concern the expression of AQP3, AQP6, AQP8 and AQP9 mRNA, as shown in Figure 19.

AQP3 and AQP6 mRNA are statistically downregulated in epithelioid MPM cell lines, while AQP8 is statistically upregulated in biphasic MPM cell line. AQP9 mRNA is downregulated in both MPM cell lines.

Figure 19 - qRT-PCR reaction analysis of AQP3, AQP5, AQP6, AQP8, AQP9 and AQP11 expression in mesothelial (MeT-5A , in white), epithelioid and biphasic MPM cell lines (REN and MSTO-211H, in blue and in green respectively)

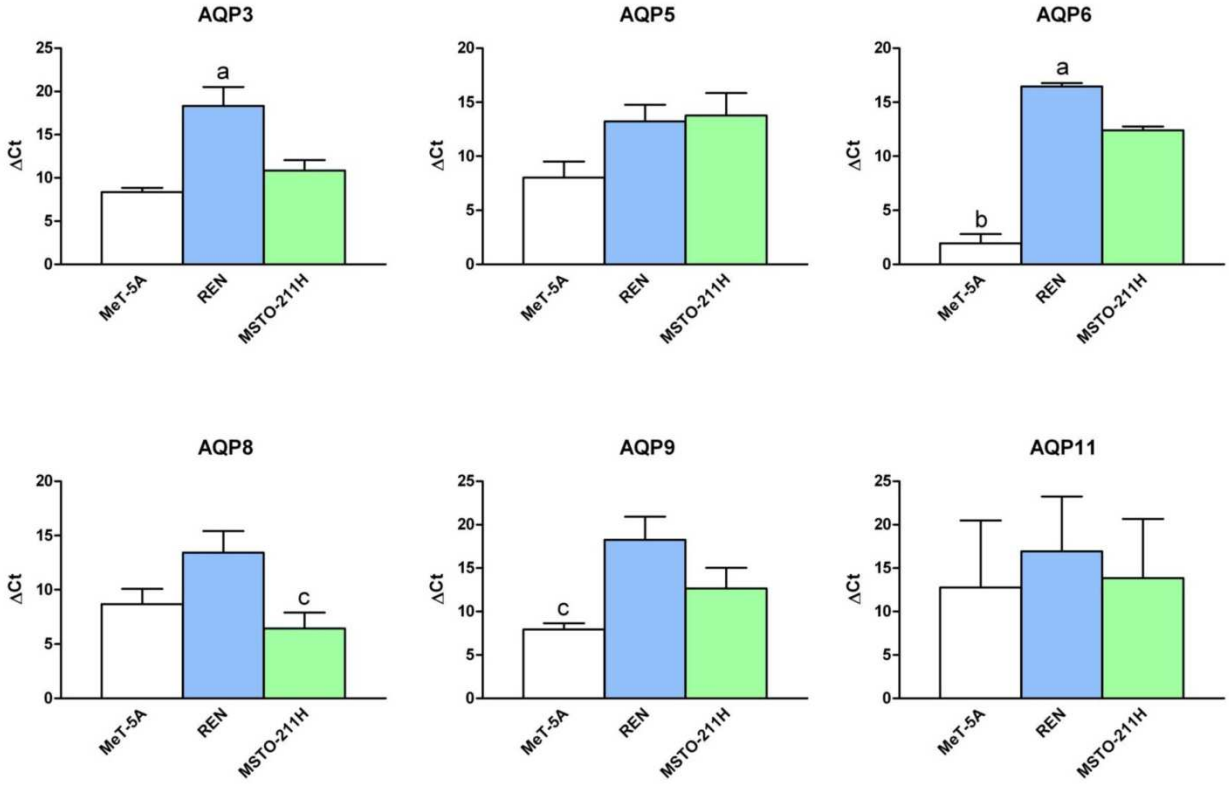

Bars represent mean ± SEM of ΔCt values (n = 4). a: p < 0.01 versus Met-5A, MSTO-211H, b: p < 0.01 versus REN, MSTO-211H, c: p < 0.05 versus REN, (ANOVA followed by Newman–Keuls Q-test).

Immunoblotting of AQP3, AQP5, AQP6, AQP9, AQP11 in MeT-5A, REN, MSTO-211H cell lines

Plasma membranes from MeT-5A, REN, MSTO-211H cell lines were analyzed by immunoblotting using affinity-purified antibodies against human AQP3, AQP5, AQP6, AQP9 and AQP11. The results showed that all the AQP proteins considered were expressed in cell lines (Figure 20-24).

A major band of 36 kDa was observed in immunoblots probed with anti-AQP3 antibody (Figure 20). Immunoblots of AQP5 showed a major band at approximately 35 kDa (Figure 21), while immunoblots of AQP6 protein showed a major band of 29 kDa (Figure 22). AQP9 and AQP11 showed major bands of about 33 and 30kDa, respectively. The specificity of the reactions was confirmed by preadsorption experiments for all the AQPs, in which the proteins bands were absent (data not shown).

AQP3 protein expression is statistically upregulated in MPM cell lines (Figure 20), especially in the biphasic one. AQP5 and AQP6 protein expressions are unmodified in REN and downregulated in MSTO-211H of about 30 and 8 percent, respectively (Figure 21, 22), while AQP9 is upregulated in MSTO-211H of about 35 percent (Figure 23). The expression of AQP11 protein does not change in the three cell lines (Figure 24).

Figure 20 - Immunoblotting and densitometric analysis of AQP3 in mesothelial (MeT-5A , in white), epithelioid and biphasic MPM cell lines (REN and MSTO 211H, in blue and in green respectively)

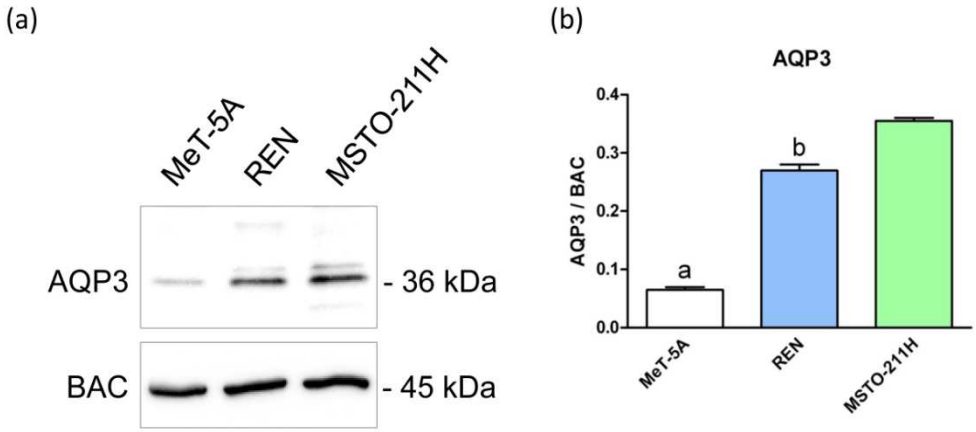

(a) Blots representative of three were shown. Lanes were loaded with 30 µg of proteins, probed with affinity purified antibody and processed as described in Materials and Methods. The same blots were stripped and re-probed with anti-β-actin (BAC) antibody, as housekeeping. Major bands of the expected molecular weights were shown. (b) Densitometric analysis, each bar represents the mean ± SEM of the normalized values of AQP protein expression. a: p < 0.001 versus REN, MSTO-211H; b: p < 0.01 versus MSTO-211H (ANOVA followed by Newman–Keuls Q-test).

Figure 21 - Immunoblotting and densitometric analysis of AQP5 in mesothelial (MeT-5A , in white), epithelioid and biphasic MPM cell lines (REN and MSTO-211H, in blue and in green respectively)

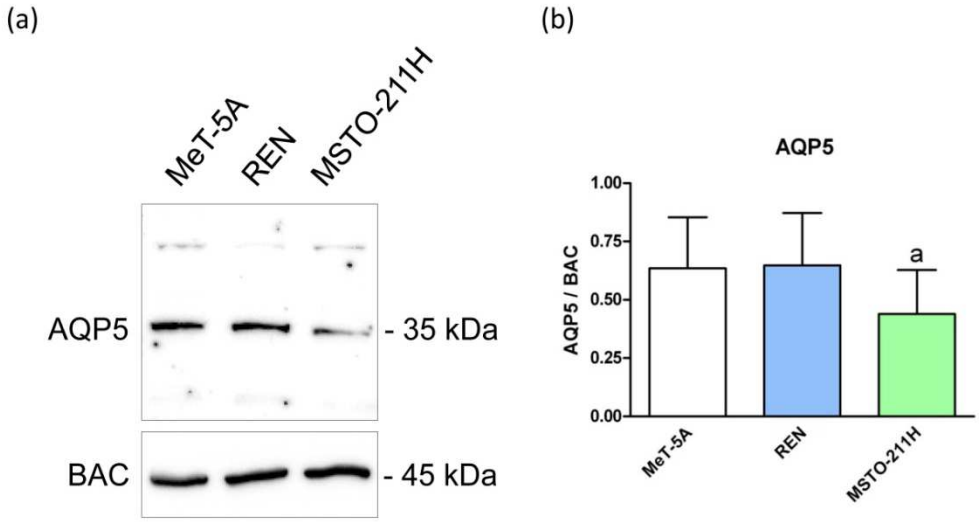

(a) Blots representative of three were shown. Lanes were loaded with 30 µg of proteins, probed with affinity purified antibody and processed as described in Materials and Methods. The same blots were stripped and re-probed with anti-β-actin (BAC) antibody, as housekeeping. Major bands of the expected molecular weights were shown. (b) Densitometric analysis, each bar represents the mean ± SEM of the normalized values of AQP protein expression. a: p < 0.01 versus Met-5A, REN (ANOVA followed by Newman–Keuls Q-test).

Figure 22 - Immunoblotting and densitometric analysis of AQP6 in mesothelial (MeT-5A , in white), epithelioid and biphasic MPM cell lines (REN and MSTO-211H, in blue and in green respectively)

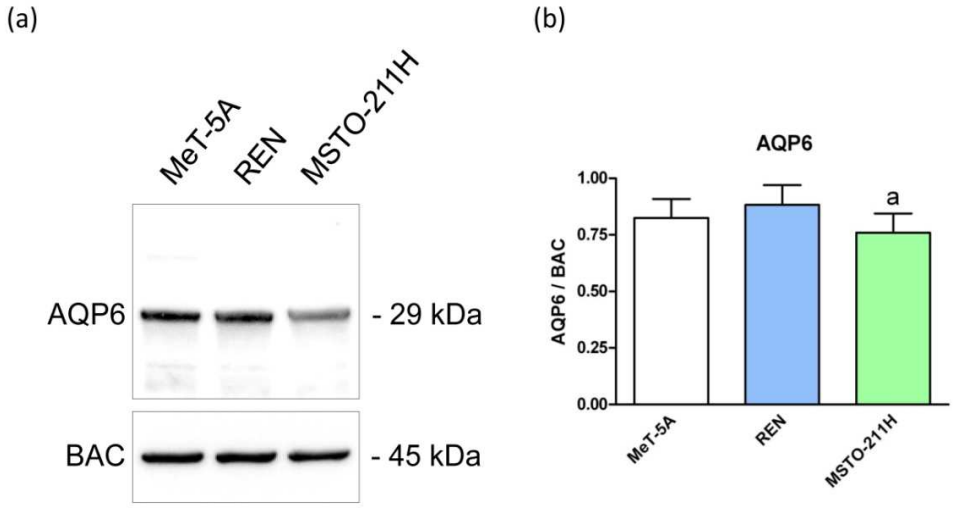

(a) Blots representative of three were shown. Lanes were loaded with 30 µg of proteins, probed with affinity purified antibody and processed as described in Materials and Methods. The same blots were stripped and re-probed with anti-β-actin (BAC) antibody, as housekeeping. Major bands of the expected molecular weights were shown. (b) Densitometric analysis, each bar represents the mean ± SEM of the normalized values of AQP protein expression. a: p < 0.05 versus MeT-5A, REN (ANOVA followed by Newman–Keuls Q-test).

Figure 23 - Immunoblotting and densitometric analysis of AQP9 in mesothelial (MeT-5A , in white), epithelioid and biphasic MPM cell lines (REN and MSTO-211H, in blue and in green respectively)

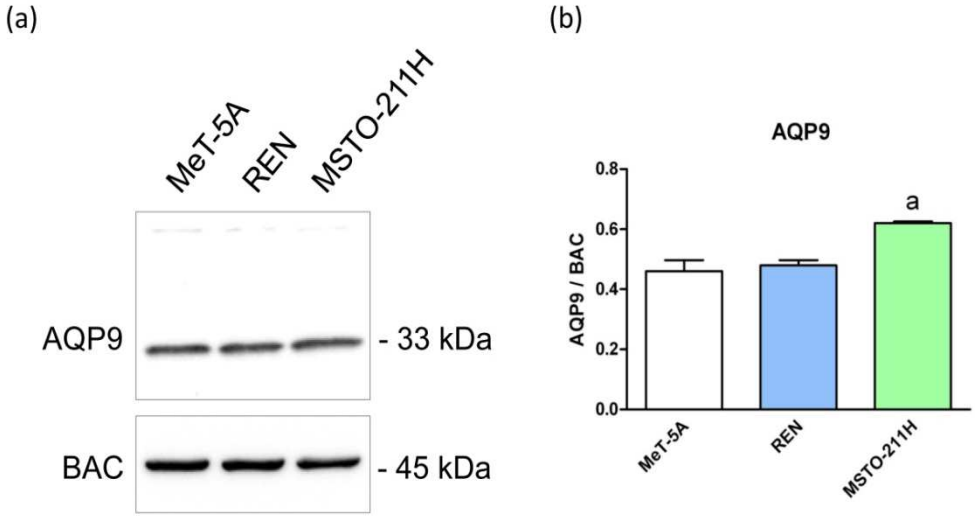

(a) Blots representative of three were shown. Lanes were loaded with 30 µg of proteins, probed with affinity purified antibody and processed as described in Materials and Methods. The same blots were stripped and re-probed with anti-β-actin (BAC) antibody, as housekeeping. Major bands of the expected molecular weights were shown. (b) Densitometric analysis, each bar represents the mean ± SEM of the normalized values of AQP protein expression. a: p < 0.05 versus MeT-5A, REN (ANOVA followed by Newman–Keuls Q-test).

Figure 24 - Immunoblotting and densitometric analysis of AQP11 in mesothelial (MeT-5A , in white), epithelioid and biphasic MPM cell lines (REN and MSTO-211H, in blue and in green respectively)

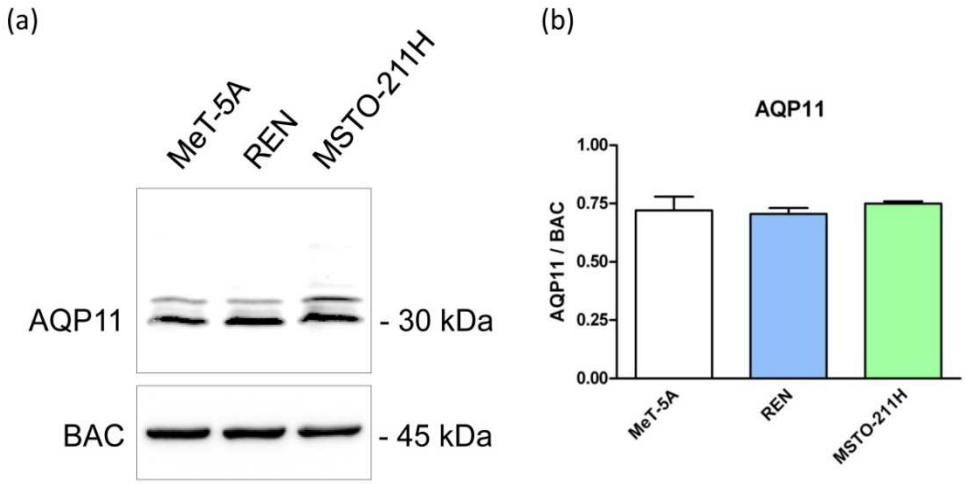

(a) Blots representative of three were shown. Lanes were loaded with 30 µg of proteins, probed with affinity purified antibody and processed as described in Materials and Methods. The same blots were stripped and re-probed with anti-β-actin (BAC) antibody, as housekeeping. Major bands of the expected molecular weights were shown. (b) Densitometric analysis, each bar represents the mean ± SEM of the normalized values of AQP protein expression (ANOVA followed by Newman–Keuls Q-test).

Immunolocalization of AQP3, AQP5, AQP6, AQP8, AQP9 and AQP11 in MeT-5A, REN, MSTO-211H cell lines

The cellular and subcellular localization of AQP3, AQP5, AQP6, AQP8, AQP9 and AQP11 protein in mesothelial and MPM cell lines was investigated by immunocytochemistry.
As showed in Figure 25 the anti-AQP3 and anti-AQP5 antibodies labeled only intracellular structures (Figure 25A, B), while anti-AQP6, anti-AQP9 and AQP11 antibodies in addition to an intracellular staining showed a strong labelling in discrete areas of the plasma membrane of MPM cell lines (Figure 25C, E, F). Anti-AQP8 gave a negligible signal in the three cell lines (Figure 25D) like the negative controls (Figure 26).

Colocalization experiments were performed to gain more evidence about the localization of AQP6 on the plasma membrane (Figure 27). Double label immunofluorescence showed that AQP6 and ConA, a leptin that recognizes the plasma membrane, colocalized, as per the resulting yellow fluorescence in merged images of REN and MSTO-211H cell lines (Figure 27A). Colocalization graphs showed the overlap of the fluorescence signal originated by AQP6 (red) and ConA (green) labeling (Figure 27E). On the contrary, MeT-5A cells did not show any overlap of the fluorescence signal between AQP6 and ConA (Figure 27A), as per the absence of yellow fluorescence in merged image (Figure 27E). Control experiments were performed using non-immune serum which did not show any labeling (Figure 28).

Figure 25 - Immunocytochemical localization of AQP3 (A), AQP5 (B), AQP6 (C), AQP8 (D), AQP9 (E) and AQP11 (F) proteins in MeT-5A, REN, MSTO-211H cell lines

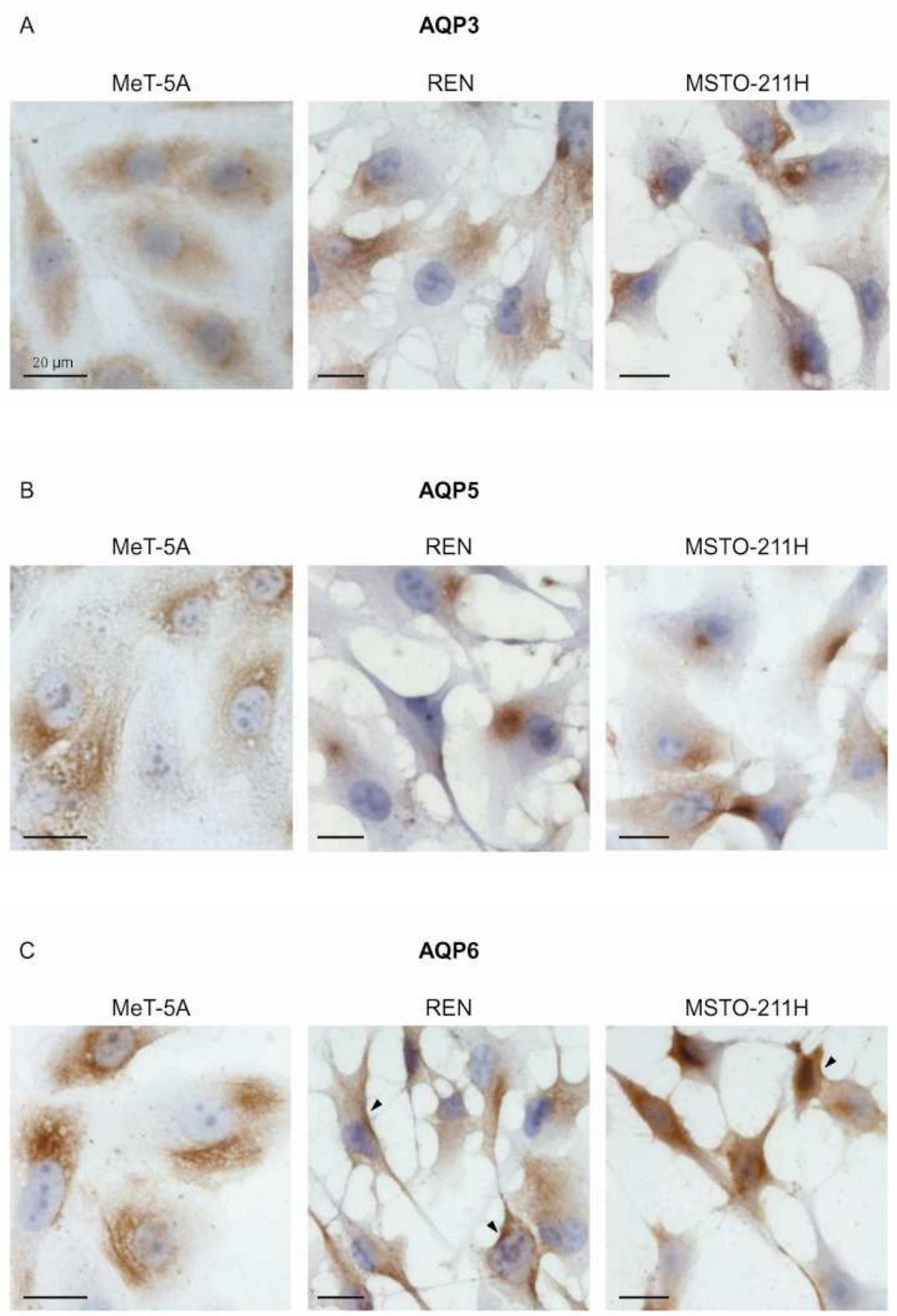

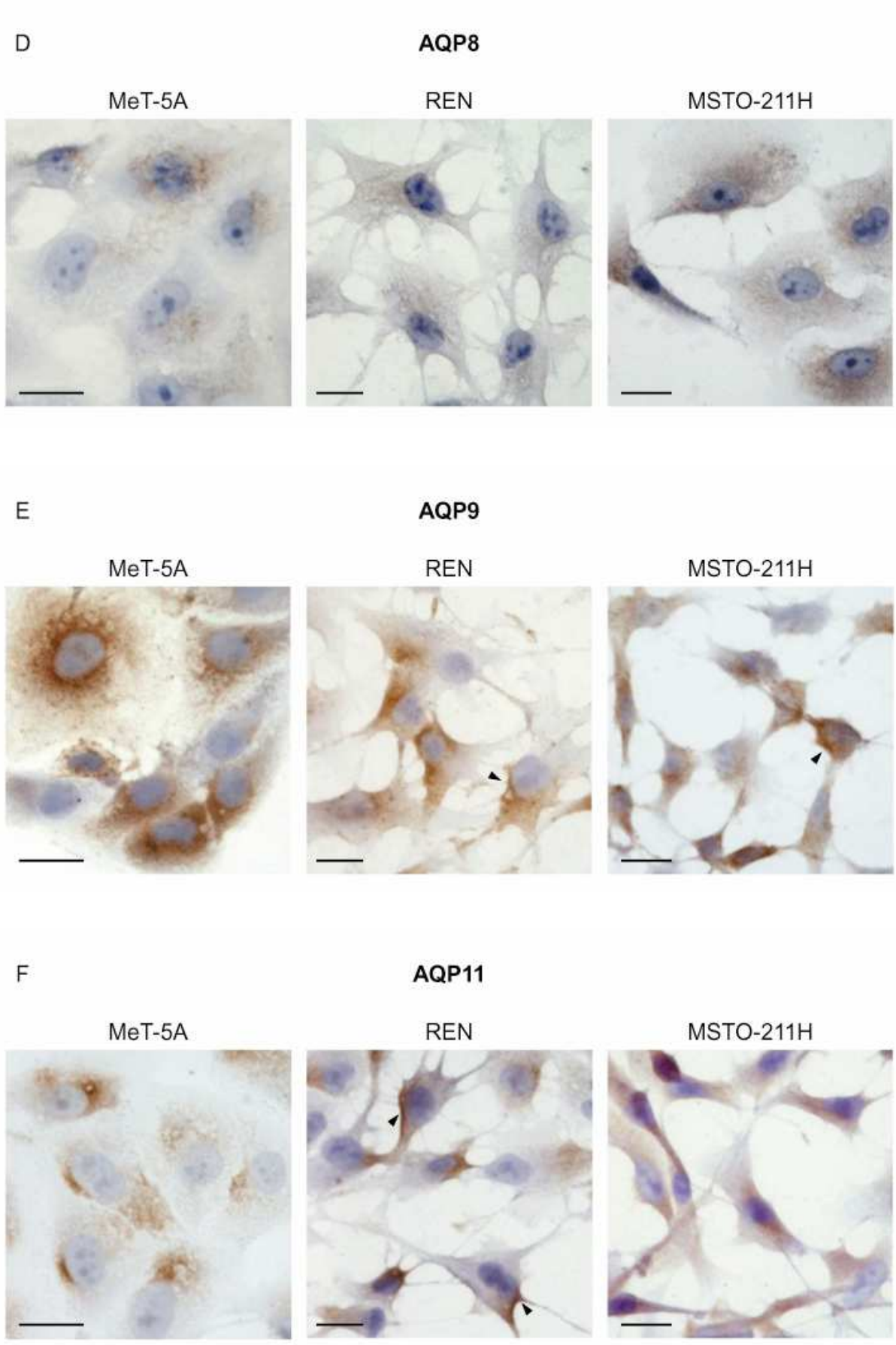

Arrowheads indicates the localization in plasma membranes. Scale bar, 20 μm.

Figure 26 - Immunocytochemical negative control of MeT5A, REN and MSTO-211H cell lines

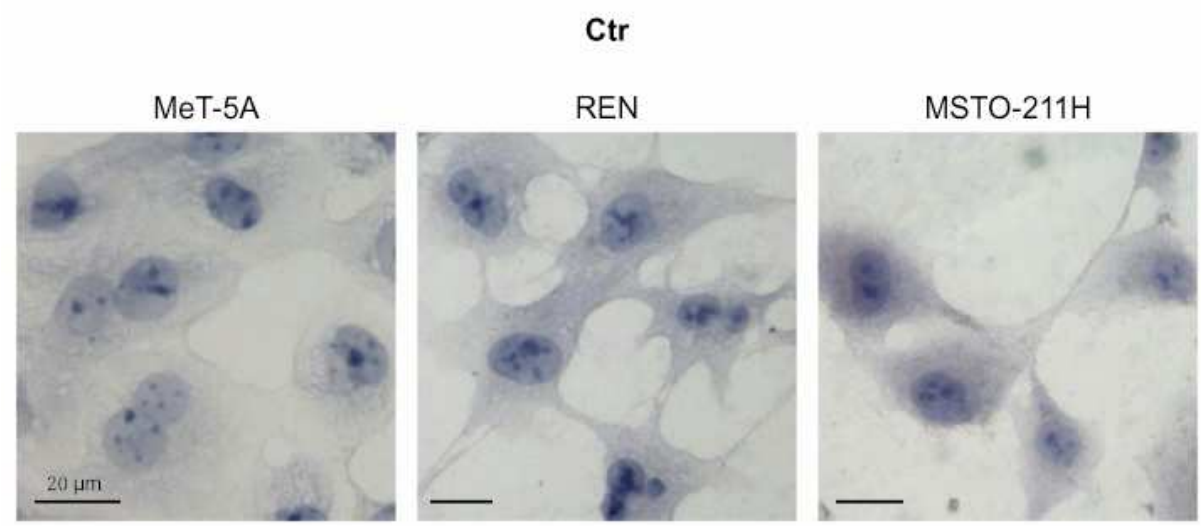

The primary antibody was substituted with non-immune serum. Scale bar, 20 µm.

Figure 27 - Representative immunofluorescence confocal microscopy images of colocalization of Conacavalin A and AQP6 in MeT-5A, REN and MSTO-211H cell lines

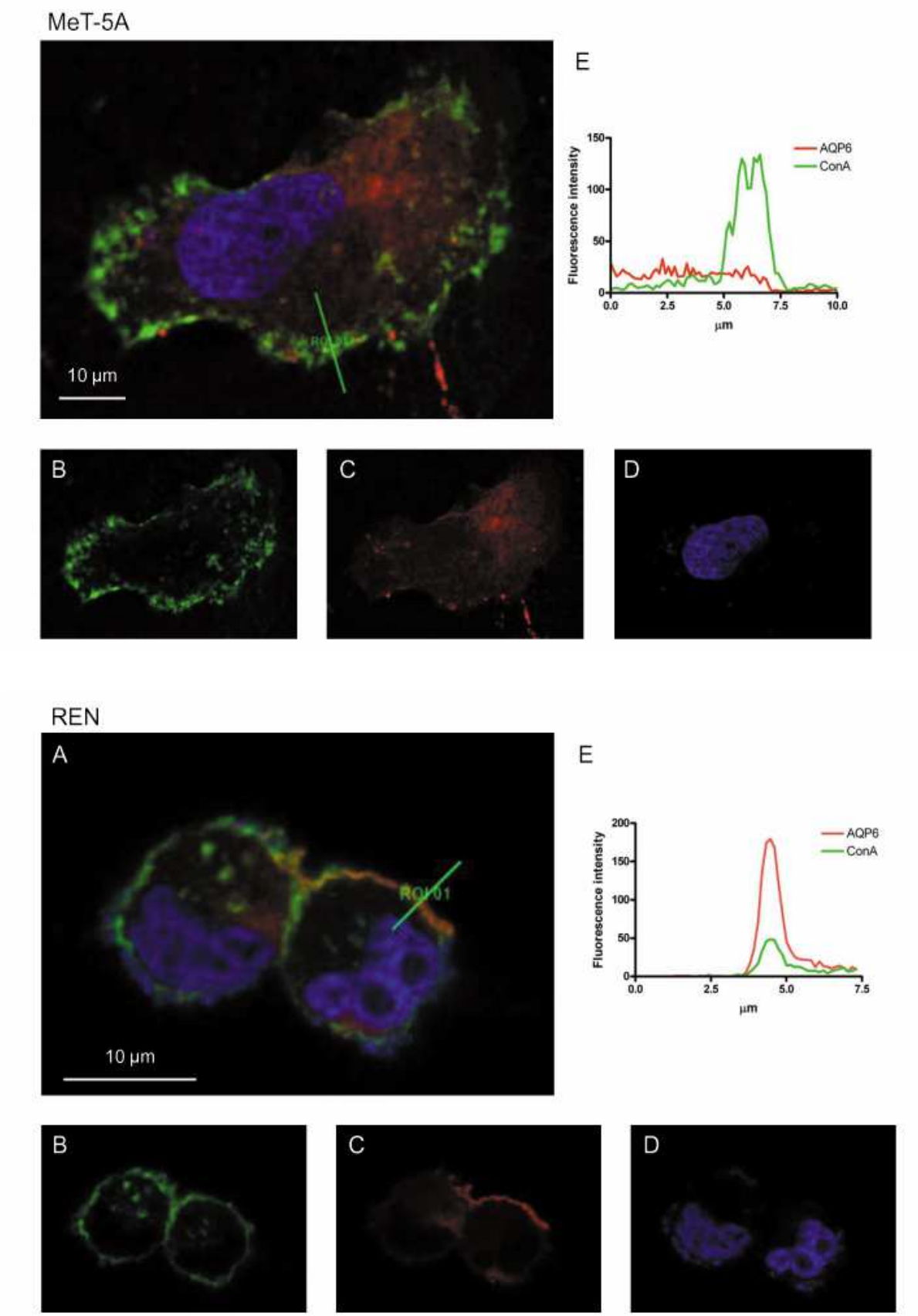

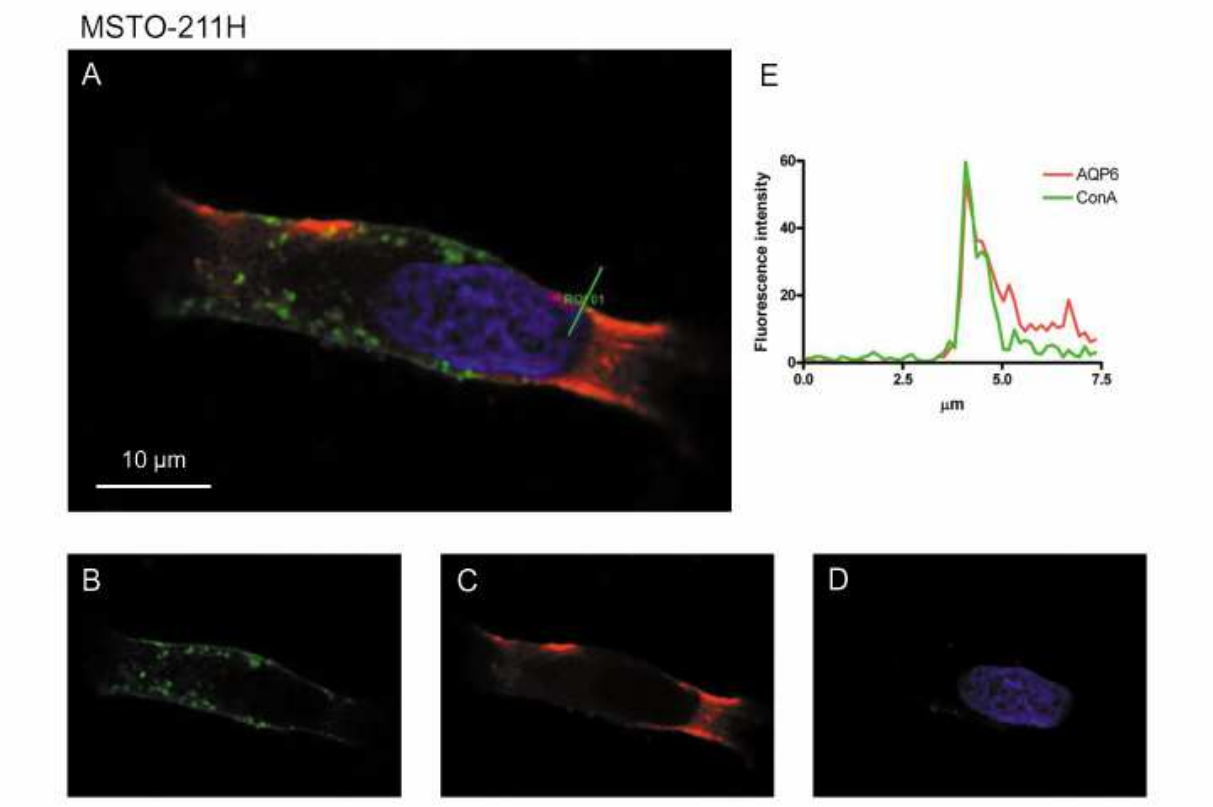

(A) Green labeling indicates the Conacavalin A, red labeling the expression of AQP6, while nuclei were counterstained by DAPI (blue). Yellow labeling shows colocalization signal of AQP6 with Conacavalin A. Scale bar, 10 µm. (B-D) Images show single labeling for Conacavalin A (green; B), AQP6 (red; C) and nuclei (DAPI; D). (E) Colocalization graphs, measured in the green line position in panel A, showing the fluorescence signals originated by AQP6 and Conacavalin A (ConA) staining. The graph in panel E of REN and MSTO-211H shows the overlap of the fluorescence signals originated by AQP6 and ConA staining.

Figure 28 - Immunofluorescence negative control

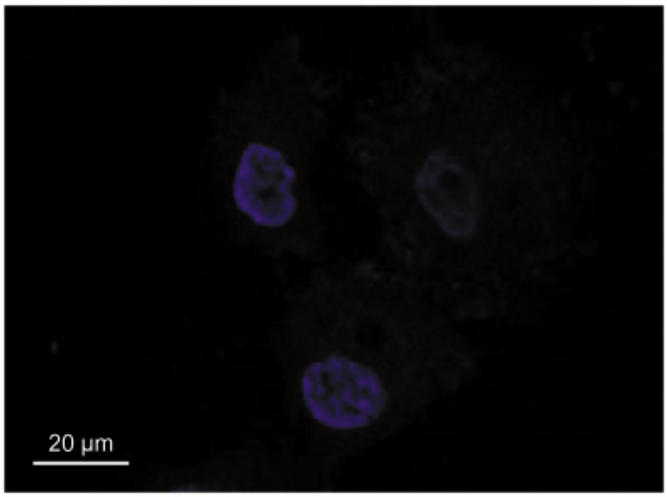

No or faint staining was observed when anti-aquaporins and anti-Conacavalin A antibodies were substituted with preimmune serum. Nuclei were counterstained by DAPI (blue). Scale bar, 20 µm.

Effect of oxidative stress and mercury chloride on water permeability of MeT-5A, REN, MSTO211-H cell lines

Cells exposed to hypotonic buffer behaved as functional osmometers showing a sudden swelling (Figure 29). The decrease in scattered light intensity could be fitted by a one phase exponential decay equation and the initial rate constant *k* was obtained. Firstly, we wanted to compare the osmotic permeability of the three cell lines by calculating the osmotic permeability coefficient Pf as indicated in Materials and methods. MeT-5A cells have a significantly higher Pf as compared to REN and MSTO-211H cells [4.88E-02±1.60E-03 cm/sec (n=24) versus 2.87E-02±7.31E-04 cm/sec (n=25) and 3.23E-02±5.48E-04 cm/sec (n=24)].

Mesothelial cells (MeT-5A) treated with H_2O_2 showed a significant water permeability reduction, which was restored by the subsequent β-mercaptoethanol treatment. On the contrary, the cells subjected to heat stress not only did not show a reduction in water permeability but rather increased it of about 55%. The enhanced AQP-permeability was reversed also by pre-treating with DPI, a potent inhibitor of NADPH oxidase and also of iNOS/eNOS (Figure 30a-b). Moreover, the AQPs localization on cell membranes was demonstrated in a functional way, evaluating the water permeability and the effect of mercury chloride, a well-known AQP inhibitor (Martins et al 2012). Surprisingly, the results showed an increase of water permeability (45%; $p < 0.05$, ANOVA followed by Newman–Keuls Q-test), probably due to the presence of AQP6 (Yasui et al., 1999). The subsequent treatment with β-mercaptoethanol restored the water permeability values (Figure 30c).

The results of epithelioid and biphasic MPM cell lines, REN and MSTO211-H, showed that H_2O_2 treatment did not change water permeability, while heat stress treatment increased water permeability of about 20% and 60%, respectively. The pretreatment with DPI prevented the enhanced AQP-permeability by heat stress (Figure 31a-b, 32a-b). The mercury treatment increases water permeability of 62% for epitheliod MPM cells and 66% for biphasic MPM cells ($p < 0.05$, ANOVA followed by Newman–Keuls Q-test). The subsequent treatment with β-mercaptoethanol partially restored the water permeability (Figure 31c, 32c).

Figure 29 - Representative curve of stopped flow osmotic permeability measurement obtained from MeT-5A cell line

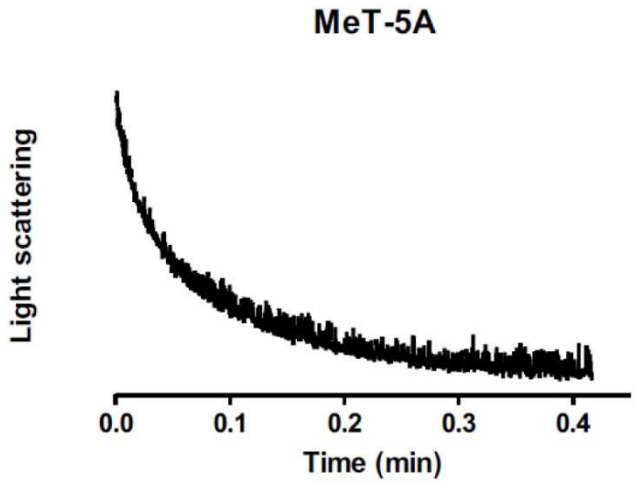

Cells were exposed to 150 mOsm hypotonic gradient.

Figure 30 - Effect of oxidative stress (a) (b) and mercury (c) on water permeability of mesothelial cells, MeT-5A

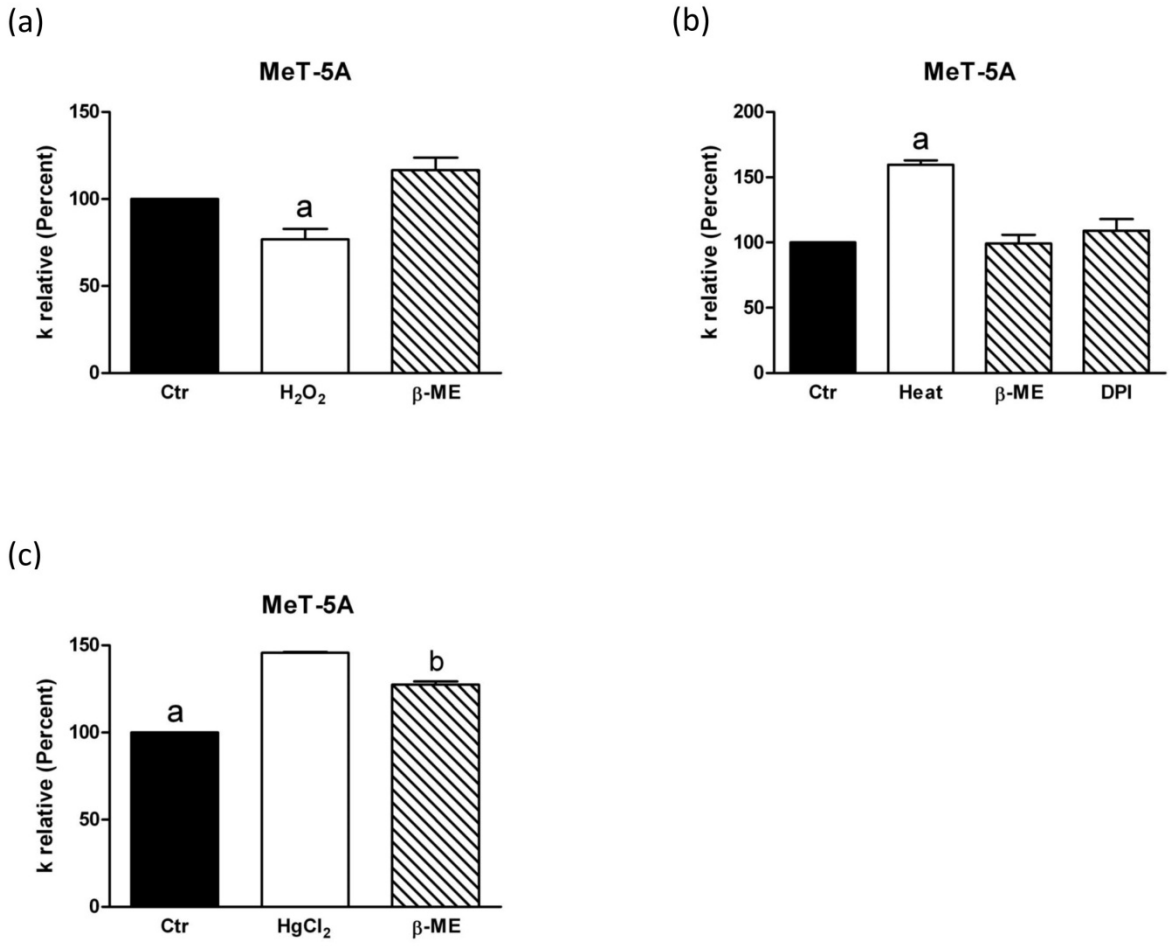

(a) Cells were exposed to 150 mOsm osmotic gradient in three different conditions: untreated cells (Ctr), cells treated with H_2O_2 (H_2O_2) and cell treated with β-mercaptoethanol after H_2O_2 treatment (β-ME). a, $p < 0.05$ versus Ctr, β-ME.
(b) Cells were exposed to 150 mOsm osmotic gradient in four different conditions: untreated cells (Ctr), heat stressed cells (Heat), cell treated with β-mercaptoethanol after heat stress (β-ME) and cells treated with DPI before heat stress (DPI). a, $p < 0.05$ versus Ctr, β-ME, DPI.
(c) Cells were exposed to 150 mOsm osmotic gradient in three different conditions: untreated cells (Ctr), cells treated with mercury ($HgCl_2$) and cells treated with β-mercaptoethanol after mercury treatment (β-ME). a, $p < 0.05$ versus $HgCl_2$, β-ME; b, $p < 0.05$ versus $HgCl_2$.
Bars represent the osmotic water permeability of MeT-5A cells expressed as percent of k relative. Values are means ±SEM of 4–15 single shots for each of 4 different experiments (ANOVA, followed by Newman–Keuls's Q test).

Figure 31 - Effect of oxidative stress (a) (b) and mercury (c) on water permeability of epithelioid MPM cells, REN

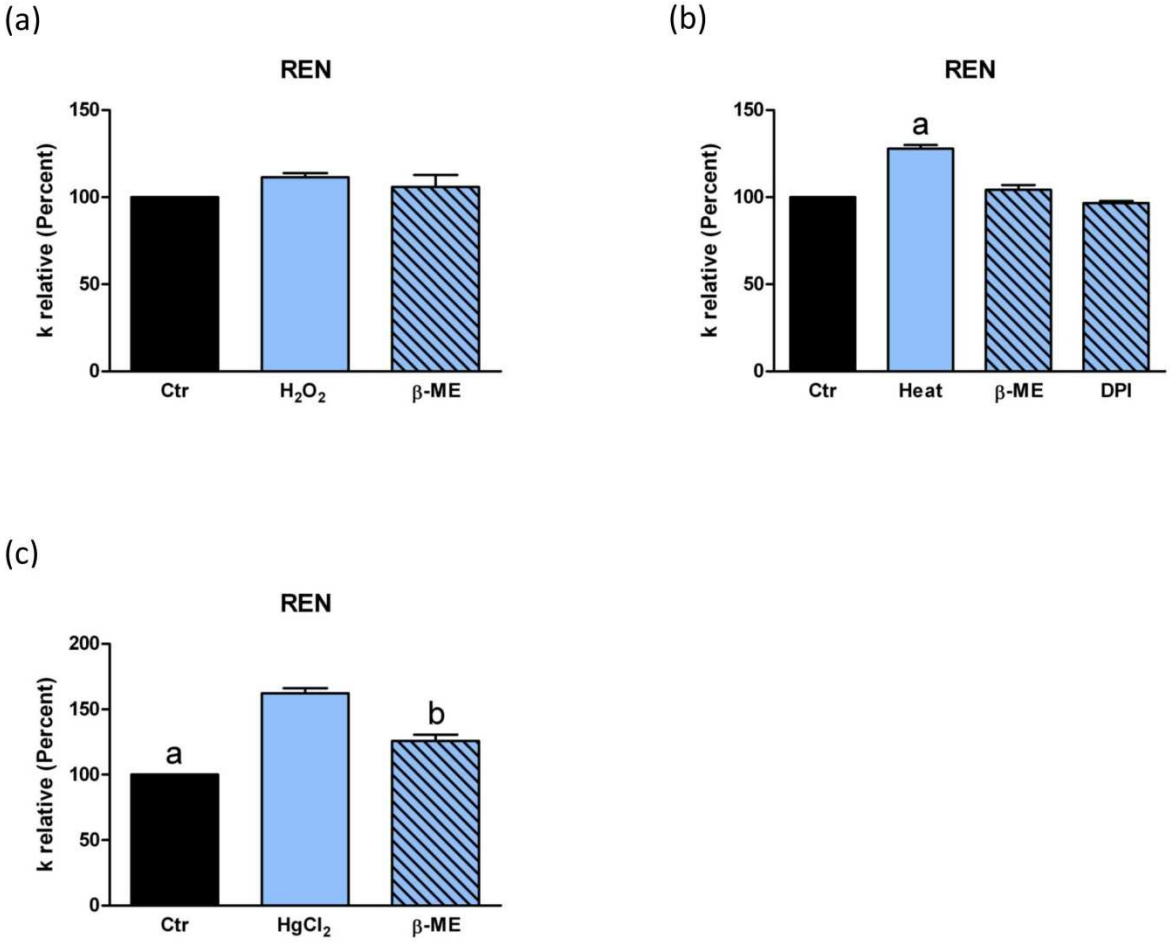

(a) Cells were exposed to 150 mOsm osmotic gradient in three different conditions: untreated cells (Ctr), cells treated with H_2O_2 (H_2O_2) and cell treated with β-mercaptoethanol after H_2O_2 treatment (β-ME).
(b) Cells were exposed to 150 mOsm osmotic gradient in four different conditions: untreated cells (Ctr), heat stressed cells (Heat), cell treated with β-mercaptoethanol after heat stress (β-ME) and cells treated with DPI before heat stress (DPI). a, $p < 0.05$ versus Ctr, β-ME, DPI.
(c) Cells were exposed to 150 mOsm osmotic gradient in three different conditions: untreated cells (Ctr), cells treated with mercury ($HgCl_2$) and cells treated with β-mercaptoethanol after mercury treatment (β-ME). a, $p < 0.05$ versus $HgCl_2$, β-ME; b, $p < 0.05$ versus $HgCl_2$.
Bars represent the osmotic water permeability of REN cells expressed as percent of k relative. Values are means ±SEM of 4–15 single shots for each of 4 different experiments (ANOVA, followed by Newman–Keuls's Q test).

Figure 32 - Effect of oxidative stress (a) (b) and mercury (c) on water permeability of biphasic MPM cells, MSTO-211H

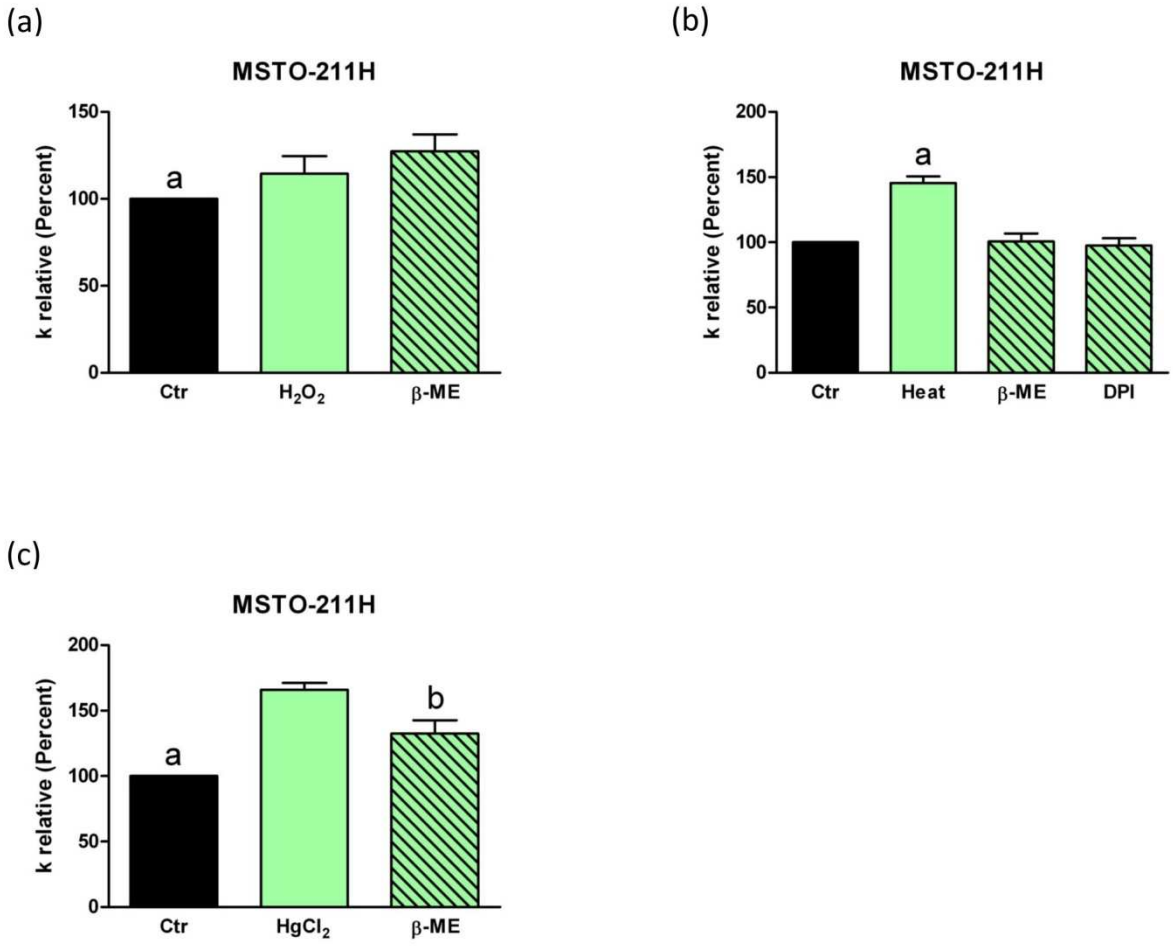

(a) Cells were exposed to 150 mOsm osmotic gradient in three different conditions: untreated cells (Ctr), cells treated with H_2O_2 (H_2O_2) and cell treated with β-mercaptoethanol after H_2O_2 treatment (β-ME). a, $p < 0.05$ versus β-ME.
(b) Cells were exposed to 150 mOsm osmotic gradient in four different conditions: untreated cells (Ctr), heat stressed cells (Heat), cell treated with β-mercaptoethanol after heat stress (β-ME) and cells treated with DPI before heat stress (DPI). a, $p < 0.05$ versus Ctr, β-ME, DPI.
(c) Cells were exposed to 150 mOsm osmotic gradient in three different conditions: untreated cells (Ctr), cells treated with mercury ($HgCl_2$) and cells treated with β-mercaptoethanol after mercury treatment (β-ME). a, $p < 0.05$ versus $HgCl_2$, β-ME; b, $p < 0.05$ versus $HgCl_2$.
Bars represent the osmotic water permeability of MSTO-211H cells expressed as percent of k relative. Values are means ±SEM of 4–15 single shots for each of 4 different experiments (ANOVA, followed by Newman–Keuls's Q test).

Effect of mercury chloride treatment on hydrogen peroxide permeability of MeT-5A, REN, MSTO-211H cell lines

H_2O_2 permeability of mesothelial and MPM cell lines (and the involvement of AQPs) was measured by a fluorescence method using the CM-H2DCFDA reagent. Two different experimental conditions were used: untreated cells (Ctr) and cells treated with 100 μM $HgCl_2$. $HgCl_2$, an AQPs inhibitor (Martins et al 2012), did not decrease the H_2O_2 permeability of each cell line, on the contrary it increased the H_2O_2 permeability of about 66% in MeT-5A. 53% in REN and 90% in MSTO-211H cells (Figure 33).

Figure 33 - Effect of mercury chloride (HgCl2) treatment on the hydrogen peroxide permeability of mesothelial (MeT-5A), epithelioid and biphasic MPM cell lines (REN and MSTO211-H)

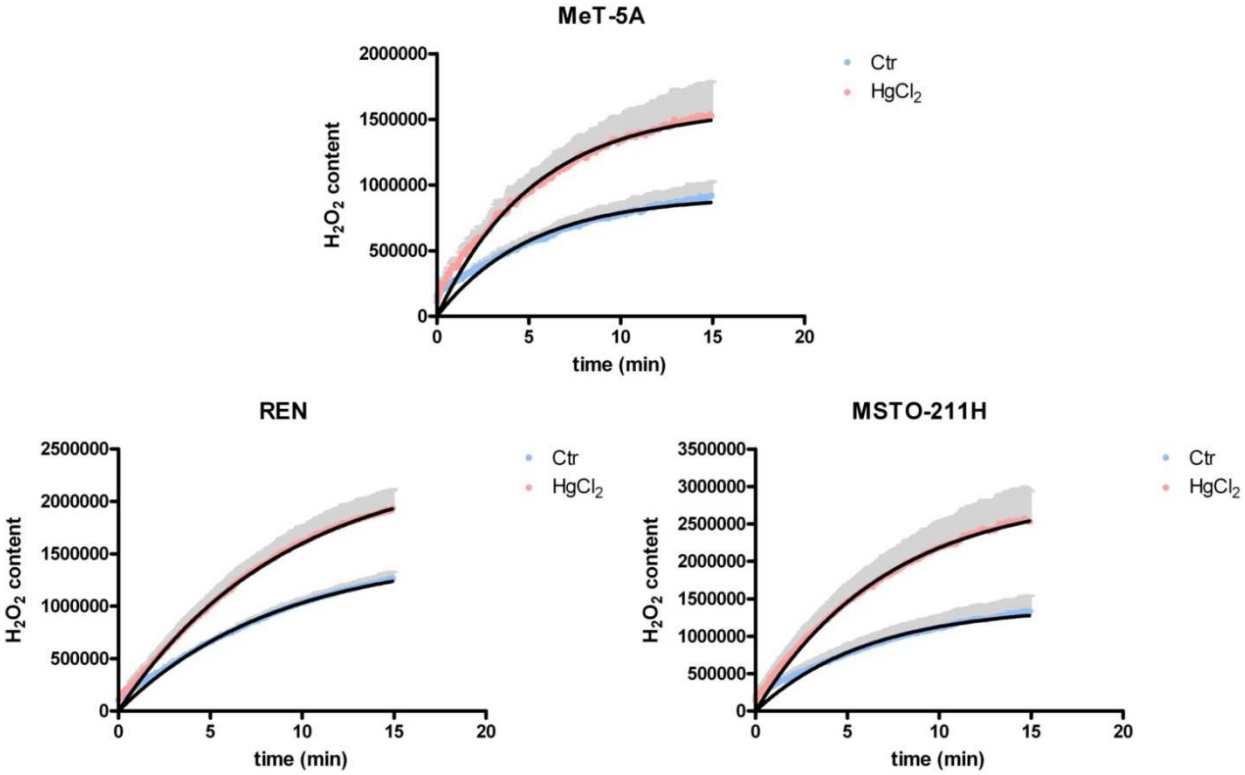

Hydrogen peroxide permeability was measured by loading the cells with CM-H2DCFDA reagent as described in Materials and Methods. Curves represent the H_2O_2 permeability of cells expressed as H_2O_2 content. Values are mean ±SEM (in gray) of three time courses for each of four different experiments. Ctr, controls ($p < 0.0001$, Student's t-test).

Silencing of AQP6 in MeT-5A, REN, MSTO-211H cell lines

The increase in water and H_2O_2 permeability after mercury treatment suggested the involvement of AQP6. To demonstrate it, silencing of AQP6 was performed with specific siRNAs as described in Materials and Methods. The silencing happened successfully in REN cell line after 48 h of incubation and in MeT-5A after 24h. Unfortunately, the silencing did not happen in MSTO-211H, at least in our experimental condition. To determine the effectiveness of siRNA in silencing AQP6 gene expression, cells were harvested and analyzed for AQP6 protein levels by immunoblotting (Figure 34).

AQP6 was silenced 70% in MeT-5A cells, 62% in REN cells.

Figure 34 - AQP6 silencing in mesothelial (a)(MeT-5A), (b) epithelioid and (c) biphasic MPM cells (REN and MSTO211-H)

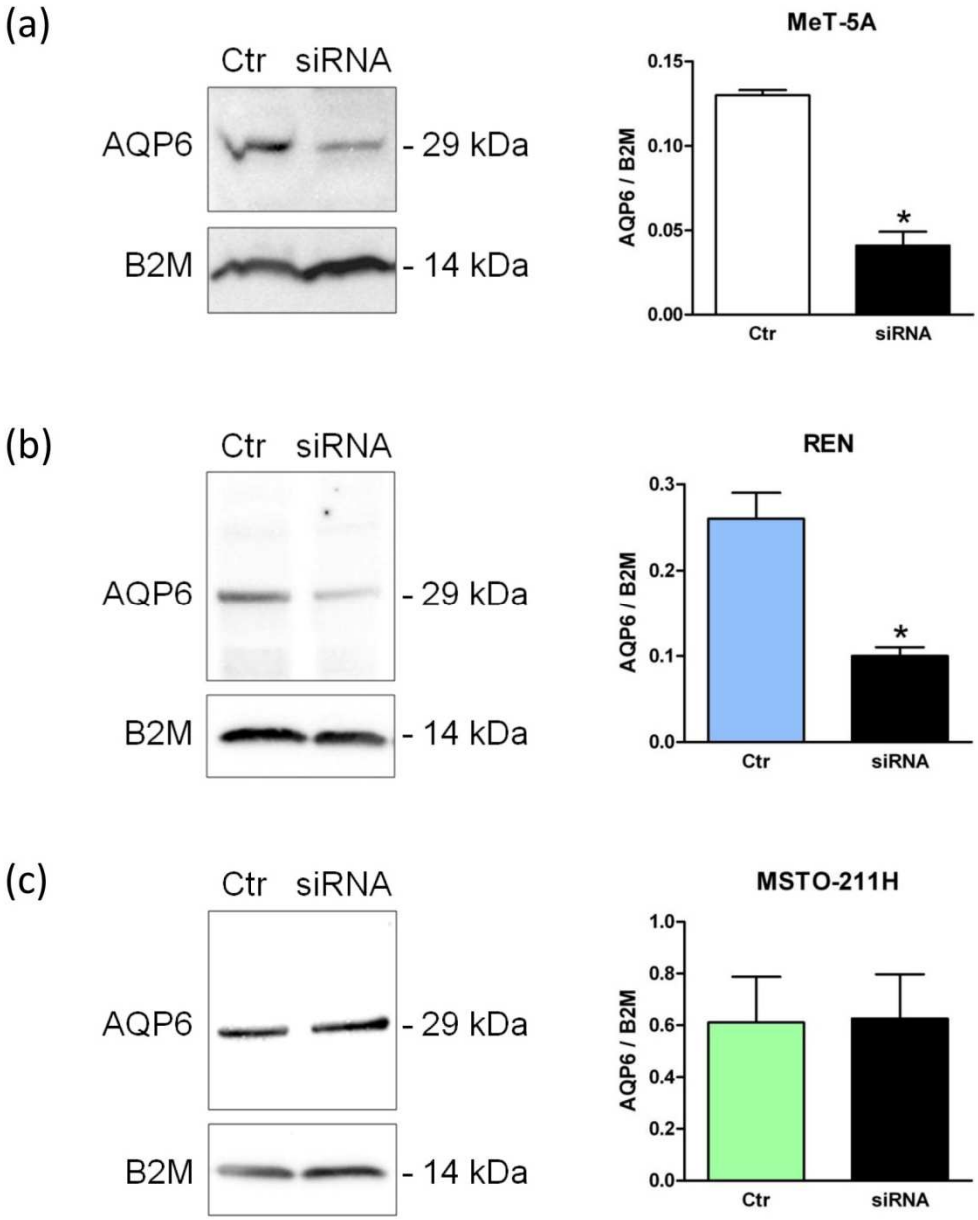

Cells were silenced and the effectiveness in silencing was tested by immunoblotting and densitometry demonstrating a significant reduced protein expression in silenced (siRNA) cells compared to controls (scrambled; Ctr) (, $p < 0.05$; Student's t test). Blots representative of three were shown. Lanes were loaded with 30 µg of proteins, then probed with anti-AQP6 rabbit polyclonal antibody and managed as described in the Materials and Methods. The same blots were stripped and re-probed with anti-β2 microglobulin (B2M) antibody, as housekeeping (* $p < 0.05$, Student's t-test). Densitometry was performed by acquiring the blot with the iBright CL1000 imaging system. Semiquantitation was performed by iBA 316 (iBright Analysis Software) and the results were normalized to the corresponding B2M.*

Effect of oxidative stress on water permeability of MeT-5A and REN cell lines after AQP6 gene silencing

AQP6 silencing differently affected the water permeability of normal mesothelial cells and REN cells: no effect in the former and a significant inhibition in the latter. This supports the results of immunostaining experiments suggesting the presence of a functioning AQP6 in the plasma membrane of REN cells. In addition, Figure 35 shows how the silencing of AQP3 and AQP5, intracellular AQPs (Figure 25a-b), do not affect the water permeability in the three cell lines.

AQP6-null MeT-5A cells treated with H_2O_2 showed the same behaviour of mock control cells demonstrating a reduced water permeability after H_2O_2 treatment (Figure 36a).

In addition to a water permeability lower than REN-normal cells, AQP6-null REN cells showed that the treatment with H_2O_2 did not increase the water permeability as in normal cells ($p < 0.05$, ANOVA followed by Newman–Keuls Q-test).

REN silenced cells both H_2O_2 treated and untreated had the same permeability (Figure 36b). This result demonstrates the involvement of AQP6 in the increased water permeability following H_2O_2 treatment.

Figure 35 - Effect of AQP3(a), AQP5 (b) and AQP6 (c) silencing on water permeability of MeT-5A, REN and MSTO-211H cells

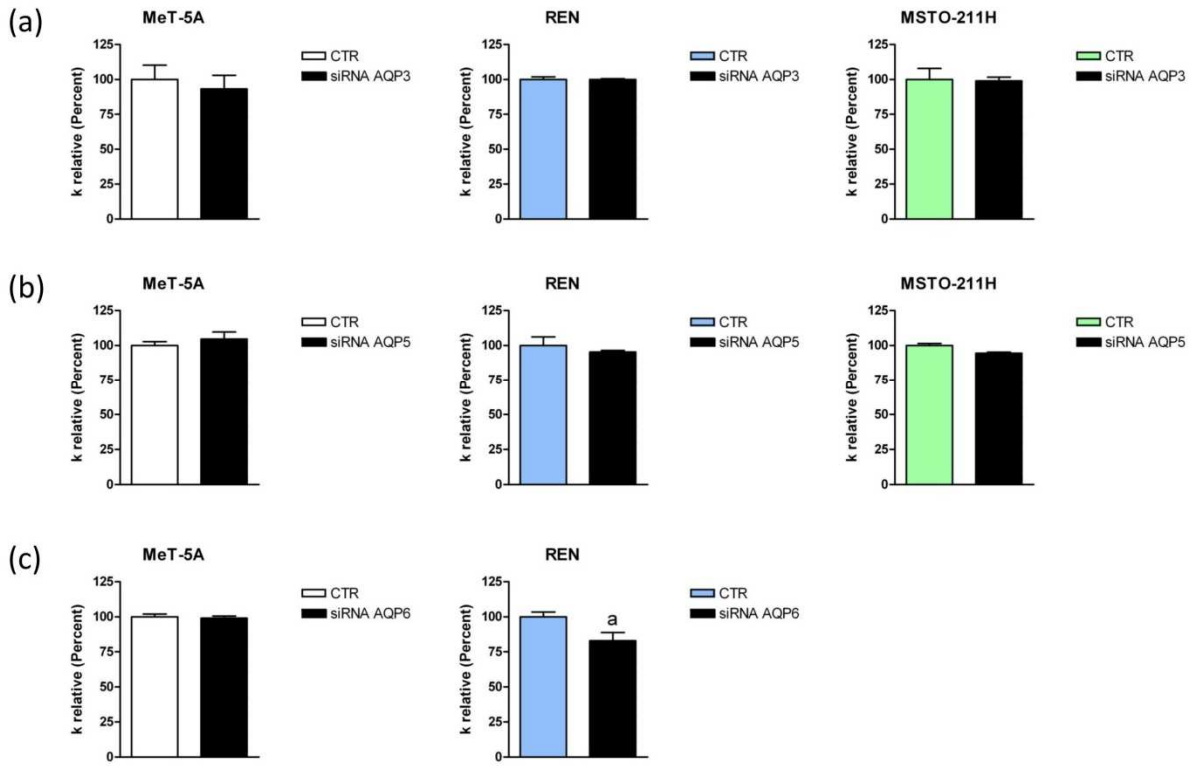

The effect of AQP6 silencing on water permeability of MSTO-211H is not presented due to the failure in AQP6-silencing. Control (CTR) and silenced cells (siRNA AQP) were exposed to 150 mOsm osmotic gradient. Bars represent the osmotic water permeability of cells expressed as percent of k relative. Values are means ±SEM of 4–15 single shots for each of 4 different experiments (a, $p < 0.05$, Student's t-test).

Figure 36 - Effect of oxidative stress on water permeability of AQP6-null epithelial (a) and epithelioid MPM cells (REN)(b)

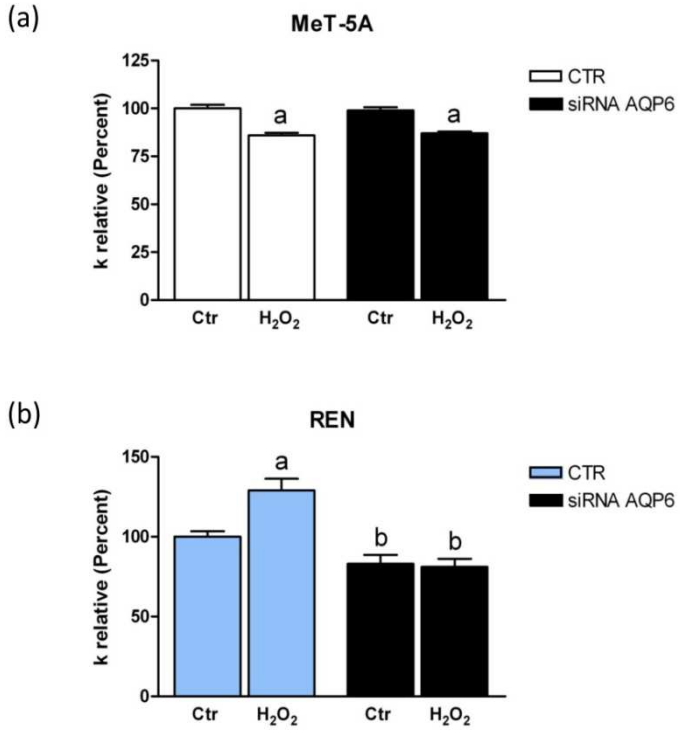

Controls (scrambled; CTR) and silenced cells (siRNA AQP6) were exposed to 150 mOsm osmotic gradient in two different conditions: untreated cells (Ctr), cells treated with H_2O_2 (H_2O_2). (a) a, $p < 0.001$ versus Ctr. (b) a, $p < 0.001$ versus Ctr of not silenced cells; b, $p < 0.05$ versus Ctr and H_2O_2 of not silenced cells.
Bars represent the osmotic water permeability of cells expressed as percent of k relative. Values are means ±SEM of 4–15 single shots for each of 4 different experiments (ANOVA, followed by Newman–Keuls's Q test).

5. Discussion

MPM is an aggressive cancer of the pleural mesothelium and it is associated with previous asbestos exposure, which often occurs 40 years previously. The prognosis is poor and the median survival ranges from 8 to 14 month from diagnosis (Bibby et al., 2016). There are three main histological sub-types: the epithelioid, the sarcomatoid and the biphasic. The standard therapeutic strategies for each MPM sub-types are the radiotherapy and the chemotherapy, even if the results are discouraging.

The need to find biomarkers, for an early diagnosis of MPM, led to the study of some proteins, including AQPs. Recent studies discovered that high levels of AQP1 expression of MPM tumor cells predict an increase in the survival rate (Driml et al., 2016; Ledda et al., 2018). In addition, AQP1 plays a role in the equilibration of the osmotic gradient in pleural effusions and in proliferation, movement and anchorage-independent growth in MPM (Klebe et al., 2015). Moreover, the discovery of peroxiporins, AQPs permeable to H_2O_2, is an evidence for their functional involvement in cancer, considering that the high intracellular concentration of ROS has been shown to have a role in cancer progression, proliferation and metastasis (Bienert and Chaumont, 2014; Moloney and Cotter, 2017). In literature unfortunately, there are no information about the expression and the functions of other AQPs normally present in MPM cells.

This study aimed to characterize the AQPs expression and function in MPM cells, in particular their involvement in ROS (H_2O_2) transport. Recently, some AQPs were shown to mediate H_2O_2 transport across the cell plasma membrane and were involved in signaling cascades and tumorigenesis (Prata et al., 2019). Two immortalized cell lines were used as models of two histological MPM subtypes, REN cell line for epithelioid MPM and MSTO-211H for biphasic MPM, while MeT-5A immortalized cell line was the normal pleural mesothelium.

Firstly, data about AQPs expression were obtained performing RT-qPCR and immunoblotting in the three cell lines (Figure 19). The expression of peroxiporins (AQP3, AQP5, AQP8, AQP9, AQP11) and of AQP6 were considered because of preliminary functional data about the behavior of these cells to mercury treatment (Figure 31c, 32c, 33c). All the AQPs tested, except AQP8, were expressed at mRNA and protein level in MeT-5A, REN and MSTO-211H cell lines. AQP3 was down regulated at mRNA level and upregulated at protein level in REN cells, probably due to a slower turnover of AQP3. AQP5 protein was downregulated in MSTO-211H and this expression

corresponded to the trend of AQP5 mRNA expression. AQP6 was downregulated at mRNA level but the protein levels were unchanged in REN and only slightly downregulated in MSTO-211H cells. AQP9 was upregulated in REN at mRNA level, while it was upregulated in MSTO-211H at protein level, while the mRNA and protein expression levels of AQP11 did not change among the different cell lines (Figure 19–24).

Despite immunoblotting results did not point out a smaller elected set of AQPs, subsequent immunolabelling techniques gave important information about the localization of this set of AQPs in the three cell lines (Figure 25). Unexpectedly, AQP3 and AQP5 were expressed in the cytoplasm in the three cell lines, while the immunolabelling signal of anti-AQP6, anti-AQP9 and anti-AQP11 in mesothelial cells changed from a cytoplasmatic localization in mesothelial cells to a plasma membrane localization in MPM cells. This shifted localization may suggest a development in cancer progression, and a possible change in AQPs function due to the different localization from normal cells to cancer cells. In addition, the anti-AQP6, anti-AQP9 and anti-AQP11 immunolabeling signals were not equally distributed on plasma membranes, but they localized in specific regions of plasma membranes and cellular protrusions facing other cells. AQP9 was already identified in cellular protrusions involved in cell migration (Morishita et al., 2019). It is important to underline that the plasma membrane's localization on MPM cells was detected only in samples with a high percentage of cellular confluency, during the proliferating phase, and not in sample with a low percentage of cellular confluency (data not shown). These results suggest the key role of AQPs localization in MPM cells in cancer proliferation, migration and progression.

The AQP6 localization on plasma membrane was studied with confocal immunofluorescence in the three cell lines (Figure 27). REN and MSTO-211H cells showed a yellow co-localization signal between AQP6 and the plasma membrane marker, confirming the localization on plasma membrane.

The osmotic water permeability of benign human mesothelial cells was measured and compare to that of MPM cells. The Pf of REN and MSTO-211H was significantly lower than that of MeT-5A (see Results). Katkova et al. (2019) reported similar results with a significantly lower Pf in epithelioid (M14K) and sarcomatoid (ZL34) cells compared to that of MeT-5A cells. Successively, functional experiments were also performed to evaluate the effect of oxidative stress on water and H_2O_2 permeability of mesothelial and MPM cells. ROS are important tumor-inducing factors but also tumor-suppressing (Wang and Yi, 2008). Different mechanisms significantly increase ROS levels in cancer

cells, ROS that influence the tumor development by mediating initiation, progression and metastasis. Most cancer chemotherapeutic agents act by increasing the already high level of intracellular ROS (Yang et al., 2018). The exceeding of a ROS concentration above a critical threshold lead to cell death, mostly via apoptosis. Redox-homeostasis of tumor cells should be carefully considered since normally elevated levels favor cancer cell functions (progression and metastasis) but a further ROS elevation lead to apoptosis (Liou and Storz, 2010).

In our experiments the oxidative stress conditions were achieved via cellular incubation with H_2O_2 (exogenous stress) and via heat stress (endogenous stress). Results showed that the water permeability of mesothelial cells was reduced by H_2O_2 treatment, and not by heat stress (Figure 30a, b). On the contrary, the water permeability of MPM cells was not influenced by H_2O_2 treatment, but it was considerably increased by heat stress (Figure 31a-b, 32a-b). These data suggest that MPM cells could be resistant to endogenous oxidative stress increasing H_2O_2 efflux via AQPs. These results asses the hypothesis that AQPs, intended as "ROS scavengers", prevent the apoptosis of MPM cells by setting them free from the high levels of H_2O_2. This hypothesis could explain why radiotherapy and chemotherapy are ineffective in MPM treatment: MPM cells could avoid apoptosis due to the presence of H_2O_2-permeable AQPs. A recent study by Soverall's group showed that AQP5 gating could be involved in the fine-tuning of cell sensitivity and/ or resistance to oxidative external conditions and could induce cell proliferation and migration (Rodrigues et al., 2019).

The presence in the plasma membrane of the three types of cells of a functioning AQP6 was also demonstrated in a functional way, evaluating the water permeability and the effect of mercury chloride (Figure 30c, 31c, 32c). The increase in water permeability in the three cell lines is due to the presence of AQP6, an AQP that increases its water and anion permeability under mercury treatment (Yasui et al., 1999). This result was further confirmed by results of H_2O_2 permeability experiments obtained using the CM-H2DCFDA probe: treatment with mercury chloride increased the H_2O_2 influx in each cell line considered (Figure 33). This is the first study demonstrating that AQP6 possesses a H_2O_2 permeability.

The involvement of AQP6 in morphological and functional characterization of MPM cells led to the decision to further understand the impact of AQP6 in oxidative stress and in cancer proliferation. For this reason, functional experiments were performed in AQP6-

null cells. AQP6 was silenced in Met-5A and REN cells with an efficacy of 70% and 62% respectively, but it was not knocked down in MSTO-211H cells (Figure 34).

In this regard, several hypotheses can be formulated. The first is that the transfectant reagent is unable to permeabilize MSTO-211H cells to siRNA. The second is that MSTO-211H cells may have mutations in the target sequences of siRNAs. For this reason, the effect of the endogenous oxidative stress was studied only in AQP6-null mesothelial cells and epithelioid MPM cells.

The H_2O_2 treatment in AQP6-silenced MeT-5A cells decreased the water permeability as previously reported for not silenced cells (Figure 36a). In opposite to previous functional data of REN cells, the H_2O_2 treatment did not increase the water permeability in silenced REN cells (Figure 36b). This data could make the AQP6 a possible target to make MPM cells more sensitive to oxidative stress created by conventional chemotherapy and radiotherapy. In addition, the AQP6 silencing did not decrease the water permeability in untreated MeT-5A cells, but it decreased the water permeability in untreated REN cells, confirming the intracellular and plasma membrane localization of AQP6 in MeT-5A and REN cells, respectively.

6. Conclusions

This is the first study analyzing the AQPs functioning role as H_2O_2 channel in MPM cells and their possible involvement in chemotherapy drug resistance. The results seem to suggest a great capacity of MPM cells to resist to oxidative stress and this, unfortunately, would explain the resistance of this cancer to chemotherapeutics drugs.

More experiments are necessary to complete the presented data, but we could speculate that a possible genetic mutation/s of one or more AQPs might alter H_2O_2 handling by MPM cells and makes them resistant to chemotherapy-induced apoptosis.
Medraño-Fernandez et al. (2016) found that cells expressing the mutant AQP8 C53S are more resistant to stressful stimuli and to apoptosis than the wt expressing ones. Reduction of AQP/s functionality could make chemotherapy more effective.

The identification of the cellular mechanisms underlying this could lead to the development of pharmacological/biological strategies, not new chemotherapy drugs but agents that make effective therapeutic ROS-inducing anticancer molecules.

7. Future Perspectives

Covid19 pandemic has slowed down the MPM research plan. The research will go on silencing AQP6 in the biphasic cell line, then proliferation and migration assays will be performed in the three cell lines to verify the involvement of AQP6 protein in cancer propagation. Subsequently, we will silence the other two plasma membrane AQPs, AQP9 and AQP11, to verify their role in H_2O_2 permeability, progression and migration.

3th Research Plan:

Dual Aquaporins and Sigma1 Receptor modulators (DAS) are new compounds to counteract Oxidative Stress

1. Introduction

The discovery of Sigma1 Receptor

The Sigma1 Receptor (S1R) was discovered for the first time in 1976 during pharmacological studies of opioid and opioid-like compounds in the nondependent and opioid-dependent chronic spinal dog (Martin et al., 1976). These studies led to the classification of three distinct opioid receptor subtypes: Mu, Kappa and Sigma. Mu and Kappa receptors are closely related to one another than Sigma receptors that have different characteristics. Unlike canonical opioid receptors, the Sigma receptors have a divergent ligand binding profile, they binds with high affinity only the (-)-enantiomers and have no affinity for naloxone and naltrexone (Largent et al., 1987). Other pharmacological studies divided the Sigma receptors in Sigma1 and Sigma2 subtypes (Hellewell and Bowen, 1990). Sigma2 receptor localizes in the endoplasmic reticulum and lysosomes, where it may bind to cholesterol and it is overexpressed in some cancers (Schmidt and Kruse, 2019). In 1995, the different characteristics of S1R were confirmed by its molecular cloning, and thereafter called Sigma non-opioid intracellular receptor 1 (Hanner et al., 1996).

Molecular structure of S1R

The S1R gene is located on human chromosome 9 in a region that is associated with several psychiatric disorders (Prasad et al.; 1998). The protein consists of 223 amino acids, with a predicted molecular weight of 25.3 kDa. S1R is not similar to any other mammalian proteins, but its sequence is shared among different species with a >93% identity (Hanner et al., 1996). The molecular structure of S1R was extensively studied from its discovery until now, but it remains controversial about two topology aspects. The first topology aspect concerns the transmembrane architecture, while the second regards the position of N- and C-termini.

The two-pass transmembrane architecture is supported by solution NMR studies (Ortega-Roldan et al., 2015) and a 3D homology model (Laurini et al., 2017) validated by ligand binding, in silico/in vitro mutagenesis and NMR studies. The two-pass architecture is characterized by the transmembrane domains TMI, TMII and by two hydrophobic domains, called *steroid binding domain like I and II* (SBDL I and II) because of their homology of the *steroid binding domains* of yeast and other fungal sterol isomerases. SBDL I partially overlaps with the TMII domain, while SBDL II is positioned in the membrane flanking region of the receptor C-terminus (Figure 37a). The N- and C-terminus facing the ER lumen. The two-pass architecture is characterized by two other structurally elements: the first is a typical arginine-arginine endoplasmatic reticulum retention signal near the N-terminus of the protein. The second is a signature motif in TMII that occurs with high frequency in membrane proteins that favor helix-helix interactions, involved in oligomerization. In addition, the S1R ligand binding site is formed by SBDL I, SBDL II and a part of TMI domain (Figure 37a) (Laurini et al., 2017). The two-transmembrane domain model of S1R was based on biochemical and molecular biology studies in Xenopus oocytes (Aydar et al., 2002), in Chinese hamster ovary cells (Hayashi and Su, 2007) and in vitro dimerization studies performed by Gromek and collaborators (2014).

On the other side, the single-pass transmembrane architecture is supported by Schmidt and coworkers that undertook biochemical and crystallographic studies to elucidate the protein structure in complex with two distinct ligands (Schmidt et al., 2016). The crystallography structure reveals a trimeric organization with a single transmembrane domain in each monomer. The C-termini of monomers are cytosolic and show a beta-barrel fold with the ligand at its center, flanked by four alpha helices (Figure 37b). The

ligand binding domain is highly conserved in sequence across species (Schmidt et al., 2016 and 2018). In addition, the single-transmembrane domain is corroborated by later proximity labeling (Mavylutov et al.,2018) and by a novel receptor homomer assays (Yano et al., 2018) in cells.

The second controversial topology aspect concerns the position of N- and C- termini. Some supporters of the two-transmembrane architecture suggested the N- and C-termini facing the cytosol (Aydar et al., 2002), while others suggested that both termini facing the ER lumen (Hayashi and Su, 2007; Laurini et al., 2017). While Schmidt and collaborators, supporters of single-transmembrane architecture, suggested the N-terminus in the lumen and the C-terminus in the cytosol. Mavylutov and collaborators, to clarify the exact topology of N- and C- terminus, applied the ascorbate peroxidase 2 (APE2) approach using electron microscopy (Mavylutov et al.,2018). Their study is consistent with the crystal structure proposed by Schmidt et al (2016), except that the N-terminus of the protein faces the cytosol (Figure 37c).

Laurini et al. (2017) suggest that the differences between NMR and crystal structures of membrane proteins may arise from a combination of different technical conditions adopted in the two procedures. To support the validity of these studies is necessary to perform crystallographic experiments under the conditions adopted for NMR/in silico experiments and vice versa. In conclusion, Laurini and collaborators (2017) proposed that Sigma1 Receptor probably adopts different structures under solid (revealed by the crystal structure) and solution states (revealed by the in silico and NMR models).

Figure 37 - The controversial molecular structures of Sigma1 Receptor (S1R)

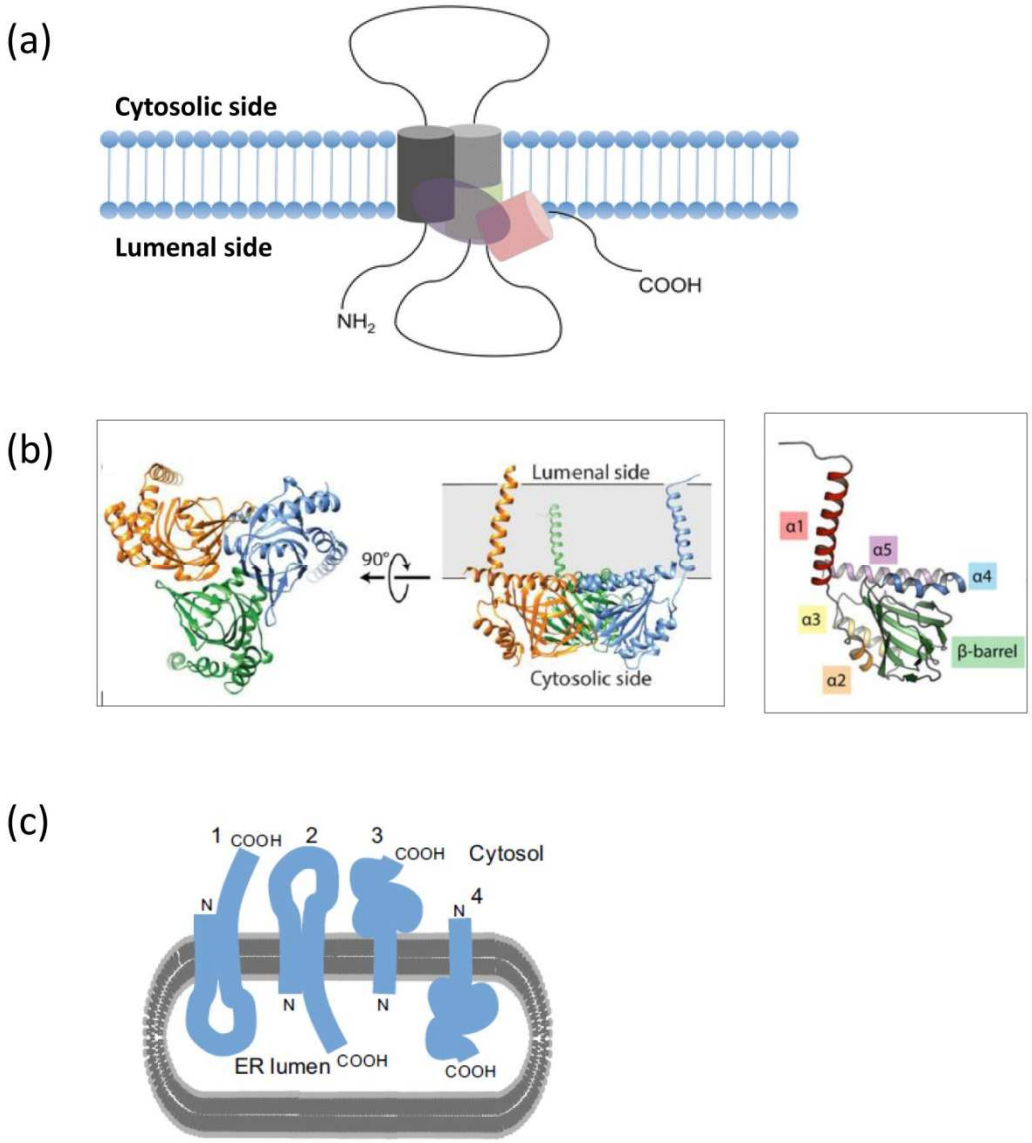

(a) Two-pass transmembrane architecture of S1R and its ligand binding site consisting of TMI (dark gray), TM II (light gray), SBDL I (light green) and SBDL II (light pink) as hypothesized from photoaffinity studies. The binding site is encircled in the transparent (light purple area) (Laurini et al., 2017).
(b) Single –pass transmembrane architecture of S1R. Left panel: Viewed perpendicular to the membrane plane, the receptor shows a triangular structure comprised of three tightly associated monomers, each with a single transmembrane domain at a corner of the oligomeric triangle. From the side, the receptor reveals a flat membrane-associate surface. The location of the membrane plane is shown in grey (Schmidt et al., 2016). Right panel: The structure of a single S1R monomer, with the secondary structural elements (Schmidt et al., 2018).
(c) Three topologies of S1R in the endoplasmatic reticulum (ER) membrane have been proposed. 1) Both N- and C-termini are cytosolic with two TM domains (Aydar et al., 2002), 2) Both N- and C-termini are luminal with two TM domains (Hayashi and Su 2007; Laurini et al., 2017), 3) N-terminus in the lumen with one TM domain (Schmidt et al., 2016), 4) N-terminus in the cytosol with one TM domain (Mavylutov et al., 2018).

Molecular roles of S1R

The S1R is a ligand-operated chaperone that modulates signaling pathways inside of the cell. Ligands of the S1R are classified in agonists and antagonists. Antagonist ligands mimic as a genetic knockdown of the S1R, while agonists exert an S1R-dependent effect. The lack of mammalian proteins similar to the S1R represents a problem in functional studies. The closest homolog of the S1R is a sterol isomerase of the yeast, however the S1R has no sterol isomerase activity (Schmidt and Krouse, 2019).

The role of S1R in cellular signaling

The S1R is involved in intracellular calcium, ion channel and G protein-coupled receptor (GPCR) signaling. Co-immunoprecipitation experiments demonstrated the interaction of the S1R with the inositol triphosphate receptor (IP_3) and with a potassium channel ($K_v1.4$) (Hayashi and Su, 2001; Aydar et al., 2002). Many experiments report the modulation of other signaling pathways through S1R-protein interactions. Until now, the S1R has been demonstrated to interact to at least 49 proteins, which are divergent in sequence and structure (Schmidt and Krouse, 2019). Despite these S1R-protein interactions studies, more work is necessary to clarify if these modulatory effects result from a direct S1R-protein interaction or if sigma ligands directly modulate proteins independently of the S1R (Schmidt and Krouse, 2019).

The most well-characterized S1R-protein interaction is its association with itself. In vitro and in vivo studies demonstrated that S1R exist in monomeric and oligomeric form. Many of these studies suggested that monomer and dimer forms favor agonists, while antagonists are favored by higher order oligomers (Ramachandran et al., 2007; Chu et al., 2013; Gromek et al., 2014; Mishra et al., 2015). In addition, these in vivo experiments confirmed the existence of S1R oligomeric forms that are constitutively regulated by the ligand types, agonist or antagonist. Higher oligomeric forms may work as a storage for the active forms of S1R, while the dimer and the monomer may represent the functional chaperone state. However, the S1R monomer has been shown to bind to protein partners as a functional unit, which may suggest a secondary function independent of the chaperone activity of the S1R (Figure 38). Subsequent crystallographic experiments demonstrated that agonist ligands bind the receptor in the same binding pocket as antagonists, but it occupies a distinct region of that pocket. This binding could induce a small conformational change in helix alpha4 that could explain why these ligands may favor smaller molecular weight forms of S1R (Schmidt and Kruse, 2019).

The role of S1R as a ligand-operated chaperone

The discovery of a large number of S1R-protein interactions is consistent with the idea that S1R is a ligand-operated chaperone. The S1R in the chaperone model, proposed for the first time by Hayashi and Su (2007), exist in a resting state at the mitochondrion-associated membrane (MAM) of the endoplasmatic reticulum (ER). The MAM is a specialized region of the ER membrane that forms a contact with the mitochondrial membrane, thought to be important for the control of calcium homeostasis, lipid metabolism and autophagy (Weng et al., 2017). The ER can change is shape forming a reticular structure throughout the entire cytoplasm, thus enabling physical connections to other subcellular structures, such as the plasma membrane and mitochondria (Hayashi et al., 2009; Kerkhofs et al., 2017). At the MAM, S1R interact with a chaperone called the Binding immunoglobulin Protein (BiP) forming a complex, which has a role in protein folding and quality control. However, S1R dissociates from BiP and interacts with other proteins and other organelles when there is an agonist or a decrease in ER calcium concentration (Figure 38) (Weng et al., 2017).

Figure 38 - Model of S1R oligomeric forms in vivo

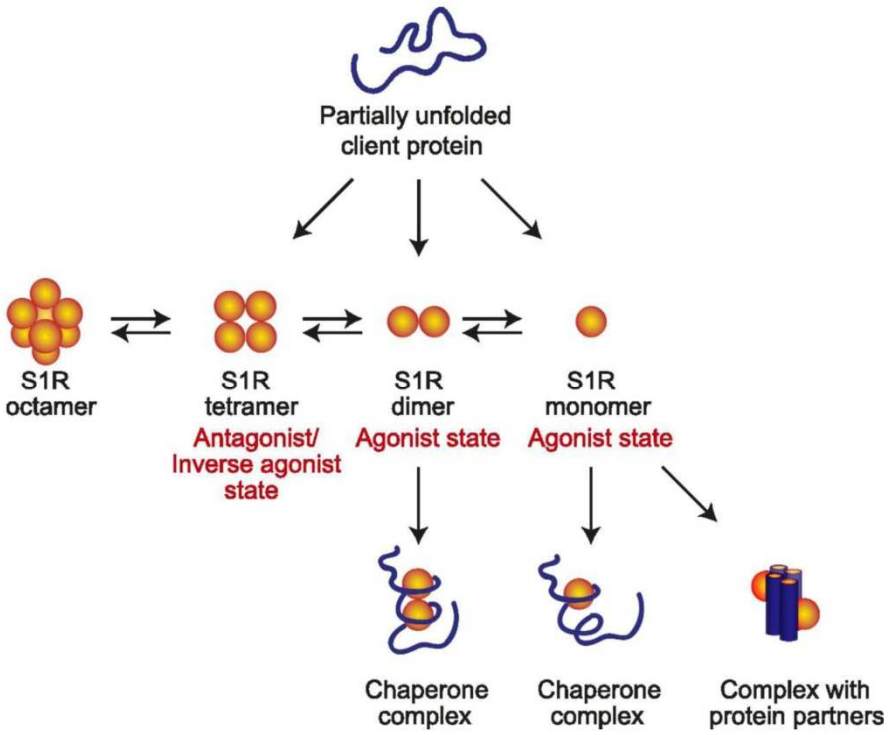

(Chu and Ruoho ,2015)

The role of S1R in bioenergetics

The contact between ER and mitochondria outer membrane permits the passage of Ca2+ from ER to mitochondria through IP3 receptors. The S1R stabilizes the activated IP3 receptor ensuring Ca2+ influx at MAMs. The flux of Ca2+ enables the regulation of bioenergetics via activation of enzymes involved in TCA cycle and the subsequent production of ATP. In addition, the flux of Ca2+ regulates the free radical formation in mitochondria (Hayashi and Su, 2007).

The role of S1R in oxidative stress

Cells are protected against ER stress by the overexpression of S1R and by the treatment of its agonist, on the other side, S1R knockdown and antagonist treatment can make cells more sensitive to stress (Hayashi and Su, 2007). This idea correlates with the chaperone model of the S1R. According to the role of S1R in pathway signaling, S1R can modulate the ER stress pathway interacting with ER stress response regulatory protein IRE1 (Rosen et al., 2019). The association of S1R with IRE1 is also triggered by high level of ROS in mitochondria (Mori et al., 2013). Happy and collaborators (2015), inducing ROS generation and ER stress in S1R-knockdown cancer cells, observed an inhibition of cellular proliferation. Another study has demonstrated that S1R activates the antioxidant response element (ARE) to over-express the mRNA of NAD(P)H quinone oxidoreductase 1 and superoxide dismutase 1 (Pal et al., 2012).

Additionally, changes in ER lipid composition are associated with ER stress response and these changes can be influenced by the S1R that localizes to cholesterol-rich lipid microdomains (Hayashi and Su, 2003). Recently, Goguadze and collaborators (2019) confirmed that the S1R activity is strictly related to mitochondrial physiopathology. In physiological condition S1R agonists generate a moderate oxidative stress, while in pathological/stressed conditions they contribute to a rapid restoration of mitochondrial physiology, upregulating cellular antioxidant pathways.

Accumulating evidence suggests that modulation of S1R is an effective strategy to counteract oxidative stress, although mechanisms responsible for the antioxidant effects exerted by S1R have not been completely clarified yet (Pal et al., 2012; Wang et al., 2012; Goguadze et al., 2019). S1R modulators are under investigation for treating several diseases involved in oxidative stress (Maurice and Su, 2009) such as cardiovascular diseases, neurodegenerative disorders, diabetes, ischemia/reperfusion, Alzheimer's (Villard et al., 2009; Villard et al., 2011; Su et al., 2010) and CNS inflammatory conditions associated with cocaine and HIV (Su et al., 2010; Yao et al., 2010).

New antioxidant compounds

For many debilitating pathological conditions, oxidative stress is one of the underpinning mechanisms, and therapies implementing antioxidant effects may enhance healing potential. Professor Simona Collina and coworkers have recently discovered a series of aryl aminoalkyl ketones endowed with good S1R binding affinity and antioxidant properties (compounds 1-3, Figure 39) (Rui et al., 2018), as viable neuroprotective pharmacological tools (Vigani et al., 2019). Of note, the potent S1R agonist, called RC-33, identified in their lab is currently under investigation in vivo for its potential against Amyotrophic Lateral Sclerosis and for recovery of the damage of Spinal Cord Injury (Vigani et al., 2019).

Aquaporins modulators and oxidative stress

As stated above (see Conclusions of the 1st Research Plan, pag. 70, and of the 2nd Research Plan, pag. 113), the control of peroxiporins-mediated H_2O_2 permeability seems to have a great importance in regulating cell signaling and survival during oxidative stress (Medraño-Fernandez et al., 2016; Laforenza et al., 2016; Pellavio et al., 2017). For living cells, the functioning of peroxiporins is critical to ensure ROS wasting and is considered an antioxidant system. Various cellular stress conditions, including heat and incubation with H_2O_2, reduce the AQP-mediated H_2O_2 transport (Medraño-Fernandez et al., 2016; Laforenza et al., 2016; Pellavio et al., 2017). Recently, a number of natural antioxidants, such as flavonoids, flavanones and terpenoids, has been identified as AQPs modulators (Pellavio et al., 2017).

The natural antioxidants studied are quercetin, marrubin, curcumin, ASME ((R)-aloesaponol III-8 methyl ether) and naringenin that are characterized by different scaffolds and different aromatic substitutions. These natural compounds have different profiles of free radical scavenging properties (FRS), quercetin possess the higher FRS. The addition of quercetin, naringenin, ASME and marrubin, during or after heat-treatment, are able to prevent or restore the AQP permeability. Curcumin do not prevent or restore the AQP permeability, on the contrary, inhibits AQP-mediated water permeability also in the absence of oxidative stress (Pellavio et al., 2017).

This suggests the possibility to chemically modulate the pore gating of peroxiporins, supporting the idea that AQPs are druggable targets.

As a whole, these results open new direction to the development of novel therapeutic treatments to regulate cell signaling and survival during oxidative stress in normal and pathologic conditions, like cancer and degenerative diseases (Thanan et al., 2014; Uttara et al., 2009).

2. Objectives

This work aims to evaluate the potential of S1R modulators as AQPs interfering compounds, studying:

1) the *in vitro* effect of the well-established S1R agonists PRE-084 (Su et al., 1991), RC-33 (in racemic and enantiomeric configured form) (Rossi et al., 2013a) and of the S1R antagonist NE-100 (Okuyama et al., 1993), on AQPs permeability

2) the *in vitro* effect of three S1R ligands (compounds 1-3) developed by Professor Simona Collina and coworkers (Rui et al., 2018) on AQPs permeability. These ligands have been developed and synthesized starting from natural substances previously tested on the permeability of AQPs, such as curcumin (Pellavio et al., 2017; Rui et al., 2018). This step is essential to understand if the modifications made to these substances could improve the permeability of AQPs in oxidative stress conditions.

3) the *in vitro* effect of the S1R modulators on AQP-mediated water permeability of S1R-silenced cells. These experiments were necessary to understand if the protective effect of the compounds on oxidative stress was indirect, S1R-mediated, or direct on the AQPs functioning.

3. Materials and Methods

Compound synthesis

Our collaborators, Professor Simona Collina and coworkers, have recently discovered a series of aryl aminoalkyl ketones endowed with good S1R binding affinity and antioxidant properties (compounds 1-3, Figure 39), as viable neuroprotective pharmacological tools (Vigani et al., 2019). Of note, the potent S1R agonist, called RC-33, identified in their lab is currently under investigation in vivo for its potential against Amyotrophic Lateral Sclerosis and for recovery of the damage of Spinal Cord Injury (Vigani et al., 2019).

The group of Professor Simona Collina has synthetized RC-33 and compounds 1-3. The racemic and enantiomeric RC-33 was synthetized according to the procedures published by Rossi et al. (2013), while compounds 1-3 were prepared following the procedure reported by Rui et al. (2018).

Figure 39 - S1R ligands tested in this study to evaluate their AQPs-mediated antioxidant effect

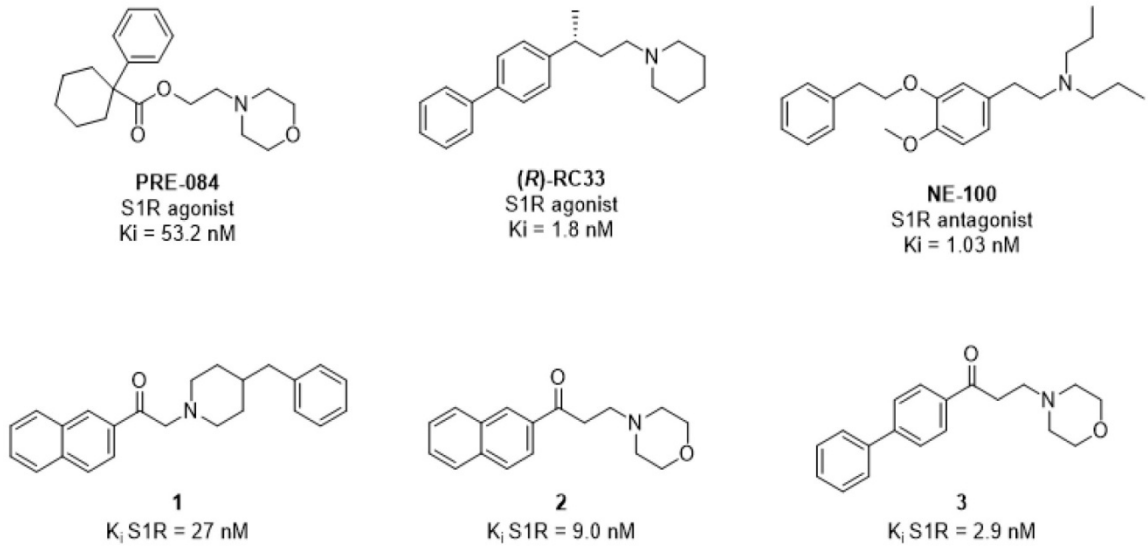

Cell Culture

HeLa cells were grown in plastic tissue culture flasks using Dulbecco's modified minimal essential medium high glucose, supplemented with 10% fetal bovine serum, 1% L-glutamine, 1% penicillin and streptomycin and maintained at 37°C in a humidified atmosphere of 5% CO2, 95% air.

Water Permeability Measurements

Osmotic water permeability was measured in HeLa cells suspension by the stopped-flow light scattering method (Laforenza et al., 2016) (for more details pag. 50). To evaluate the antioxidant effect of the test compounds on water permeability HeLa cells were divided into different groups: a) controls, cells left at room temperature (21°C); b) heat-stressed cells, cells subjected to heat-treatment by placing them in a water thermostatic and shacking bath at 42°C for 3 h; c) heat-stressed cells pre-treated, cells heat-stressed with the antioxidants compounds at 20 μM final concentration (dissolved in methanol). Moreover, to test the possible capacity of the molecules to affect the AQP gating in eustress condition, HeLa cells were treated in the presence and in the absence of the compounds by incubating at 21°C for 3 h.

Hydrogen Peroxide Permeability Measurements

Dose-response relationship was assessed for compound 2 and 3 by measuring the hydrogen peroxide concentrations in heat-stressed HeLa cells. Hydrogen peroxide levels were measured by a fluorescence method using the 5-(and-6)-chloromethyl-20,70-dichlorodihydro-fluorescein diacetate, acetyl ester reagent (CM-H2DCFDA) (Thermo Fisher Scientific Inc., Italy) (Pellavio et al., 2017). Briefly, cells were centrifuged at 200 rcf for 5 min. The cell pellet was resuspended in PBS with increasing concentrations of the compounds 2 and 3 (0, 5, 10, 20, 40 μM final concentration) and subjected to heat-stress as above indicated. Before terminating the incubation, the CM-H2DCFDA reagent was added at 10 μM final concentration and leaved for further 15 min at 42°C. Then, cells were centrifuged, and the pellet resuspended in PBS. Hydrogen peroxide levels were measured by using a CLARIOstar® microplate reader (BMG LABTECH, Ortenberg, Germany). Values are expressed as arbitrary unit per mg total protein.

Gene silencing

S1R knockdown was performed by treating HeLa cells with ON-TARGETplus SMARTpool Human SIGMAR1 siRNA (FE5LHUMANXX0005; Carlo Erba Reagents Srl, Italy) at a 25 nM final concentration. Negative controls were done with scrambled siRNA. siRNAs were diluted in siRNA Diluition Buffer (N0413, Sigma-Aldrich, USA) and mixed with N-TER peptide (N2788, Sigma-Aldrich, USA) pre-diluted in distilled water, according to the manufacturer's instructions to create the Target siRNA Nanoparticle Formation Solution (NFS). HeLa cells at 50% confluence were removed from the medium and replaced with fresh medium containing NFS. After 30 min incubation at 37°C, the NFS was diluted in the culture medium and added to the cells and incubated at 37 °C for 24 h.
Immunoblotting was used to validate the gene silencing and the silenced cells were used 24 hours after transfection.

Immunoblotting

Cells were homogenized with a Dounce homogenizer in RIPA buffer (150 mM NaCl, 0.5% sodium deoxycholate, 0.1% SDS, 0.1% Triton X-100, 50 mM Tris-HCl, pH 8) supplemented with a protease inhibitor cocktail (cOmplete Tablets EASYpack, 04693116001, Roche, Germany).
Immunoblotting was carried out as previously described (pag. 52) loading 30 µg proteins. Membranes were incubated overnight with anti-Sigma1 Receptor (B-5) (sc-137075, 1:500 dilution; Santa Cruz Biotechnology, Inc., USA) in a blocking solution (Tris buffered saline, 5% skimmed dry milk and 0.1% Tween). The membranes were washed thrice and incubated for 1 h with peroxidase-conjugated rabbit anti-mouse IgG (Dakocytomation, P0260, Agilent, Italy), diluted 1:100000 in blocking solution. The bands were detected with Westar Supernova western blotting detection system (CYANAGEN) and pre-stained molecular weight markers (ab116028, Abcam) used to calculate the molecular weights of the bands.
Blots were stripped following Yeung and Stanley (2009) and reprobed with anti β-2-microglobulin (B2M) rabbit antibody (ab75853, Abcam, Cambridge, UK) diluted 1:10000 in blocking solution.
Densitometry was performed by acquiring the blots with the iBrightTM CL1000 Imaging System (Thermo Fisher Scientific Inc., USA). The semiquantitation of the bands was

performed using the iBA (iBright Analysis Software; Thermo Fisher Scientific Inc., Italy) and the results were expressed as S1R/B2M ratio.

Protein Content

The protein content was determined with the Bradford method (Bradford, 1976), using bovine serum albumin as standard.

Statistic

All data were expressed as mean ± S.E.M. The significance of the differences of the means was evaluated by using repeated measures one-way ANOVA followed by Newman-Keuls's Q test. All statistical tests were carried out using GraphPad Prism 4.00, 2003.

4. Results

Effect of PRE-084, RC-33 and NE-100 on the water permeability in the presence and in the absence of oxidative stress

A first set of experiments was performed using well characterized S1R modulators, the S1R antagonist NE-100 (Okuyama et al., 1993), the S1R agonists PRE-084 (Su et al., 1991), and RC-33 (racemic and (R)-configured) (Rossi et al., 2013a). Results reported in Figure 40 clearly evidenced a different behavior of S1R modulators, depending on their agonist/antagonist profile. Heat-stress reduced the water permeability and the pre-treatment with PRE-084 and racemic RC-33 restored water permeability in heat-stressed cells, whereas the Sigma-1 antagonist NE-100 was unable to counteract oxidative stress conditions (Figure 40A).

Conversely, the treatment of cells under normal conditions (incubation in the absence of heat-stress) with the S1R modulators had no effect on water permeability (Figure 40B). Moreover, NE-100, co-administered with (R/S)-RC-33 totally counteracted its ability to prevent or restore the water permeability decrease in heat-stressed cells, confirming that S1R agonists are involved in modulation of water and hydrogen peroxide permeability in Hela cells (Figure 41).

As a further confirmation, it has been probed whether RC-33 stereochemistry plays a role in the modulation of AQPs. Previous studies demonstrated that the racemic RC-33 and both (R) and (S) enantiomers show nearly the same affinity toward the binding site of S1R and are equally effective in promoting neurite outgrowth in PC12 cellular model (Rossi et al., 2013a). Subsequent investigations demonstrated that (R)-RC-33 is endowed with higher in vitro metabolic stability, and for this reason was selected as the eutomer for further in vivo studies (Rossi et al., 2013b). Here, we compared the effect of (R/S)-RC-33 with that of (R)-RC-33. Racemic and (R)-configured RC-33 showed a similar behavior in the experiments on water permeability (Figure 42).

Figure 40 - *Effect of Pre084, (R/S)-RC-33, NE-100 on the water permeability of HeLa cells in heat-stress condition (A) and in normal non-stressed condition (B)*

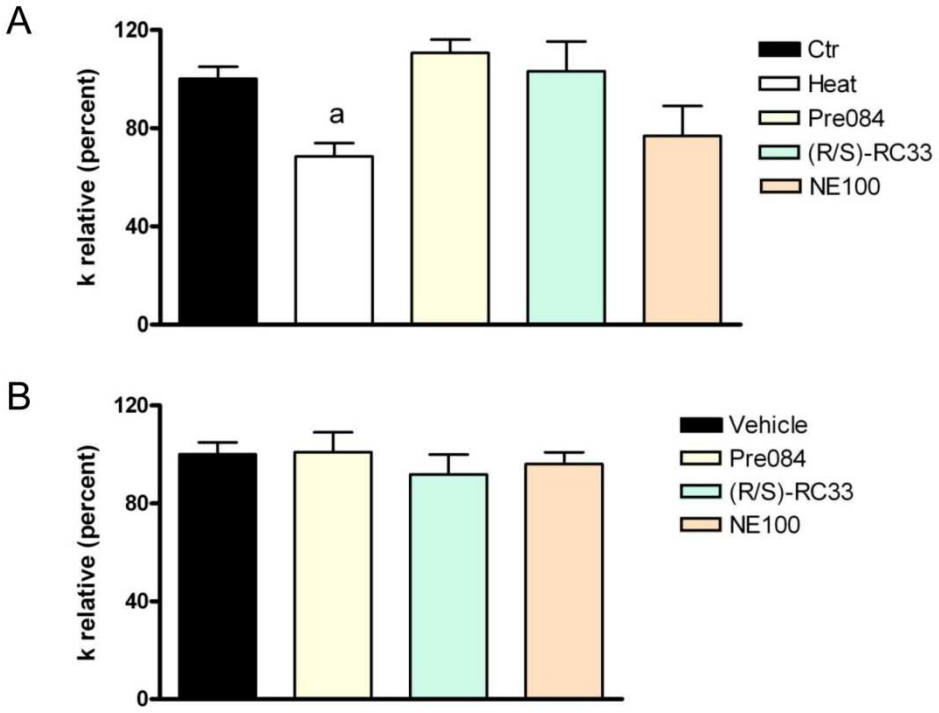

(A) HeLa cells were exposed to a 150 mOsm osmotic gradient in different conditions: 1) untreated cells (Controls, Ctr); 2) cells treated at 42°C for 3 h (heat-stressed, Heat); 3) heat-stressed cells pre-treated with the compounds at 20 μM final concentration. (B) Effect of test compounds on water permeability in absence of oxidative stress. Hela cells were incubated at 21°C for 3 h with the compounds at 20 μM final concentration and, successively, were exposed to a 150 mOsm osmotic gradient. Vehicle indicates cells incubated without compounds. Bars represent the osmotic water permeability of HeLa cells expressed as percent of k relative. Values are means ± SEM of 4-15 single shots (time course curves) for each of 4-6 different experiments. a, P < 0.05 vs. Ctr, Pre084, (R/S)-RC-33 (Repeated measures ANOVA, followed by Newman-Keuls's Q test).

Figure 41 - *Effect of the NE-100 and (R/S)-RC-33 co-administration on the water permeability of HeLa cells in heat-stress condition*

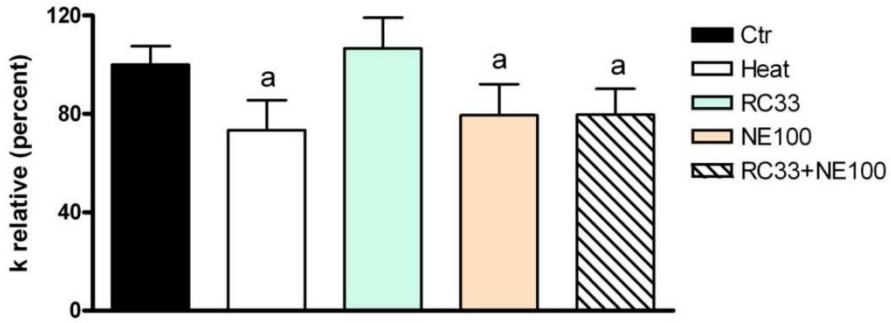

HeLa cells were exposed to a 150 mOsm osmotic gradient in four different conditions: 1) untreated cells (Controls, Ctr); 2) cells treated at 42°C for 3 h (heat-stressed, Heat); 3) heat-stressed cells pre-treated separately with NE-100 and (R/S)-RC-33 at 20 μM final concentration; 4) heat-stressed cells pre-treated simultaneously with NE-100 and (R/S)-RC-33. Bars represent the osmotic water permeability of HeLa cells expressed as percent of k relative. a, P < 0.05 vs. Ctr, (R/S)-RC-33 (Repeated measures ANOVA, followed by Newman-Keuls's Q test).

Figure 42 - *Effect of the RC-33 stereochemistry on the water permeability of HeLa cells in heat-stress condition*

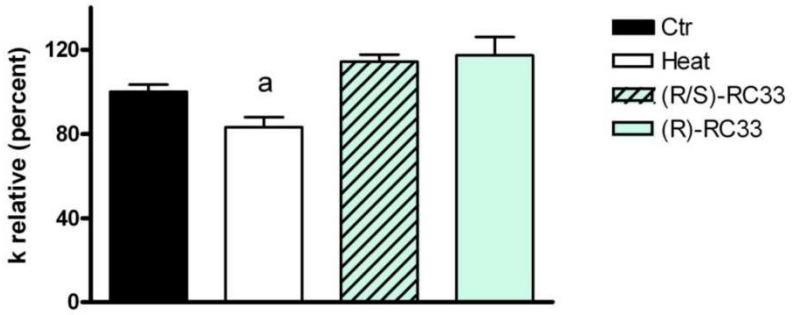

HeLa cells were exposed to a 150 mOsm osmotic gradient in three different conditions: 1) untreated cells (Controls, Ctr); 2) cells treated at 42°C for 3 h (heat-stressed, Heat); 3) heat-stressed cells pre-treated with the racemic ((R/S)-RC33) or the R-configured ((R)-RC33) RC33 at 20 μM final concentration. Bars represent the osmotic water permeability of HeLa cells expressed as percent of k relative. Values are means ± SEM of 4-15 single shots (time course curves) for each of 4-6 different experiments. a, P < 0.05 vs. Ctr, (R/S)-RC33, (R)-RC33 (Repeated measures ANOVA, followed by Newman-Keuls's Q test).

Effect of compound 1, 2 and 3 on the water permeability in the presence and in the absence of oxidative stress

Heat-stressed cells treated with compounds 1-3 displayed a restored water permeability (Figure 43A). HeLa cells treated with compound 3 had a significantly higher water permeability than those incubated with compound 2 (Figure 43A). The behavior is similar with the trend of PRE-084 and RC-33, well-established S1R agonists. On the other hand, the treatment of the cells with compounds 1-3 under normal conditions had no effect on water permeability (Figure 43B).

Figure 43 - *Effect of compounds 1- 3 on the water permeability of HeLa cells in heat-stress condition (A) and in normal non-stressed condition (B)*

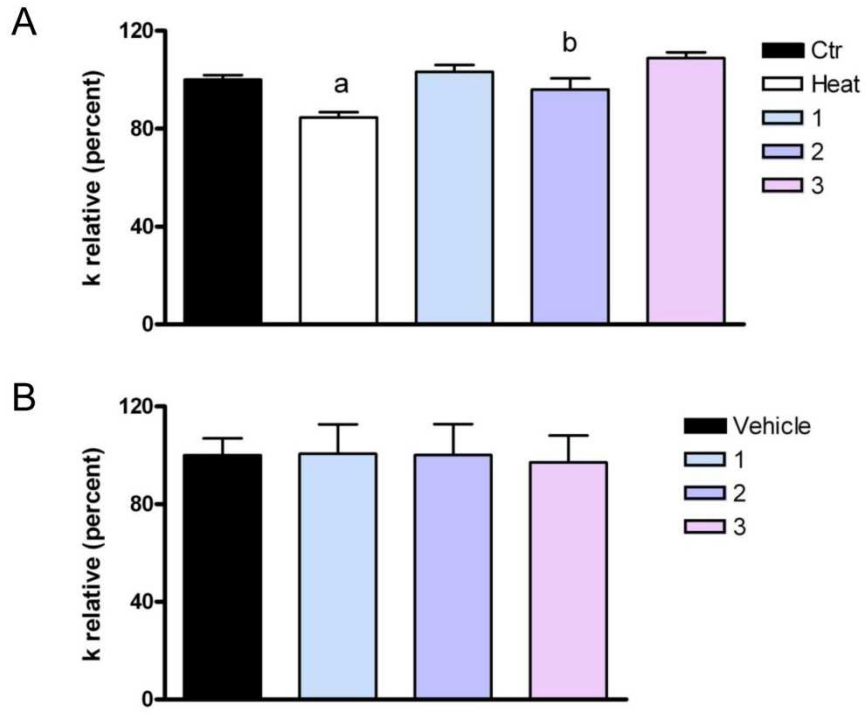

(A) HeLa cells were exposed to a 150 mOsm osmotic gradient in three different conditions: 1) untreated cells (Controls, Ctr); 2) cells treated at 42°C for 3 h (heat-stressed, Heat); 3) heat-stressed cells pre-treated with the compounds at 20 μM final concentration. (B) The effect of the compounds on water permeability independently on their antioxidant properties. Hela cells were incubated at 21°C for 3 h with the single compounds at 20 μM final concentration and, successively, were exposed to a 150 mOsm osmotic gradient. Vehicle, cells incubated without compounds. Bars represent the osmotic water permeability of HeLa cells expressed as percent of k relative. Values are means ± SEM of 4-15 single shots (time course curves) for each of 4-6 different experiments. a, P < 0.01 vs. Ctr, 1, 2, 3; b, P < 0.05 vs. 3 (Repeated measures ANOVA, followed by Newman-Keuls's Q test).

Oxidative stress dose-response relationship for compound 2-3

Results showed that compound 2 and 3 are effective in reduction of H_2O_2 levels within the cell in a dose-dependent fashion (Figure 44). The compounds had a similar response per unit dose since the slopes of the lines did not statistically differ (compound 2: -56.98±4.7; compound 3: -48.00±13.0; P= 0.54, Student's t test).

Figure 44 - *Dose–response effect of compounds 2 and 3 on HeLa cells H_2O_2 content*

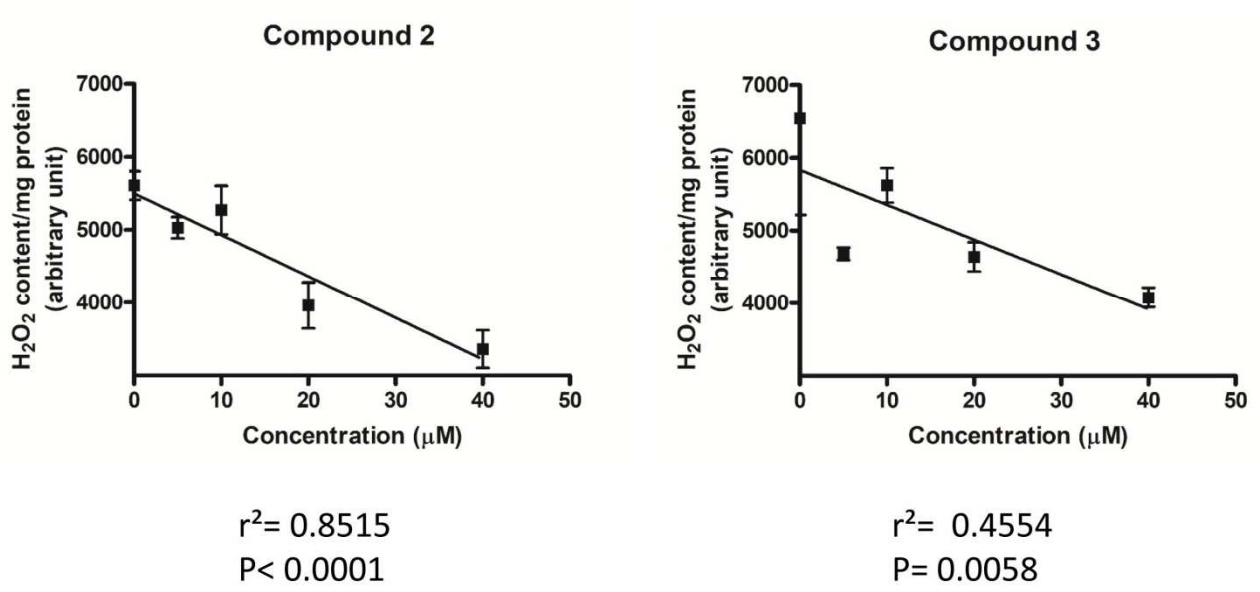

HeLa cells were heat-stressed at 42°C for 3 h and pre-treated with increasing concentrations of test compounds. H_2O_2 was measured using the CM-H2DCFDA reagent (see Materials and methods). Values represent mean ± SEM (n = 4) and are expressed as H_2O_2 content (arbitrary unit) per mg protein. Overall linear regression (black line) is presented. P and r^2 values are shown.

Effect of S1R modulators on the water permeability in the presence of oxidative stress in S1R-silenced cells

siRNAs targeting human S1R were used to knockdown the S1R in HeLa cells. Figure 45A and B show the effectiveness in silencing (50% compared to control), assessed by immunoblotting. Successively, silenced HeLa cells were heat-stressed in the presence and in the absence of S1R agonists and the water permeability was measured. The water permeability of controls is similar to the water permeability of heat-stressed, demonstrating that S1R silencing induced an oxidative stress even in the absence of heat treatment (Figure 45C). Heat treatment of the S1R-silenced cells in the presence of Pre084, and compounds 1-3 increased the water permeability from 38 to 58%, while RC-33 did not significantly modify the water permeability (Figure 45C).

Figure 45 - S1R silencing in HeLa cells.

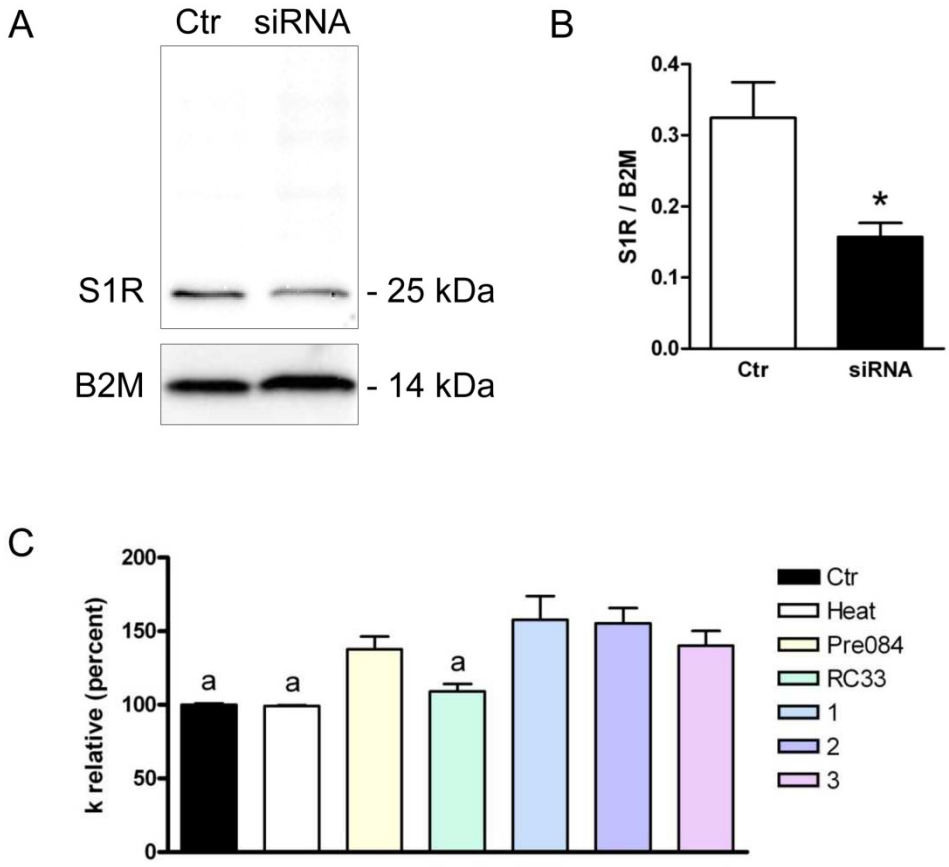

HeLa cells were silenced and the effectiveness in silencing was tested by immunoblotting and densitometry demonstrating a significant reduced protein expression in silenced (siRNA) cells compared to controls (scrambled; Ctr) (, P<0.001; Student's t test). (A) A representative blot is shown. 30 mg of proteins were loaded and the blots incubated with anti-S1R antibody. Blots were stripped and re-probed with anti-b b macroglobulin (B2M) antibody. Bands of 25 and 14 kDa were obtained for S1R and B2M, respectively. (B) Densitometry was performed by acquiring the blot with the iBright CL1000 imaging system. Semiquantitation was performed by iBA (iBright Analysis Software) and the results were normalized to the corresponding B2M. (C) Effect of S1R agonist treatment on the water permeability of S1R-null HeLa cells heat-stressed (Heat). The compounds were used at 20 μM final concentration. Ctr, control, untreated HeLa cells silenced for S1R. a, P<0.05 vs. Pre084, 1, 2, 3 (ANOVA, followed by Newman-Keuls's Q test).*

5. Discussion

In the first set of experiments, the effect of the well characterized S1R agonists PRE-084 and racemic RC-33 was evaluated in HeLa cells, and the results were compared with the known S1R antagonist NE-100. All compounds were tested in the presence and in absence of oxidative stress conditions. The distress condition was recreated via heat shock, and the resulting variation in osmotic water permeability was measured by a stopped-flow light scattering method. All compounds had no effect on water permeability under normal conditions (non-stressed cells). It can be assumed that the compounds can act on AQPs only in the "oxidized" form. A previous study demonstrated that some antioxidant compounds were able to protect (pre-treatment) or reverse (post-treatment) the water permeability of HeLa cells heat-stressed (Pellavio et al., 2017). Particularly, curcumin was the only compound showing a different behavior, inhibiting the water permeability in the absence of oxidative stress (Pellavio et al., 2017).

Conversely, two distinct profiles could be drawn under oxidative stress: S1R agonists PRE-084 and RC-33 were able to restore water permeability, whereas NE-100 was ineffective (Figure 40). The subsequent co-administration of RC-33 and NE-100 to heat-stressed cells, evidenced that the effect of the antagonist quenched the antioxidant properties of the agonist, confirming that the effect appears S1R mediated (Figure 41). Moreover, the effects of racemic RC-33 and of (R)-RC-33 are superimposable, as expected by their S1R binding profile (Figure 42).

After the first set of experiments, the effect of compound 1-3 was investigated in the same way. Compounds 1-3 were originally designed by merging the pharmacophoric elements of different neuroprotective and/or antioxidant molecules, including the already mentioned curcumin. Compound 1 possesses a good binding profile, a free radical scavenging activity in the 2,2-diphenyl-1-picrylhydrazyl (DPPH) assay and it is able to reduce ROS in SH-SY5Y cells, after an exposure to oxidative damages mediated by H_2O_2, in the 2',7'-dichlorofluorescein diacetate assay. Compounds 2 and 3 showed a better binding affinity toward S1R than compound 1, but a lower antioxidant profile. Compounds 1-3 resulted able to protect the water permeability in heat-stressed cells like RC-33 and PRE-084 that do not display any intrinsic antioxidant activity as observed in DPPH assay (Rui et al., 2018). Although compounds 1-3 possess the pharmacophoric

elements of curcumin, they show a different behavior, since they do not inhibit the water permeability in the absence of oxidative stress, thus suggesting a successful optimization of the biological profile (Figure 43).

A dose-response correlation, assessing the cellular H_2O_2 content, has been determined for compounds with the best binding affinity toward S1R: compounds 2 and 3. Based on obtained results (Figure 44) and since that both compounds (2 and 3) displayed poor free radical scavenging activity in the DPPH assay, we can conclude that antioxidant activity might be mainly AQP-mediated and that there is a correlation between S1R and AQP modulation.

However, the possibility that the compounds could act on S1R and that the restoring effect on osmotic permeability was indirect could not be ruled out. Other experiments were performed in HeLa cells knocked down for S1R to discriminate the effect on the two targets. The results clearly showed that RC-33 is unable to recover S1R-silenced cells from oxidative stress and thus it acts only through S1R modulation (Figure 45). Conversely, Pre084, 1, 2 and 3 are able also to increase ROS scavenging thereby protecting the cells from oxidative stress damage. Therefore, compounds 1-3 exert their activity on both S1R and AQP. They are the first members of a new series of dual modulators of AQP and S1R, by now called DAS 1-3.

6. Conclusion

The investigated S1R agonists showed antioxidant properties through a double mechanism: the interaction with S1R and the direct modulation of AQP, with the only exception of the S1R agonist RC-33. Although S1R are undoubtedly involved in the oxidative stress process, the roles of S1R are not completely understood and thus results herein presented add a piece to the complex puzzle of S1R. S1R has been extensively studied in the past decades, and its modulators have been proposed as viable tools for different therapeutic applications, reaching advanced stages of drug development (Linciano et al., 2020). On the other hand, aquaporins are still largely unexplored from a medicinal chemistry standpoint and have been recognized as druggable molecular targets only recently (Pellavio et al., 2017; Cataldo et al., 2019; Calamita et al., 2018; Portincasa and Calamita, 2019; Tesse et al., 2018; Sonntag et al., 2019) .

This work represents the first report involving modulators of both AQP and S1R. Results herein presented support the hypothesis that drug-like small molecules can modulate AQPs. The mutual correlation of AQPs and S1R opens a new avenue for the development of new bioactive molecules with synergistic activities. In fact, oxidative stress is a typical condition in debilitating pathologies where S1R is involved, namely neurodegenerative diseases and cancer.

DAS 1-3 represent the first members of a new class of AQP and S1R modulators. Further research on such small molecules is warranted to create an opportunity to develop novel therapies to treat diseases involving oxidative stress.

Conclusions

This study has investigated the role and the functioning of peroxiporins to clarify the "scavenging role" of peroxiporins in different oxidative stress environments: the HPV infection and the MPM cancer. Moreover, the effect of S1R modulators on the AQP-dependent water/hydrogen peroxide permeability in the presence and in the absence of oxidative stress was also taken into account.

In HPV infected spermatozoa, HPV reduces AQP8-mediated detoxification mechanism leading to sperm distress and sperm dysfunction. Results obtained confirm the deleterious effect of HPV on male fertility, clarifying a possible target and a mechanism by which HPV infection alters sperm functioning.

MPM cells, showing a high permeability in stressful conditions, seem to resist to oxidative stress and this would explain the resistance of this cancer to chemotherapy-induced apoptosis. The identification of the cellular mechanisms underlying this resistance could lead to the development of drug strategies that make ROS-inducing anticancer molecules more effective.

Moreover, this work has identified new chemical compounds (DAS 1-3) which have a dual target, S1R and AQPs, with synergistic activities against the oxidative stress condition. Their possible use for therapeutic strategies was also suggested in pathological conditions, such as cancer and degenerative diseases, to reduce the oxidative stress.

References

Abir-Awan M , Kitchen P , Salman MM et al. Inhibitors of mammalian aquaporin water channels. Int J Mol Sci 2019;20:1589.

Agostoni E and Zocchi L. Pleural liquid and its exchanges. Respir Physiol Neurobiol 2007;159:311-323.

Agre P, Preston GM, Smith BL et al. Aquaporin CHIP: the archetypal molecular water channel. Am J Phys 1993;265:F463–F476.

Agre P. The aquaporin water channels. Proc Am Thorac Soc 2006;3(1):5-13.

Aitken RJ and Drevet JR. The Importance of Oxidative Stress in Determining the Functionality of Mammalian Spermatozoa: A Two-Edged Sword. Antioxidants (Basel) 2020;9(2):E111.

Almasalmeh A, Krenc D, Wu B et al. Structural determinants of the hydrogen peroxide permeability of aquaporins. FEBS J 2014;281:647–656.

Aydar E, Palmer CP, Klyachko VA et al. The sigma receptor as a ligand-regulated auxiliary potassium channel subunit. Neuron 2002;34(3):399-410.

Beckett P, Edwards J, Fennell D et al. Demographics, management and survival of patients with malignant pleural mesothelioma in the National Lung Cancer Audit in England and Wales. Lung Cancer 2015;88(3):344-8.

Beitz E, Wu B, Holm LM et al. Point mutations in the aromatic/arginine region in aquaporin 1 allow passage of urea, glycerol, ammonia, and protons. Proc Natl Acad Sci U S A 2006;103(2):269-274.

Benga G. The first discovered water channel protein, later called aquaporin 1: molecular characteristics, functions and medical implications. Mol Asp Med 2012;33:518–534.

Bepler G, Koehler A, Kiefer P, et al. Characterization of the state of differentiation of six newly established human non-small-cell lung cancer cell lines. Differentiation 1988;37(2):158-171.

Bestetti S, Galli M, Sorrentino I et al. Human aquaporin-11 guarantees efficient transport of H_2O_2 across the endoplasmic reticulum membrane. Redox Biol 2020;28:101326.

Bibby AC, Tsim S, Kanellakis N et al. Malignant pleural mesothelioma: an update on investigation, diagnosis and treatment. Eur Respir Rev 2016;25(142):472-486.

Bienert GP and Chaumont F. Aquaporin-facilitated transmembrane diffusion of hydrogen peroxide. Biochim Biophys Acta 2014;1840:1596–1604.

Boj M, Chauvigné F, Cerdà J. Aquaporin biology of spermatogenesis and sperm physiology in mammals and teleosts. Biol Bull 2015a;229(1):93-108.

Boj M, Chauvigné F, Cerdà J. Coordinated action of aquaporins regulates sperm motility in a marine teleost. Biol Reprod 2015b;93(2):40.

Bradford M. A rapid and sensitive method for the quantitation of microgram quantities of protein utilizing the principle of protein-dye binding. Anal Biochem 1976;72:248-254.

Brooks HL, Regan JW, Yool AJ. Inhibition of aquaporin-1 water permeability by tetraethylammonium: involvement of the loop E pore region. Mol Pharmacol 2000;57:1021–1026.

Brossfield JE, Chan PJ, Patton WC et al. Tenacity of exogenous human papillomavirus DNA in sperm washing. J Assist Reprod Genet 1999;16(6):325-8.

Brown D. The Discovery of Water Channels (Aquaporins). Ann Nutr Metab 2017;70 Suppl 1:37-42.

Calamita G, Ferri D, Gena P et al. The inner mitochondrial membrane has aquaporin-8 water channels and is highly permeable to water. J Biol Chem 2005;280:17149-53.

Calamita G, Perret J, Delporte C. Aquaglyceroporins: Drug Targets for Metabolic Diseases? Front Physiol 2018;9:851.

Carbone M, Adusumilli PS, Alexander HR Jr et al. Mesothelioma: Scientific clues for prevention, diagnosis, and therapy. CA Cancer J Clin 2019;69(5):402-429.

Carrageta DF, Bernardino RL, Soveral G et al. Aquaporins and male (in)fertility: Expression and role throughout the male reproductive tract. Arch Biochem Biophys 2020;679:108222.

Cataldo I, Maggio A, Gena P et al. Modulation of Aquaporins by Dietary Patterns and Plant Bioactive Compounds. Curr Med Chem 2019;26(19):3457-3470.

Ceresoli G, Aerts J, Madrzak J et al. MA12.06 STELLAR - final results of a phase 2 trial of TTFields with chemotherapy for first-line treatment of malignant pleural mesothelioma. J Thorac Oncol 2018;13:S397–8.

Chan PJ, Su BC, Kalugdan T et al. Human papillomavirus gene sequences in washed human sperm deoxyribonucleic acid. Fertil Steril 1994;61(5):982-5.

Chauvigné F, Boj M, Finn RN et al. Mitochondrial aquaporin-8-mediated hydrogen peroxide transport is essential for teleost spermatozoon motility. Sci Rep 2015;14:7789.

Chauvigné F, Boj M, Vilella S et al. Subcellular localization of selectively permeable aquaporins in the male germ line of a marine teleost reveals spatial redistribution in activated spermatozoa. Biol Reprod 2013;89:37.

Chen Q, Peng H, Lei L et al. Aquaporin3 is a sperm water channel essential for postcopulatory sperm osmoadaptation and migration. Cell Res 2011;21(6):922-33.

Cheung PW, Bouley R, Brown D. Targeting the Trafficking of Kidney Water Channels for Therapeutic Benefit. Annu Rev Pharmacol Toxicol. 2020;60:175-194.

Chu UB, Ruoho AE. Biochemical Pharmacology of the Sigma-1 Receptor. Mol Pharmacol 2016;89(1):142-53.

Chung HJ, Choi YE, Kim ES et al. miR-29b attenuates tumorigenicity and stemness maintenance in human glioblastoma multiforme by directly targeting BCL2L2. Oncotarget 2015;6(21):18429-44.

Clemens DM, Nemeth-Cahalan KL, Trinh L et al. In vivo analysis of aquaporin 0 function in zebrafish: permeability regulation is required for lens transparency. Invest Ophthalmol Vis Sci 2013;54:5136–5143.

Connelly DA, Chan PJ, Patton WC et al. Human sperm deoxyribonucleic acid fragmentation by specific types of papillomavirus. Am J Obstet Gynecol 2001;184(6):1068-70.

Cruz-Gregorio A, Manzo-Merino J, Lizano M. Cellular redox, cancer and human papillomavirus. Virus Res 2018;246:35-45.

Curry MR, Millar JD, Tamuli SM et al. Surface area and volume measurements for ram and human spermatozoa. Biol Reprod 1996;55(6):1325-1332.

Dacic S, Le Stang N, Husain A et al. Interobserver variation in the assessment of the sarcomatoid and transitional components in biphasic mesotheliomas. Mod Pathol 2020;33(2):255-262.

Danielli M, Marrone J, Capiglioni AM et al. Data of H_2O_2 release from AQP8-knockdown rat hepatocyte mitochondria. Data Brief 2019;23:103722.

de Almeida A, Martins AP, Mosca AF et al. Exploring the gating mechanisms of aquaporin-3: new clues for the design of inhibitors?. Mol BioSyst 2016;12:1564–1573.

De Ieso ML and Yool AJ. Mechanisms of Aquaporin-Facilitated Cancer Invasion and Metastasis. Front Chem 2018;6:135.

de Lamirande E and Gagnon C. Human sperm hyperactivation and capacitation as parts of an oxidative process. Free Radic Biol Med 1993;14(2):157-66.

Denker BM, Smith BL, Kuhajda FP et al. Identification, purification, and partial characterization of a novel Mr 28,000 integral membrane protein from erythrocytes and renal tubules. J Biol Chem 1988;263:15634–15642.

Depuydt CE, Beert J, Bosmans E et al. Human Papillomavirus (HPV) virion induced cancer and subfertility, two sides of the same coin. Facts Views Vis Obgyn 2016;8(4):211-222.

Dias TR, Alves MG, Silva BM et al. Sperm glucose transport and metabolism in diabetic individuals. Mol Cell Endocrinol 2014;396(1-2):37-45.

Driml J, Pulford E, Moffat D et al. Usefulness of Aquaporin 1 as a Prognostic Marker in a Prospective Cohort of Malignant Mesotheliomas. Int J Mol Sci 2016;17(7):1041.

Esteva-Font C, Phuan PW, Anderson MO et al. A small molecule screen identifies selective inhibitors of urea transporter UT-A. Chem Biol 2013;20:1235–1244.

Fang X, Yang B, Matthay MA et al. Evidence against aquaporin-1-dependent CO2 permeability in lung and kidney. J Physiol 2002;542:63–69.

Finn RN and Cerda J. Evolution and functional diversity of aquaporins. Biol Bull 2015;229:6–23.

Finn RN, Chauvigné F, Hlidberg JB et al. The lineage-specific evolution of aquaporin gene clusters facilitated tetrapod terrestrial adaptation. PLoS ONE 2014;9:e113686.

Foresta C, Garolla A, Zuccarello D et al. Human papillomavirus found in sperm head of young adult males affects the progressive motility. Fertil Steril 2010a;93(3):802–6.

Foresta C, Noventa M, De Toni L et al. HPV-DNA sperm infection and infertility: from a systematic literature review to a possible clinical management proposal. Andrology 2015;3(2):163-73.

Foresta C, Pizzol D, Moretti A et al. Clinical and prognostic significance of human papillomavirus DNA in the sperm or exfoliated cells of infertile patients and subjects with risk factors. Fertil Steril 2010b;94(5):1723–7.

Garland LL, Chansky K, Wozniak AJ et al. Phase II study of cediranib in patients with malignant pleural mesothelioma: SWOG S0509. J Thorac Oncol 2011;6(11):1938-45.

Garolla A, Lenzi A, Palu G et al. Human papillomavirus sperm infection and assisted reproduction: a dangerous hazard with a possible safe solution. Human reproduction (Oxford England) 2012;27(4):967–73.

Garolla A, Pizzol D, Bertoldo A et al. Association, prevalence, and clearance of human papillomavirus and antisperm antibodies in infected semen samples from infertile patients. Fertil Steril 2013;99(1):125-31.

Geyer RR, Musa-Aziz R, Qin X et al. Relative CO(2)/NH(3) selectivities of mammalian aquaporins 0-9. Am J Phys Cell Physiol 2013;304:C985–C994.

Giuliano AR, Nyitray AG, Kreimer AR et al. EUROGIN 2014 roadmap: differences in human papillomavirus infection natural history, transmission and human papillomavirus-related cancer incidence by gender and anatomic site of infection. Int J Cancer 2015;136(12):2752-60.

Goguadze N, Zhuravliova E, Morin D et al. Sigma-1 Receptor Agonists Induce Oxidative Stress in Mitochondria and Enhance Complex I Activity in Physiological Condition but Protect Against Pathological Oxidative Stress. Neurotox Res 2019;35(1):1-18.

Gonen T, Cheng Y, Kistler J et al. Aquaporin-0 membrane junctions form upon proteolytic cleavage. J Mol Biol 2004;342:1337–1345.

Gotfryd K, Mósca AF, Missel JW et al. Human adipose glycerol flux is regulated by a pH gate in AQP10. Nat Commun 2018;9(1):4749.

Grantham JJ and Burg MB. Effect of vasopressin and cyclic AMP on permeability of isolated collecting tubules. Am J Physiol 1966;211:255-9.

Gromek KA, Suchy FP, Meddaugh HR et al. The oligomeric states of the purified sigma-1 receptor are stabilized by ligands. J Biol Chem 2014;289(29):20333-44.

Guo G, Chmielecki J, Goparaju C et al. Whole-exome sequencing reveals frequent genetic alterations in BAP1, NF2, CDKN2A, and CUL1 in malignant pleural mesothelioma. Cancer Res 2015;75(2):264-9.

Halsey AM, Conner AC, Bill RM et al. Aquaporins and Their Regulation after Spinal Cord Injury. Cells 2018;7:174.

Hanner M, Moebius FF, Flandorfer A et al. Purification, molecular cloning, and expression of the mammalian sigma1-binding site. Proc Natl Acad Sci U S A 1996;93(15):8072-7.

Hanner M, Moebius FF, Flandorfer A et al. Purification, molecular cloning, and expression of the mammalian sigma1-binding site. Proc Natl Acad Sci U S A 1996;93(15):8072-7.

Hansen JS, Krintel C, Hernebring M et al. Perilipin 1 binds to aquaporin 7 in human adipocytes and controls its mobility via protein kinase a mediated phosphorylation. Metabolism 2016;65:1731–1742.

Happy M, Dejoie J, Zajac CK et al. Sigma 1 Receptor antagonist potentiates the anti-cancer effect of p53 by regulating ER stress, ROS production, Bax levels, and caspase-3 activation. Biochem Biophys Res Commun 2015;456(2):683-8.

Hara-Chikuma M and Verkman AS. Prevention of skin tumorigenesis and impairment of epidermal cell proliferation by targeted aquaporin-3 gene disruption. Mol Cell Biol 2008;28:326-32.

Hara-Chikuma M, Watanabe S, Satooka H. Involvement of aquaporin-3 in epidermal growth factor receptor signaling via hydrogen peroxide transport in cancer cells. Biochem Biophys Res Commun 2016;471(4):603-9.

Harling L, Kolokotroni SM, Nair A et al. Differential Survival Characteristics of Sarcomatoid Subtype in Biphasic Pleural Mesothelioma. Ann Thorac Surg 2019;107(3):929-935.

Hayashi T, Rizzuto R, Hajnoczky G et al. MAM: more than just a housekeeper. Trends Cell Biol 2009;19(2):81-8.

Hayashi T, Su TP. Regulating ankyrin dynamics: Roles of sigma-1 receptors. Proc Natl Acad Sci U S A 2001;98(2):491-6.

Hayashi T, Su TP. Sigma-1 receptor chaperones at the ER-mitochondrion interface regulate Ca(2+) signaling and cell survival. Cell 2007;131(3):596-610.

Hayashi T, Su TP. Sigma-1 receptors (sigma(1) binding sites) form raft-like microdomains and target lipid droplets on the endoplasmic reticulum: roles in endoplasmic reticulum lipid compartmentalization and export. J Pharmacol Exp Ther 2003;306(2):718-25.

Hazama A, Kozono D, Guggino WB et al. Ion permeation of AQP6 water channel protein. Single channel recordings after Hg2+ activation. J Biol Chem 2002;277:29224-30.

Hellewell SB, Bowen WD. A sigma-like binding site in rat pheochromocytoma (PC12) cells: decreased affinity for (+)-benzomorphans and lower molecular weight suggest a different sigma receptor form from that of guinea pig brain. Brain Res 1990;527(2):244-53.

Herrera M, Garvin JL. Novel role of AQP-1 in NO-dependent vasorelaxation. Am J Physiol Ren Physiol 2007;292:F1443–F145.

Hintze JM and O'Neill J. Strengthening the case for gender-neutral and the nonavalent HPV vaccine. Eur Arch Otorhinolaryngol 2018;275(4):857-865.

Holm LM, Klaerke DA, Zeuthen T. Aquaporin 6 is permeable to glycerol and urea. Pflugers Arch 2004;448:181–186.

Hooper C, Gary Lee YC, Maskell N. On behalf of the BTS Pleural Guideline Group: Investigation of a unilateral pleural effusion in adults: British Thoracic Society pleural disease guideline 2010. Thorax 2010;65:ii4-ii17.

Huang ML, Chiang S, Kalinowski DS et al. The Role of the Antioxidant Response in Mitochondrial Dysfunction in Degenerative Diseases: Cross-Talk between Antioxidant Defense, Autophagy, and Apoptosis. Oxid Med Cell Longev 2019;6392763.

Ikeda M, Andoo A, Shimono M et al. The NPC motif of aquaporin-11, unlike the NPA motif of known aquaporins, is essential for full expression of molecular function. J Biol Chem 2011;286:3342–3350.

Ikeda M, Beitz E, Kozono D et al. Characterization of aquaporin-6 as a nitrate channel in mammalian cells. Requirement of pore-lining residue threonine 63. J Biol Chem 2002;277:39873–39879.

Ishibashi K, Kondo S, Hara S et al. The evolutionary aspects of aquaporin family. Am J Physiol Regul Integr Comp Physiol 2011;300(3):R566–R576.

Itoh T, Rai T, Kuwahara M et al. Identification of a novel aquaporin, AQP12, expressed in pancreatic acinar cells. Biochem Biophys Res Commun 2005;330:832–838.

Jagirdar RM, Apostolidou E, Molyvdas PA et al. Influence of AQP1 on cell adhesion, migration, and tumor sphere formation in malignant pleural mesothelioma is substratum- and histological-type dependent. Am J Physiol Lung Cell Mol Physiol 2016;310(6):L489-95.

Jarius S, Paul F, Franciotta D et al. Mechanisms of disease: aquaporin-4 antibodies in neuromyelitis optica. Nat Clin Pract Neurol 2008;4:202-14.

Jiang JJ, Bai CX, Hong QY et al. Effect of aquaporin-1 deletion on pleural fluid transport. Acta Pharmacol Sin 2003;24(4):301–305.

Jozefkowicz C, Bern MC, Chaumont F et al. Heteromerization of plant aquaporins. In *Plant Aquaporins*; Chaumont F, Tyerman SD, Eds; Springer International Publishing 2017;29–46.

Kaspersen MD, Bungum M, Fedder J et al. No increased sperm DNA fragmentation index in semen containing human papillomavirus or herpesvirus. Andrology 2013;1(3):361-4.

Kaspersen MD, Larsen PB, Ingerslev HJ et al. Identification of multiple HPV types on spermatozoa from human sperm donors. PLoS One. 2011;6(3):e18095.

Katkova LE, Baturina GS, Bondar AA et al. Benign Pleural Mesothelial Cells Have Higher Osmotic Water Permeability than Malignant Pleural Mesothelioma Cells and Differentially Respond to Hyperosmolality. Cell Physiol Biochem 2019;52(4):869-878.

Ke Y, Reddel RR, Gerwin BI, et al. Establishment of a human in vitro mesothelial cell model system for investigating mechanisms of asbestos-induced mesothelioma. Am J Pathol 1989;134(5):979-991.

Kerkhofs M, Giorgi C, Marchi S et al. Alterations in Ca2+ Signalling via ER-Mitochondria Contact Site Remodelling in Cancer. Adv Exp Med Biol 2017;997:225-254.

Kindler HL, Ismaila N, Armato SG et al. Treatment of Malignant Pleural Mesothelioma: American Society of Clinical Oncology Clinical Practice Guideline. J Clin Oncol 2018;36(13):1343-1373.

King LS, Kozono D, Agre P. From structure to disease: The evolving tale of aquaporin biology. Nat Rev Mol Cell Biol 2004;5:687–698.

Klebe S, Griggs K, Cheng Y et al. Blockade of aquaporin 1 inhibits proliferation, motility, and metastatic potential of mesothelioma in vitro but not in an in vivo model. Dis Markers 2015;2015:286719.

Krane CM, Fortner CN, Hand AR, et al. Aquaporin 5-deficient mouse lungs are hyperresponsive to cholinergic stimulation. Proc Natl Acad Sci USA 2001;98(24):14114-14119.

Krasinskas AM, Borczuk AC, Hartman DJ et al. Prognostic significance of morphological growth patterns and mitotic index of epithelioid malignant peritoneal mesothelioma. Histopathology 2016;68(5):729-37.

Kreida S and Törnroth-Horsefield S. Structural insights into aquaporin selectivity and regulation. Curr Opin Struct Biol 2015;33:126-34.

Krishnan S, Bakker E, Lee C et al. Successful combined intratumoral immunotherapy of established murine mesotheliomas requires B-cell involvement. J Interferon Cytokine Res 2015;35(2):100-7.

Krissinel E, Henrick K. Inference of macromolecular assemblies from crystalline state. J Mol Biol 2007;372:774–797.

Laemmli UK. Cleavage of structural proteins during the assembly of the head of bacteriophage T4. Nature 1970;227:680–685.

Laforenza U, Bottino C, Gastaldi G. Mammalian aquaglyceroporin function in metabolism. Biochim Biophys Acta 2016a;1858(1):1-11.

Laforenza U, Gastaldi G, Grazioli M et al. Expression and immunolocalization of aquaporin-7 in rat gastrointestinal tract. Biol Cel. 2005;97(8):605-13.

Laforenza U, Pellavio G, Marchetti AL et al. Aquaporin-Mediated Water and Hydrogen Peroxide Transport Is Involved in Normal Human Spermatozoa Functioning. Int J Mol Sci 2016b;18(1):66.

Laforenza U, Scaffino MF, Gastaldi G. Aquaporin-10 represents an alternative pathway for glycerol efflux from human adipocytes. PLoS One 2013;8:e54474.

Lai YM, Lee JF, Huang HY et al. The effect of human papillomavirus infection on sperm cell motility. Fertil Steril 1997;67(6):1152-5.

Lai-Fook SJ. Pleural mechanics and fluid exchange. Physiol Rev 2004;84:385–410.

Lanzafame FM, La Vignera S, Vicari E et al. Oxidative stress and medical antioxidant treatment in male infertility. Reprod Biomed Online 2009;19(5):638-59.

Largent BL, Wikström H, Gundlach AL et al. Structural determinants of sigma receptor affinity. Mol Pharmacol 1987;32(6):772-84.

Laurie SA, Hao D, Leighl NB et al. A phase II trial of dovitinib in previously-treated advanced pleural mesothelioma: The Ontario Clinical Oncology Group. Lung Cancer 2017;104:65-69.

Laurini E, Marson D, Fermeglia M et al. 3D Homology Model of Sigma1 Receptor. Handb Exp Pharmacol 2017;244:27-50.

Ledda C, Senia P, Rapisarda V. Biomarkers for Early Diagnosis and Prognosis of Malignant Pleural Mesothelioma: The Quest Goes on. Cancers (Basel). 2018;10(6):203.

Li Z, Yan X, Yu H et al. The C-Terminal Arm of the Human Papillomavirus Major Capsid Protein Is Immunogenic and Involved in Virus-Host Interaction. Structure 2016;24(6):874-85.

Linciano P, Rossino G, Listro R et al. Sigma-1 receptor antagonists: promising players in fighting neuropathic pain. Pharm Pat Anal 2020;9(3):77-85.

Liou GY, Storz P. Reactive oxygen species in cancer. Free Radic Res 2010;44(5):479-96.

Liu K, Kozono D, Kato Y et al. Conversion of aquaporin 6 from an anion channel to a water-selective channel by a single amino acid substitution. Proc Natl Acad Sci U S A 2005;102:2192-7.

Lu HA, Sun TX, Matsuzaki T et al. Heat shock protein 70 interacts with aquaporin-2 and regulates its trafficking. J Biol Chem 2007;282:28721–28732.

Lyu Z, Feng X, Li N et al. Human papillomavirus in semen and the risk for male infertility: a systematic review and meta-analysis. BMC Infect Dis 2017;17(1):714.

Macey RI, Farmer RE. Inhibition of water and solute permeability in human red cells. Biochim Biophys Acta 1970;211:104–106.

Maeda N, Funahashi T, Shimomura I Metabolic impact of adipose and hepatic glycerol channels aquaporin 7 and aquaporin 9. Nat Clin Pract Endocrinol Metab 2008;4:627-34.

Mansfield AS, Symanowski JT, Peikert T. Systematic review of response rates of sarcomatoid malignant pleural mesotheliomas in clinical trials. Lung Cancer 2014;86(2):133-6.

Martin WR, Eades CG, Thompson JA et al. The effects of morphine- and nalorphine- like drugs in the nondependent and morphine-dependent chronic spinal dog. J Pharmacol Exp Ther 1976;197(3):517-32.

Martins AP, Marrone A, Ciancetta A et al. Targeting aquaporin function: Potent inhibition of aquaglyceroporin-3 by a gold-based compound. PLoS ONE 2012;7:e37435.

Maurice T, Su TP. The pharmacology of sigma-1 receptors. Pharmacol Ther 2009;124(2):195-206.

Mavylutov T, Chen X, Guo L et al. APEX2- tagging of Sigma 1-receptor indicates subcellular protein topology with cytosolic N-terminus and ER luminal C-terminus. Protein Cell 2018;9(8):733-737.

Medraño-Fernandez I, Bestetti S, Bertolotti M et al. Stress Regulates Aquaporin-8 Permeability to Impact Cell Growth and Survival. Antioxid Redox Signal 2016 Jun 20;24(18):1031-44.

Mishra AK, Mavlyutov T, Singh DR et al. The sigma-1 receptors are present in monomeric and oligomeric forms in living cells in the presence and absence of ligands. Biochem J 2015;466(2):263-271.

Moeller HB, Praetorius J, Rutzler MR et al. Phosphorylation of aquaporin-2 regulates its endocytosis and protein-protein interactions. Proc Natl Acad Sci 2010;107:424–429.

Moloney JN and Cotter TG: ROS signalling in the biology of cancer. Semin Cell Dev Biol 2017;80:50–64.

Moretti E, Terzuoli G, Mazzi L et al. Immunolocalization of aquaporin 7 in human sperm and its relationship with semen parameters. Syst Biol Reprod Med 2012;58(3):129-35.

Moretti R, Lyskov S, Das R et al. Web-accessible molecular modeling with Rosetta: The Rosetta Online Server that Includes Everyone (ROSIE). Protein Sci 2018;27:259-268.

Morgan T and Berliner RW. Permeability of the loop of Henle, vasa recta, and collecting duct to water, urea, and sodium. Am J Physiol 1968;215:108-15.

Mori T, Hayashi T, Hayashi E et al. Sigma-1 receptor chaperone at the ER-mitochondrion interface mediates the mitochondrion-ER-nucleus signaling for cellular survival. PLoS One 2013;8(10):e76941.

Morinaga T, Nakakoshi M, Hirao A et al. Mouse aquaporin 10 gene (AQP10) is a pseudogene. Biochem Biophys Res Commun 2002;294(3):630-4.

Morishita K, Watanabe K, Ichijo H. Cell volume regulation in cancer cell migration driven by osmotic water flow. Cancer Sci 2019;110(8):2337–2347.

Morishita Y, Matsuzaki T, Hara-chikuma M et al. Disruption of aquaporin-11 produces polycystic kidneys following vacuolization of the proximal tubule. Mol Cell Biol 2005;25:7770–7779.

Moser JC, Peikert T, Roden AC et al. Spontaneous Regression of Malignant Pleural Mesothelioma in a Patient with New-Onset Inflammatory Arthropathy. Ann Am Thorac Soc 2015;12(9):1416-7.

Murata KK, Mitsuoka T, Hirai T et al. Structural determinants of water permeation through aquaporin-1. Nature 2000;407: 599-605.

Nave M, Castro RE, Rodrigues CM et al. Nanoformulations of a potent copper-based aquaporin inhibitor with cytotoxic effect against cancer cells. Nanomedicine 2016;11:1817–1830.

Németh-Cahalan KL and Hall JE. pH and calcium regulate the water permeability of aquaporin 0. J Biol Chem 2000;275:6777-82.

Nemeth-Cahalan KL, Kalman K, Hall JE. Molecular basis of pH and Ca^{2+} regulation of aquaporin water permeability. J Gen Physiol 2004;123:573–580.

Nesverova V and Törnroth-Horsefield S. Phosphorylation-Dependent Regulation of Mammalian Aquaporins. Cells 2019;8:82.

Nico B and Ribatti D. Aquaporins in tumor growth and angiogenesis. Cancer Lett 2010;294:135–138.

Nicolini F, Bocchini M, Bronte G et al. Malignant Pleural Mesothelioma: State-of-the-Art on Current Therapies and Promises for the Future. Front Oncol 2020;9:1519.

Niemietz CM and Tyerman SD. New potent inhibitors of aquaporins: Silver and gold compounds inhibit aquaporins of plant and human origin. FEBS Lett 2002;531:443–447.

Noda Y and Sasaki S. Regulation of aquaporin-2 trafficking and its binding protein complex. Biochim Biophys Acta 2006;1758:1117-25.

Nowicka-Bauer K and Nixon B. Molecular Changes Induced by Oxidative Stress that Impair Human Sperm Motility. Antioxidants (Basel) 2020;9(2):E134.

Ohashi Y, Tsuzaka K, Takeuchi T et al. Altered distribution of aquaporin 5 and its C-terminal binding protein in the lacrimal glands of a mouse model for Sjögren's syndrome. Curr Eye Res 2008;33:621–629.

Ohta E, Itoh T, Nemoto T et al. Pancreas-specific aquaporin 12 null mice showed increased susceptibility to caerulein-induced acute pancreatitis. Am J Phys Cell Physiol 2009;297:C1368–C1378.

Okuyama S, Imagawa Y, Ogawa S et al. NE-100, a novel sigma receptor ligand: in vivo tests. Life Sci 1993;53(18):PL285-90.

Ortega-Roldan JL, Ossa F, Amin NT et al. Solution NMR studies reveal the location of the second transmembrane domain of the human sigma-1 receptor. FEBS Lett 2015;589(5):659-65.

Paajanen J, Laaksonen S, Ilonen I et al. Computed tomography in the evaluation of malignant pleural mesothelioma-Association of tumor size to a sarcomatoid histology, a more advanced TNM stage and poor survival. Lung Cancer 2018;116:73-79.

Pal A, Fontanilla D, Gopalakrishnan A et al. The sigma-1 receptor protects against cellular oxidative stress and activates antioxidant response elements. Eur J Pharmacol 2012;682(1-3):12-20.

Palucka K and Banchereau J. Cancer immunotherapy via dendritic cells. Nat Rev Cancer 2012;12(4):265-77.

Papadopoulos MC and Verkman AS. Aquaporin-4 and brain edema. Pediatr Nephrol 2007;22:778-84.

Park EK, Takahashi K, Hoshuyama T et al. Global magnitude of reported and unreported mesothelioma. Environ Health Perspect 2011;119(4):514-8.

Pellavio G, Rui M, Caliogna L et al. Regulation of aquaporin functional properties mediated by the antioxidant effects of natural compounds. Int J Mol Sci 2017;18:2665.

Pérez-Andino J, Buck CB, Ribbeck K. Adsorption of human papillomavirus 16 to live human sperm. PLoS One 2009;4(6):e5847.

Pierce BG, Wiehe K, Hwang H et al. ZDOCK server: Interactive docking prediction of protein-protein complexes and symmetric multimers. Bioinformatics 2014;30:1771–1773.

Pizzino G, Irrera N, Cucinotta M et al. Oxidative Stress: Harms and Benefits for Human Health. Oxid Med Cell Longev 2017;8416763.

Portincasa P and Calamita G. Phytocompounds modulating Aquaporins: Clinical benefits are anticipated. Food Chem 2019;274:642-650.

Prasad PD, Li HW, Fei YJ et al. Exon-intron structure, analysis of promoter region, and chromosomal localization of the human type 1 sigma receptor gene. J Neurochem 1998;70(2):443-51.

Prata C, Hrelia S, Fiorentini D. Peroxiporins in Cancer. Int J Mol Sci 2019;20(6):1371.

Preston GM, Carroll TP, Guggino WB et al. Appearance of water channels in Xenopus oocytes expressing red cell CHIP28 protein. Science 1992;256:385–387.

Preston GM, Jung JS, Guggino WB et al. The mercury-sensitive residue at cysteine 189 in the CHIP28 water channel. J Biol Chem 1993;268:17–20.

Rabaud NE, Song L, Wang Y et al. Aquaporin 6 binds calmodulin in a calcium-dependent manner. Biochem Biophys Res Commun 2009;383:54–57.

Ramachandran S, Lu H, Prabhu U et al. Purification and characterization of the guinea pig sigma-1 receptor functionally expressed in Escherichia coli. Protein Expr Purif 2007;51(2):283-92.

Rash JE, Yasumura T, Hudson CS et al. Direct immunogold labeling of aquaporin-4 in square arrays of astrocyte and ependymocyte plasma membranes in rat brain and spinal cord. Proc Natl Acad Sci 1998;95:11981–11986.

Reichow SL, Clemens DM, Freites JA et al. Allosteric mechanism of water-channel gating by Ca2+−calmodulin. Nat Struct Mol Biol 2013;20:1085–1092.

Reid G, Pel ME, Kirschner MB et al. Restoring expression of miR-16: a novel approach to therapy for malignant pleural mesothelioma. Ann Oncol 2013;24(12):3128-35.

Ren H, Yang B, Ruiz JA et al. Phosphatase Inhibition Increases AQP2 Accumulation in the Rat IMCD Apical Plasma Membrane. Am J Physiol Ren Physiol 2016;311:F1189-F1197.

Robinson BW and Lake RA. Advances in malignant mesothelioma. N Engl J Med 2005;353(15):1591-603.

Roche JV and Törnroth-Horsefield S. Aquaporin Protein-Protein Interactions. Int J Mol Sci 2017;27:18.

Rodrigues C, Pimpão C, Mósca AF et al. Human Aquaporin-5 Facilitates Hydrogen Peroxide Permeation Affecting Adaption to Oxidative Stress and Cancer Cell Migration. Cancers (Basel) 2019;11(7):932.

Rosen DA, Seki SM, Fernández-Castañeda A et al. Modulation of the sigma-1 receptor-IRE1 pathway is beneficial in preclinical models of inflammation and sepsis. Sci Transl Med 2019;11(478):eaau5266.

Rosen LE, Karrison T, Ananthanarayanan V et al. Nuclear grade and necrosis predict prognosis in malignant epithelioid pleural mesothelioma: a multi-institutional study. Mod Pathol 2018;31(4):598-606.

Rossi D, Marra A, Picconi P et al. Identification of RC-33 as a potent and selective σ1 receptor agonist potentiating NGF-induced neurite outgrowth in PC12 cells. Part 2: g-scale synthesis, physicochemical characterization and in vitro metabolic stability. Bioorg Med Chem 2013a;21(9):2577-86.

Rossi D, Pedrali A, Gaggeri R et al. Chemical, pharmacological, and in vitro metabolic stability studies on enantiomerically pure RC-33 compounds: promising neuroprotective agents acting as σ_1 receptor agonists. ChemMedChem 2013b;8(9):1514-27.

Rui M, Rossino G, Coniglio S et al. Identification of dual Sigma1 receptor modulators/acetylcholinesterase inhibitors with antioxidant and neurotrophic properties, as neuroprotective agents. Eur J Med Chem 2018;158:353-370.

Saadoun S, Papadopoulos MC, Hara-Chikuma M et al. Impairment of angiogenesis and cell migration by targeted aquaporin-1 gene disruption. Nature 2005;434(7034):786-792.

Saito K, Kageyama Y, Okada Y e al. Localization of aquaporin-7 in human testis and ejaculated sperm: possible involvement in maintenance of sperm quality. J Urol 2004;172(5 Pt 1):2073-6.

Schmidt HR, Betz RM, Dror RO et al. Structural basis for σ1 receptor ligand recognition. Nat Struct Mol Biol 2018;25(10):981-987.

Schmidt HR, Kruse AC. The Molecular Function of σ Receptors: Past, Present, and Future. Trends Pharmacol Sci 2019;40(9):636-654.

Schmidt HR, Zheng S, Gurpinar E et al. Crystal structure of the human σ1 receptor. Nature 2016;532(7600):527-30.

Sekido Y. Molecular pathogenesis of malignant mesothelioma. Carcinogenesis. 2013;34(7):1413-9.

Sies H, Berndt C, Jones DP. Oxidative Stress. Annu Rev Biochem 2017;86:715-748.

Sies H. Hydrogen peroxide as a central redox signaling molecule in physiological oxidative stress: Oxidative eustress. Redox Biol 2017;11:613-619.

Sjohamn J and Hedfalk K. Unraveling aquaporin interaction partners. Biochim Biophys Acta 2014;1840:1614–1623.

Smythe WR, Hwang HC, Amin KM, et al. Use of recombinant adenovirus to transfer the herpes simplex virus thymidine kinase (HSVtk) gene to thoracic neoplasms: an effective in vitro drug sensitization system. Cancer Res 1994;54(8):2055-2059.

Sohara E, Rai T, Yang SS et al. Pathogenesis and treatment of autosomal-dominant nephrogenic diabetes insipidus caused by an aquaporin 2 mutation. Proc Natl Acad Sci 2006;103:14217–14222.

Solomon AK. The permeability of red cells to water and ions. Ann N Y Acad Sci 1958;75:175–181.

Song Y, Sonawane N, Verkman AS. Localization of aquaporin-5 in sweat glands and functional analysis using knockout mice. J Physiol 2002;541:561-568.

Song Y, Verkman AS. Aquaporin-5 dependent fluid secretion in airway submucosal glands. J Biol Chem 2001;276:41288-41292.

Song Y, Yang B, Matthay MA et al. Role of aquaporin water channels in pleural fluid dynamics. Am J Phys Cell Physiol 2000;279(6):C1744–C1750.

Sonntag Y, Gena P, Maggio A et al. Identification and characterization of potent and selective aquaporin-3 and aquaporin-7 inhibitors. J Biol Chem 2019;294(18):7377-7387.

Soria LR, Fanelli E, Altamura N et al. Aquaporin-8-facilitated mitochondrial ammonia transport. Biochem Biophys Res Commun 2010;393(2):217-21.

Soria LR, Gradilone SA, Larocca MC et al. Glucagon induces the gene expression of aquaporin-8 but not that of aquaporin-9 water channels in the rat hepatocyte. Am J Physiol Regul Integr Comp Physiol 2009;296:R1274–R1281.

Spinello A, de Almeida A, Casini A et al. The inhibition of glycerol permeation through aquaglyceroporin-3 induced by mercury(II): A molecular dynamics study. J Inorg Biochem 2016;160:78–84.

Stathopoulos GT, Zhu Z, Everhart MB et al. Nuclear factor-kB affects tumor progression in a mouse model of malignant pleural effusion. Am J Respir Cell Mol Biol 2006;34:142-150.

Sterman DH, Alley E, Stevenson JP et al. Pilot and Feasibility Trial Evaluating Immuno-Gene Therapy of Malignant Mesothelioma Using Intrapleural Delivery of Adenovirus-IFNα Combined with Chemotherapy. Clin Cancer Res 2016;22(15):3791-800.

Sterman DH, Haas A, Moon E et al. A trial of intrapleural adenoviral-mediated Interferon-α2b gene transfer for malignant pleural mesothelioma. Am J Respir Crit Care Med 2011;184(12):1395-9.

Su TP, Hayashi T, Maurice T et al. The sigma-1 receptor chaperone as an inter-organelle signaling modulator. Trends Pharmacol Sci 2010;31(12):557-566.

Su TP, Wu XZ, Cone EJ et al. Sigma compounds derived from phencyclidine: identification of PRE-084, a new, selective sigma ligand. J Pharmacol Exp Ther 1991;259(2):543-50.

Sui H, Han BG, Lee JK et al. Jap: Structural basis of water-specific transport through the AQP1 water channel. Nature 2001;414: 872-8.

Tamma G, Valenti G, Grossini E et al. Aquaporin Membrane Channels in Oxidative Stress, Cell Signaling, and Aging: Recent Advances and Research Trends. Oxid Med Cell Longev 2018;1501847.

Tang G and Yang GY. Aquaporin-4: a potential therapeutic target for cerebral edema. Int J Mol Sci 2016;17:1413.

Tesse A, Grossini E, Tamma G et al. Aquaporins as Targets of Dietary Bioactive Phytocompounds. Front Mol Biosci 2018;5:30.

Thanan R, Oikawa S, Hiraku Y et al. Oxidative stress and its significant roles in neurodegenerative diseases and cancer. Int J Mol Sci 2014;16(1):193-217.

Thiagarajah JR, Chang J, Goettel JA et al. Aquaporin-3 mediates hydrogen peroxide-dependent responses to environmental stress in colonic epithelia. Proc Natl Acad Sci U S A. 2017;114(3):568-573.

Uttara B, Singh AV, Zamboni P et al. Oxidative stress and neurodegenerative diseases: a review of upstream and downstream antioxidant therapeutic options. Curr Neuropharmacol 2009;7(1):65-74.

Verkman AS, Anderson MO, Papadopoulos MC. Aquaporins: important but elusive drug targets. Nat Rev Drug Discov 2014;13(4):259–277.

Verkman AS. Aquaporins in clinical medicine. Annu Rev Med 2012;63:303–316.

Verma V, Ahern CA, Berlind CG et al. Survival by Histologic Subtype of Malignant Pleural Mesothelioma and the Impact of Surgical Resection on Overall Survival. Clin Lung Cancer 2018;19(6):e901-e912.

Viadiu H, Gonen T, Walz T. Projection map of aquaporin-9 at 7 A resolution. J Mol Biol 2007;367:80–88.

Vigani B, Rossi S, Sandri G et al. Dual-Functioning Scaffolds for the Treatment of Spinal Cord Injury: Alginate Nanofibers Loaded with the Sigma 1 Receptor (S1R) Agonist RC-33 in Chitosan Films. Mar Drugs 2019;18(1).

Vigneswaran WT, Kircheva DY, Ananthanarayanan V et al. Amount of Epithelioid Differentiation Is a Predictor of Survival in Malignant Pleural Mesothelioma. Ann Thorac Surg 2017;103(3):962-966.

Villard V, Espallergues J, Keller E et al. Anti-amnesic and neuroprotective potentials of the mixed muscarinic receptor/sigma 1 (σ1) ligand ANAVEX2-73, a novel aminotetrahydrofuran derivative. J Psychopharmacol 2011;25(8):1101-1117.

Villard V, Espallergues J, Keller E et al. Antiamnesic and neuroprotective effects of the aminotetrahydrofuran derivative ANAVEX1-41 against amyloid beta(25-35)-induced toxicity in mice. Neuropsychopharmacology 2009;34(6):1552-1566.

Wang J, Feng L, Zhu Z et al. Aquaporins as diagnostic and therapeutic targets in cancer: How far we are?. Journal of Translational Medicine 2015;13:96.

Wang J, Yi J. Cancer cell killing via ROS: to increase or decrease, that is the question. Cancer Biol Ther 2008;7(12):1875-84.

Wang L, Eldred JA, Sidaway P et al. Sigma 1 receptor stimulation protects against oxidative damage through suppression of the ER stress responses in the human lens. Mech Ageing Dev 2012;133(11-12):665-674.

Watanabe S, Moniaga CS, Nielsen S et al. Aquaporin-9 facilitates membrane transport of hydrogen peroxide in mammalian cells. Biochem Biophys Res Commun 2016;471:191–197.

Weng TY, Tsai SA, Su TP. Roles of sigma-1 receptors on mitochondrial functions relevant to neurodegenerative diseases. J Biomed Sci 2017;24(1):74.

Wiener H, Turnheim K, van Os CH. Rabbit distal colon epithelium: I. Isolation and characterization of basolateral plasma membrane vesicles from surface and crypt cells. J Membr Biol 1989;110(2):147-162.

World Health Organization. WHO Laboratory Manual for the Examination and Processing of Human Semen, 5th ed.; World Health Organization: Geneva, Switzerland, 2010.

Yang B, Brown D, Verkman AS. The mercurial insensitive water channel (AQP-4) forms orthogonal arrays in stably transfected Chinese hamster ovary cells. J Biol Chem 1996;271:4577–4580.

Yang B, Fukuda N, van Hoek A et al. Carbon dioxide permeability of aquaporin-1 measured in erythrocytes and lung of aquaporin-1 null mice and in reconstituted proteoliposomes. J Biol Chem 2000;275:2686–2692.

Yang B, Zhang H, Verkman AS. Lack of aquaporin-4 water transport inhibition by antiepileptics and arylsulfonamides. Bioorg Med Chem 2008;16:7489–7493.

Yang B. Aquaporins. Adv Exp Med Biol 2017;969; Springer.

Yang H, Villani RM, Wang H, et al. The role of cellular reactive oxygen species in cancer chemotherapy. J Exp Clin Cancer Res 2018;37(1):266.

Yang Y, Jia CW, Ma YM et al. Correlation between HPV sperm infection and male infertility. Asian journal of andrology 2013;15(4):529–32.

Yano H, Bonifazi A, Xu M et al. Pharmacological profiling of sigma 1 receptor ligands by novel receptor homomer assays. Neuropharmacology 2018;133:264-275.

Yao H, Yang Y, Kim KJ et al. Molecular mechanisms involving sigma receptor-mediated induction of MCP-1: implication for increased monocyte transmigration. Blood 2010;115(23):4951-4962.

Yasui M, Hazama A, Kwon TH et al. Rapid gating and anion permeability of an intracellular aquaporin. Nature 1999;402:184–187.

Yasui M, Kwon TH, Knepper MA et al. Aquaporin-6: An intracellular vesicle water channel protein in renal epithelia. Proc Natl Acad Sci U S A 1999b;96:5808-13.

Yeung CH and Cooper TG. Aquaporin AQP11 in the testis: molecular identity and association with the processing of residual cytoplasm of elongated spermatids. Reproduction 2010;139(1):209-16.

Yeung CH, Callies C, Tüttelmann F et al. Aquaporins in the human testis and spermatozoa - identification, involvement in sperm volume regulation and clinical relevance. Int J Androl 2010;33(4):629-41.

Yeung YG and Stanley ER. A solution for stripping antibodies from polyvinylidene fluoride immunoblots for multiple reprobing. Anal Biochem 2009;389(1):89-91.

Yool AJ and Weinstein AM. New roles for old holes: ion channel function in aquaporin-1. News Physiol Sci Int J Physiol Prod Joint Int Union Physiol Sci Am Physiol Soc 2002;17:68–72.

Zalcman G, Mazieres J, Margery J et al. French Cooperative Thoracic Intergroup (IFCT). Bevacizumab for newly diagnosed pleural mesothelioma in the Mesothelioma Avastin Cisplatin Pemetrexed Study (MAPS): a randomised, controlled, open-label, phase 3 trial. Lancet 2016;387(10026):1405-1414.

Zeidel ML, Ambudkar SV, Smith BL et al. Reconstitution of functional water channels in liposomes containing purified red cell CHIP28 protein. Biochemistry 1992;31:7436–7440.

Zelenina M, Bondar AA, Zelenin S et al. Nickel and extracellular acidification inhibit the water permeability of human aquaporin-3 in lung epithelial cells. J Biol Chem 2003;278:30037–30043.

Zeltsman M, Dozier J, McGee E et al. CAR T-cell therapy for lung cancer and malignant pleural mesothelioma. Transl Res 2017;187:1-10.

Zeuthen T and and Klaerke DA. Transport of water and glycerol in aquaporin 3 is gated by H(+). J Biol Chem 1999;274:21631- 6.

Zhang R, van Hoek AN, Biwersi J et al. A point mutation at cysteine 189 blocks the water permeability of rat kidney water channel CHIP28k. Biochemistry 1993;32:2938-41.

Zhang Y. I-TASSER server for protein 3D structure prediction. BMC Bioinform 2008;9:40.

Zilli L, Schiavone R, Chauvigné F et al. Evidence for the involvement of aquaporins in sperm motility activation of the teleost gilthead sea bream (Sparus aurata). Biol Reprod 2009;81:880–888.

Scientific production arisen from this thesis

Peer-reviewed publications

Pellavio G, Todaro F, Alberizzi P, et al. HPV Infection Affects Human Sperm Functionality by Inhibition of Aquaporin-8. Cells. 2020 May 17;9(5):1241. doi: 10.3390/cells9051241.

(Pellavio G, Rossino G, Gastaldi G, et al. Dual Aquaporin and Sigma1 Receptor (DAS) Modulators: New Tools for Counteracting Oxidative Stress. Preprints 2020, 2020110333. doi: 10.20944/preprints202011.0333.v1)

Abstracts at international meetings

FEPS-SIF 2019 (10-13 September 2019, Bologna): HPV infection inhibits aquaporin-mediated hydrogen peroxide elimination and affect human sperm function. Pellavio G, Todaro F, Omes C, Alberizzi P, Scotti C, Gastaldi G, Caliogna L, Nappi R, Laforenza U.

ESCI Virtual Meeting 2020 – Covid19 Edition (20-30 September 2020): Aquaporins-mediated hydrogen peroxide permeability is crucial for human spermatozoa functioning and fertility. Pellavio G, Gastaldi G, Laforenza U.

Acknowledgements

I have never loved writing and in all of my thesis I have never written acknowledgements, but in this case I wanted to make an exception, because the creation of this PhD thesis is due to the trust and support of all those people who believed in me.
I consider this thesis the result of a scientific research that lasted three years, but also the result of a personal research in having the courage to follow something I love, despite the thousand doubts and difficulties.

I thank my tutor, Professor Umberto Laforenza for giving me the opportunity to follow his work and for transmitting his interest in science and for teaching to think in a scientific way, to be critical, but at the same time reasonable to face scientific problems, challenges and obstacles.

I thank Professor Gastaldi for giving me the opportunity to help her in her research with a pre-doctoral scholarship that allowed me to enrich my knowledge in the field of cell cultures, fundamental for this thesis.

I thank Dr. Caliogna for teaching me to work with cells in a precise and accurate way.

I thank the calm and helpfulness of Dr. Bottino, who in 2015 gave me confidence in undertaking a career path in scientific research.

I thank my colleagues, both past and present, who in their own way supported or encouraged me on bad days, creating a friendly working environment.

I thank all my friends, both near and far, both childhood and more recent, for having always considered me and still consider me a sort of "oracle of Science", for trusting me and for having found comfort in my answers.

I thank Simone, my boyfriend and partner, who supported and endured me especially in this last year and for trying to listen to my scientific talks.

Finally, I thank my parents for always believing in me, for supporting me in this path of personal growth, for encouraging me day after day to pursue my ideas and not to accept the simplest way, to have courage and not give up even in hard times.

To thank you, I will try to follow your advice: never lose hope.

"Never lose hope in pursuing your dreams because there is one unique creature that can stop you, and that creature you are.
The freedom is a choice that only you can do, you are only tied by chins of your fears.
It is never a real tragedy try and fail because sooner or later you learn, tragedy is do not even trying for fear of failure.
If you can accomplish great things when others believe in you, imagine what you can achieve when it's you, who believes in yourself."
Peter O'Connor from "Wings on the ocean".

Thank you,

Giorgia

Ringraziamenti

Non ho mai amato scrivere e nelle tesi di laurea non ho mai scritto i ringraziamenti, ma in questo caso ho voluto fare un'eccezione, perché la creazione di questa tesi di dottorato è dovuta alla fiducia e al sostegno di tutte quelle persone che hanno creduto in me. Non considero questa tesi solamente il frutto di una ricerca scientifica durata tre anni, ma anche di una ricerca personale nell'avere coraggio di seguire qualcosa che si ama, nonostante i mille dubbi e difficoltà.

Ringrazio il mio responsabile, il Professor Umberto Laforenza, per avermi dato la possibilità di seguire il suo lavoro in questi anni e soprattutto per avermi trasmesso il suo interesse per la scienza e per avermi insegnato a pensare in modo scientifico e ad essere critica, ma allo stesso tempo ragionevole di fronte a problemi, sfide ed ostacoli scientifici.

Ringrazio la Professoressa Gastaldi per avermi dato la possibilità di aiutarla nella sua ricerca con una borsa pre-dottorato che mi ha permesso di arricchire le mie conoscenze nel campo delle culture cellulari, fondamentali per questa tesi.

Ringrazio la Dottoressa Caliogna per avermi insegnato a lavorare con le cellule in modo preciso ed accurato.

Ringrazio la calma e la disponibilità della Dottoressa Bottino che nel 2015 mi hanno ridato fiducia nell'intraprendere un percorso lavorativo nella ricerca scientifica.

Ringrazio le mie colleghe, sia passate che presenti, che a modo loro mi hanno sostenuta o spronata nei giorni negativi, creando un amichevole ambiente lavorativo.

Ringrazio tutte le mie amiche, sia vicine che lontane, sia di infanzia che più recenti, per avermi sempre considerata e considerarmi tuttora una sorta di "oracolo della Scienza", per esservi fidate di me e per aver trovato conforto nelle mie risposte.

Ringrazio Simone, il mio ragazzo e compagno, che mi ha supportato e sopportato soprattutto in questo ultimo anno di stesura della tesi e per aver provato ad ascoltare i miei discorsi scientifici.

Infine, ringrazio i miei genitori per aver sempre creduto in me, per avermi sostenuta in questo percorso di crescita personale, per avermi spronata giorno dopo giorno nel perseguire le mie idee e nel non accettare la via più semplice, nell'avere coraggio e non arrendersi anche nei momenti di difficoltà.

Per ringraziarvi, cercherò di continuare a seguire i vostri consigli per non perdere mai la speranza.

"Non perdere mai la speranza nell'inseguire i tuoi sogni, perché c'è un'unica creatura che può fermarti, e quella creatura sei tu.
La libertà è una scelta che soltanto tu puoi fare: tu sei legata soltanto dalle catene delle tue paure.
Non è mai una vera tragedia provare a fallire, perché prima o poi si impara, la tragedia è non provarci nemmeno per paura di fallire.
Se tu puoi compiere grandi cose quando gli altri credono in te, immagina ciò che puoi raggiungere quando sei tu a credere in te stessa."
Peter O'Connor da "Ali sull'oceano".

Grazie,

Giorgia